

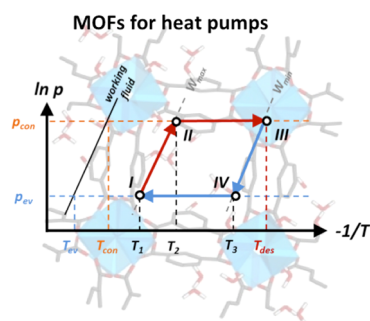
Adsorption-Driven Heat Pumps: The Potential of Metal–Organic Frameworks

Martijn F. de Lange,^{†,‡} Karlijn J. F. M. Verouden,[†] Thijs J. H. Vlugt,[‡] Jorge Gascon,[†] and Freek Kapteijn^{*,†}

[†]Catalysis Engineering, Chemical Engineering Department, Delft University of Technology, Julianalaan 136, 2628 BL Delft, The Netherlands

[‡]Engineering Thermodynamics, Process & Energy Department, Delft University of Technology, Leeghwaterstraat 39, 2628 CB Delft, The Netherlands

Supporting Information



CONTENTS

1. Introduction	12205
2. Adsorption Mechanism	12208
3. Stability	12213
4. Adsorptive Properties	12215
4.1. Water Adsorption (1Table 1)	12215
4.2. Methanol Adsorption (2Table 2)	12219
4.3. Ethanol Adsorption (3Table 3)	12220
4.4. Ammonia Adsorption (4Table 4)	12221
5. MOF Evaluation and Selection	12221
6. Performance Assessment	12222
6.1. Selected Working Pairs	12222
6.2. Heat Pump Cycle	12223
6.3. Thermodynamic Model	12225
6.4. Thermodynamic Properties	12226
6.4.1. Adsorbent Heat Capacity	12226
6.4.2. Characteristic Curve	12226
6.4.3. Enthalpy of Adsorption	12227
6.5. Results and Discussion	12228
6.5.1. Capacity	12228
6.5.2. Efficiency Comparison	12229
6.5.3. Temperature Lift	12231
7. Alternative Applications	12232
7.1. Thermochemical Energy Storage	12232
7.2. Open Cycle Air-Conditioning	12232
8. Summary and Future Perspectives	12233
8.1. Summary	12233
8.2. Future Perspectives	12234
8.2.1. Ammonia – Stage 0	12234
8.2.2. Alcohols – Stage 2	12234
8.2.3. Water – Stages 3/4	12234
Associated Content	12235

Supporting Information	12235
Author Information	12235
Corresponding Author	12235
Notes	12235
Biographies	12235
Acknowledgments	12236
Abbreviations	12236
MOF Terminology	12236
Ligands	12236
Miscellaneous	12237
List of Symbols	12237
Latin	12237
Greek	12237
Subscripts	12237
Superscripts	12237
References	12237

1. INTRODUCTION

Energy consumption is experiencing a continuous rise, despite the increased tangibility of (anthropogenic) global climate change. Households worldwide are responsible for about one-third of the world energy consumption. This energy is mainly used for heating and cooling of residential areas.¹ The building sector accounted for 25% of the total global energy consumption in 2010, predominantly for space heating and hot water production, 53% and 16%, respectively, of this sector.² Furthermore, combined energy demands for heating and especially cooling are forecasted to increase significantly in the coming years, the magnitude of which depends on model assumptions used for the prediction.¹ The urgent need to address this situation has prompted international action from governments and industries; for example, the EU-28 countries have specified ambitious energy efficiency targets, as expressed in Directive 2012/27/EU,³ to reduce primary energy consumption by 20% in 2020. The Netherlands, specifically, has committed to reduce the total annual energy consumption to 2183 PJ in 2020,^{3,4} a 38% reduction as compared to 2010.⁵ Of the total energy consumption in this country, roughly 40% is spent on heating (38.4%) and cooling (2.4%).⁵ Especially, the energy demand for cooling in The Netherlands is forecasted to

Received: February 2, 2015

Published: October 23, 2015

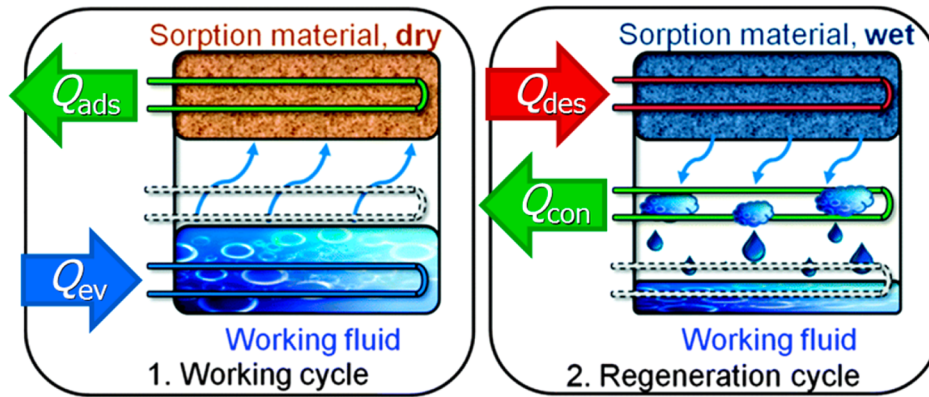


Figure 1. Principle of operation of an adsorption-driven heat cycle with the adsorption stage (left) and the desorption stage (right). Reproduced with permission from ref 22. Copyright 2013 Royal Society of Chemistry.

increase substantially in the coming years.⁵ This clearly highlights the importance of mitigating primary energy requirements for heating and cooling as a tool to decrease fossil fuel consumption and associated CO₂ emissions.

To mitigate (part of) these energetic expenses, one could opt for the utilization of solar energy for these purposes. However, the supply of solar energy and demand for heating are not always in phase.⁶ When energy supply and heating demand are in phase, for example, for air-conditioning, refrigeration, and hot water production, thermally driven heat pumps can be employed, sustainably utilizing the available energy (e.g., solar or waste heat), a clear advantage over devices based on vapor compression,⁷ which use electrical energy. There are multiple possible working principles for heat pumps driven by thermal energy,⁸ for example, chemical reactions,^{8,9} absorption,^{8,10} and adsorption.^{8,11} The main advantage of the adsorption-driven heat pump, which is the method of choice in this Review, is that low driving or regeneration temperatures (<100 °C) can be employed efficiently,^{8,10,12–14} which fits the available temperatures of the desired energy sources (solar, industrial waste heat). Further, environmentally benign working fluids (e.g., water) can be used. A drawback is that the performance of these devices is somewhat lower, for currently available devices, than for alternatives based on chemical reactions or absorption. Additionally, one could further use adsorption-based open system air-conditioning by desiccation.^{13–16} A great advantage is that water vapor can be removed directly from the ambient air, whereas the closed devices require cooling of the incoming air to temperatures below the dew point.¹⁷ Often this means that the dried air has to be reheated, resulting in an energetically expensive system. Additional advantages of desiccant air conditioning over vapor compression systems are the ability to use low-grade thermal energy (similar to adsorption-driven heat pumps) and the working fluid (ambient water) is environmentally benign by default.

When energy supply and demand are out of phase, temporary energy storage is required. Especially thermochemical storage is interesting, as it requires significantly less volume to store the same amount of energy^{18,19} as compared to systems based on latent²⁰ or sensible energy.²¹ The main alternatives for thermochemical storage primarily store and release energy on the basis of either chemical reactions (e.g., hydration of inorganic salts) or adsorption. Note however that for adsorption-based energy storage, in comparison to latent or sensible energy-based systems, additional low temperature energy is required for the evaporation of the working fluid. This

also holds in principle for, for example, the hydration of inorganic salts.

Thermochemical energy storage and desiccant air conditioning are considered alternative applications for porous adsorbents here and are concisely discussed in section 2 of this Review, the main focus being adsorption-driven heat pumps. Devices based on this principle could use thermal energy to supply cooling and heating. The working mechanism, in its simplest form, is shown in Figure 1.

An initially dry adsorbent is connected with a working fluid-filled evaporator (Figure 1, left)). During this process, heat is taken up from the surroundings by evaporation of the working fluid (Q_{evap}), due to the adsorption of the working fluid by the (porous) adsorbent. As adsorption is exothermic, heat will be released to the surroundings at an intermediate temperature (Q_{ads}). As the adsorbent will become saturated with working fluid, regeneration is required (Figure 1, right)). Energy is taken up at a relatively high temperature (Q_{des}) to desorb the working fluid, which is subsequently condensed, releasing heat at an intermediate temperature (Q_{con}). One can operate such an adsorption cycle as heat pump to produce heat at the intermediate temperature (adsorption heat pump, AHP), using effectively Q_{con} and Q_{ads} or to produce cold at the lower temperature by making use of Q_{evap} (adsorption chiller, AC). A detailed thermodynamic description of such a cycle is located in section 6 of this Review. In any case, the cycle requires thermal energy as input. The temperature of this input can be relatively low (below 100 °C),^{12,13} making efficient use of industrial waste heat or solar energy.

Adsorption-driven heat and cold allocation is not a novel technology. After the first quantitative work on adsorption by Scheele and Fontana²³ and the pioneering work of Michael Faraday, who demonstrated adsorptive-based cooling in 1823 using an ammonia–silver chloride working pair,^{24,25} and some early commercial products,^{26–28} the technology was swiftly replaced due to the development of more efficient vapor compression systems (based on chlorinated fluorocarbons, CFCs).^{23,25} However, following the prohibition of commonly used fluids in vapor compression (CFCs) because of environmental concerns,^{29,30} and the aforementioned global energy consumption prognosis, research on adsorption-driven heat pumps is again in full swing (timeline depicted in Figure 2).^{23,31}

For application, the selected working fluid should have a high enthalpy of evaporation. Furthermore, the capacity of the adsorbent should be maximized, implying that working fluid molecules are preferentially relatively small. In addition, the

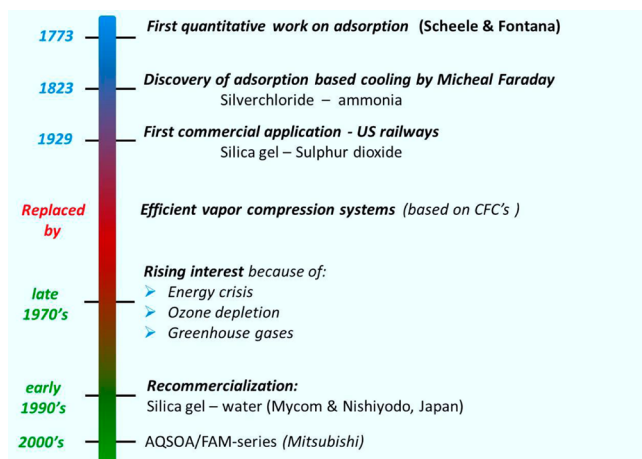


Figure 2. Historical timeline (brief) of adsorption-driven heat pump and chiller research and commercialization.

working fluid should be condensable under operating conditions. Obviously, selected working fluids should have no global warming or ozone depletion potential. It is therefore not surprising to say that commonly used working fluids for adsorption-driven purposes are water, methanol, ammonia,²³ and, because of lower toxicity as compared to methanol, ethanol is also used.^{11,32–34} As shown in Figure 3, water has the

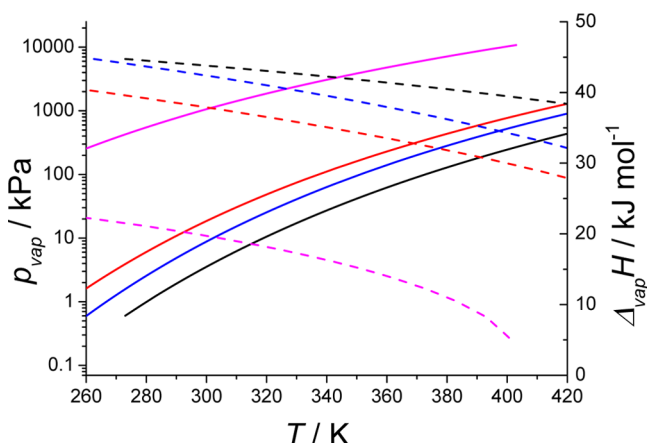


Figure 3. Vapor pressure (solid lines) and enthalpy of evaporation (dashed lines) as a function of temperature, for water (black), methanol (blue), ethanol (red), and ammonia (magenta). Data from ref 35.

highest enthalpy of evaporation and ammonia the lowest, making the latter thermodynamically less efficient.²³ However, the high vapor pressure of NH_3 ensures that mass transport limitations are eliminated in cycle times down to the order of minutes.²³ In addition, in AHP/ACs no use can be made of copper-based parts when ammonia is used.²³ Water has a significantly lower vapor pressure (see Figure 3) and cannot be used for subzero temperatures, due to its relatively high triple point temperature (273.16 K). Methanol and ethanol both are somewhat intermediate in properties as compared to water and ammonia.

In the remainder of this Review, possible working fluids under consideration are indeed water, methanol, ethanol, and ammonia. Different adsorbents can be used in conjunction with these working fluids. Silica gels (water), zeolites (water), and

activated carbons (methanol, ammonia) are popular in academia.^{23,33,36} Commercially, water is dominantly used as working fluid in combination with silica gels or zeolites (vide infra).

Regardless of the working pair, an adsorption isotherm with one single very steep uptake step is preferred from an energetic perspective, as this will display the highest thermodynamic efficiency.³⁷ Also from a dynamic perspective, a stepwise isotherm is preferred,^{38,39} as only a small change in relative sorbate pressure is needed for a large change in loading, that is, a large heat effect (see, e.g., AQSOA-Z01, Figure 4). Hysteresis

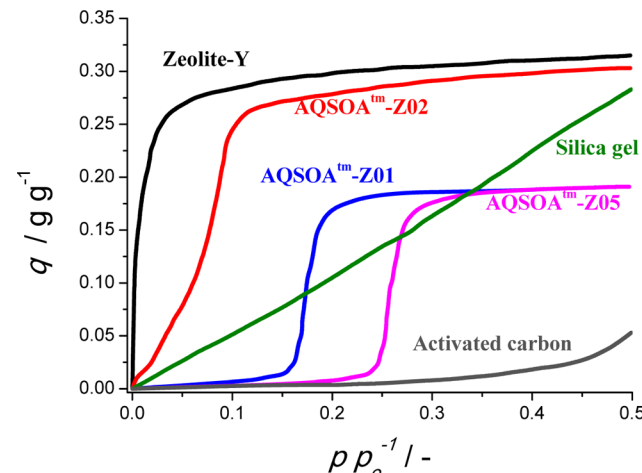


Figure 4. Water adsorption isotherms of commercially employed adsorbents. Data from ref 48.

during desorption is undesired, as this will increase the required desorption temperature. For realistic applications, the step in adsorption should be located at $p/p_o < 0.3$ ³⁷–0.4;⁴⁰ here, p_o represents the saturation pressure, for water (at room temperature), as for higher relative pressures the difference between the low (evaporator) temperature, T_e , and intermediate (adsorption/condenser) temperature, T_c , becomes increasingly smaller. For example, for $0.3 < p/p_o < 0.45$, only $T_e > 10\text{--}15^\circ\text{C}$ and $T_c < 30^\circ\text{C}$ can be used, achieving only a minor “temperature lift” (see section 6.5.3).³⁷ Furthermore, the reversible step in adsorption (or desorption in case of hysteresis) should be preferentially located at $p/p_o > 0.05$ –0.1³⁷ to ensure a sufficiently low desorption temperature. For methanol and ethanol, the operating windows are similar to that of water; for ammonia, this is shifted to higher relative pressures ($0.15 < p/p_o < 0.55$).

Nishiyodo⁴¹ and Mycom pioneered the recommercialization of adsorption-driven devices, in both cases based on silica gel–water as working pair.^{31,42} Later, Sortech marketed silica gel-based sorption systems for cooling purposes.³¹ Invensor has made a commercial coated zeolite-water-based cooling system.^{31,43} Both Vaillant and Viessmann⁴⁴ have commercialized zeolite-water-based heat pumps driven by the combustion of natural gas, which can in principle reduce the energy requirements of a conventional household boiler by up to 30%.³¹ Commercially applied sorbents that perhaps show most advantageous adsorption isotherms, when contacted with water, are those of the FAM Z-series (functional adsorbent material zeolite). FAM Z05,⁴⁵ and especially both Z01⁴⁶ and Z02⁴⁷ as commercialized by Mitsubishi Plastics, although referred to as the AQSOA™ series,⁴⁸ show very suitable adsorption character-

istics. Adsorption isotherms of commercially used adsorbents are shown in Figure 4.

Zeolite Y has a very steep uptake at extremely low p/p_0 , due to the strongly hydrophilic nature of high Al-content zeolites. This in turn means that regeneration needs to be done at unfeasibly high desorption temperatures, a commonly reported drawback for application of these materials.³⁷ On the other hand, pure silica zeolites are too hydrophobic.³⁷ The adsorption behavior of silica gel is not desired, due to the clear absence of a stepwise uptake. The FAM/AQSOA™ series show this stepwise uptake, and especially Z01 and Z02 are employed in heat pumps (Z05 is used primarily for dehumidification).⁴⁸ AQSOA-Z02 is the SAPO-34 zeotype, whereas Z01 and Z05 are AlPO-5 materials (of which Z01 is partially iron-exchanged). These materials have been shown to exhibit high cyclic stability to adsorption and desorption of water.^{49,50} The total uptake (capacity) of these materials, however, is somewhat low.

From the above, it is clear that there is a large commercial interest in the development of new adsorption-based devices, and that the market for such devices is expected to grow as performance improves.³¹ Such a scenario could be realized by different approaches.³¹ Increasing specific power input through enhanced mass and heat transport by, for example, the use of coated adsorbents,^{31,51} or decreasing the heat input by improved cycle design and/or heat integration are two approaches being explored for already defined working pairs.^{31,52} On the other hand, the development of novel working pairs can certainly improve performance^{37,53–56} for example by decreasing the required desorption temperature.³¹

In this Review, we critically assess the feasibility for application in adsorption-driven heating and cooling of one specific emerging class of porous adsorbents: metal–organic frameworks (MOFs). MOFs, comprising inorganic clusters connected by organic ligands in one, two, or three dimensions,⁵⁷ display a rich variety of topologies. The combination of organic ligands and inorganic building blocks⁵⁸ makes up for an almost infinite number of different possible structures, where seemingly the sky is the limit regarding porosity and surface area.^{59,60} In addition, the organic ligands can be decorated with functional moieties, by either pre- or postsynthesis, to tune material properties.^{61–65} No wonder that MOFs have received attention for application in, for example, adsorption/separation,^{66–69} storage,^{70,71} and catalysis.^{72–75}

In the first part of this Review, we summarize the state of the art in MOF science with regard to stability and adsorption behavior for the aforementioned working fluids.

To be able to understand, and to possibly tune, the adsorption of vapors in MOFs, one should have insight into the mechanism of adsorption. This will be described first concerning the experimental and simulation point of view (section 2). Of the utmost importance for the targeted application is further knowledge about the solvothermal (in)stability, as will be discussed second in a clear and concise manner (section 3). Subsequently, an overview of known adsorption behavior (section 4) results in a selection of the most promising MOFs in section 5. This will comprise all four selected working fluids, water (section 4.1), methanol (section 4.2), ethanol (section 4.3), and ammonia (section 4.4), although water will be dominantly present in the discussion, as it has received by far the most attention in scientific literature. In the second part of this Review, the thermodynamic efficiency and storage capacity for these materials will be determined and compared to conventional sorbents (section

6), and advantages that MOFs might hold for thermochemical energy storage and open cycle desiccant air-conditioning are discussed concisely in section 7. A comprehensive summary and a detailed future perspective are both presented in section 8.

2. ADSORPTION MECHANISM

According to Canivet et al., three different mechanisms for water adsorption in MOFs can be distinguished:⁷⁶ adsorption on the metallic cluster, which modifies the first coordination sphere of the metal ion (irreversible); layer or cluster adsorption in pores (reversible); and capillary condensation in pores (irreversible).

Note that reversibility here is defined by thermodynamics and is not meant to include irrevocable loss of structural fidelity (instability), which is discussed separately (section 3). As most MOFs consist of aromatic ligands, which are hydrophobic in nature, cluster adsorption is prevalent over layer formation when water is concerned. Clusters of water can be formed around three different types of sites. First, for MOFs that have coordinatively unsaturated sites (cus) on the metal ions after solvent removal, water can be clustered around those sites. As mentioned already, the first water molecule will then be irreversibly adsorbed, modifying the coordination sphere of said ion. Terminal groups on the metal-ions of the cluster, when present, are predominantly hydroxido- species, which can also act as nucleation sites for clustering of water. Finally, hydrophilic functional groups can be attached to the organic ligand, adding additional nucleation sites.

Whether fully reversible cluster-based adsorption or irreversible capillary condensation occurs will depend on pore size. In pores with a diameter smaller than a certain critical diameter, D_c , water adsorption occurs solely by cluster formation; for pore diameters larger than D_c , water is adsorbed due to capillary condensation, preceded by cluster adsorption.^{76,77} The former case yields continuous reversible adsorption, whereas the latter will result in a hysteretic difference between ad- and desorption behavior, due to the thermodynamic irreversibility of capillary condensation.^{76,77} According to Coasne et al., this critical pore diameter can be expressed as^{78,79}

$$D_c = \frac{4\sigma T_c}{T_c - T} \quad (1)$$

Here, σ is the approximate size of a water molecule (0.28 nm), T_c is the critical temperature of water, and T is the actual temperature. For water at room temperature, for example, this yields a critical diameter of 2 nm.^{76,77}

In a previous communication, we have shown computationally that mesoporous MIL-100(Cr) and MIL-101(Cr), with cavities bigger than the above-mentioned critical diameter, indeed show capillary condensation, preceded by clustering of water molecules around the coordinatively unsaturated chromium sites.⁸⁰ The crux of describing experimentally found adsorption behavior computationally lies in properly accounting for water–water interactions for pores with diameter larger than D_c , as water–framework interactions are of little significance.⁸⁰ Properly describing these water–water interactions is not at all trivial. In scientific literature, there is a plethora of different molecular descriptions of the water molecule available, none of which is capable of properly describing all properties of this molecule.⁸¹ To obtain a sound molecular description of adsorption in microporous materials,

Table 1. MOFs Examined for Water Adsorption in Scientific Literature^a

material	ligand	α^b [-]	q_{\max}^c [g g ⁻¹] M ₃ (μ ₃ -O)(X)(cus) ₂ ^e	$-\Delta_{\text{ads}}H$ [kJ mol ⁻¹] 80–45 ^h	V _p ^c [cm ³ g ⁻¹] 1.6	stability ^d (ThS-hi ¹⁰⁰) ^{102,196,198,203,249–252}	ref 199
MIL-101(Cr)	TPA	0.45	1	43 ^f	1.3	6.3% loss in S _{BET} after 40 ads. cycles	199
MIL-101(Cr)-NH ₂	NH ₂ -TPA	0.42	1.05	43 ^f	0.6	25% loss in S _{BET} after 40 ads. cycles	199
MIL-101(Cr)-pNH ₂ ^g	(NH ₂)-TPA	0.41	1	43 ^f	1.0	20% loss in S _{BET} after 40 ads. cycles	199
MIL-101(Cr)-NO ₂	NO ₂ -TPA	0.5	0.45	46 ^f	1.0	20% loss in S _{BET} after 40 ads. cycles	199
MIL-101(Cr)-pNO ₂ ^g	(NO ₂)-TPA	0.48	0.6	48 ^f	1.1	3.2% loss in q _{max} after 40 ads. cycles	250
MIL-101(Cr)	TPA	0.44	1	52–40 ^h	1.7	stable after 10 ads. cycles	197
MIL-101(Cr)	TPA	0.46	1.3	52–40 ^h	1.6	(ThS-hi ¹⁰⁰) ^{102,196,198,203,249–252}	203
MIL-101(Cr)	TPA	0.48	1.4	70–35 ^h	1.58	(ThS-hi ¹⁰⁰) ^{102,196,198,203,249–252}	198
MIL-101(Cr)-NH ₂	NH ₂ -TPA	0.42	0.95	75–38 ^h	1.27	(HK-hi ¹⁰⁰) ^{198,199}	198
MIL-101(Cr)-NO ₂	NO ₂ -TPA	0.48	0.65	38–20 ^h	1.19	(LK-hi ¹⁰⁰) ^{198,199}	198
MIL-101(Cr)-SO ₃ H	SO ₃ H-TPA	0.28	0.95	60–35 ^h	0.94	(ThS-hi ¹⁰⁰) ^{198,253}	198
MIL-101(Cr)	TPA	0.47	0.87	1.22	(ThS-hi ¹⁰⁰) ^{102,196,198,203,249–252}	77	
MIL-101(Cr)-NH ₂	NH ₂ -TPA	0.35	0.9	0.97	(HK-hi ¹⁰⁰) ^{198,199}	77	
MIL-101(Cr)-NO ₂	NO ₂ -TPA	0.45	0.7	0.95	(LK-hi ¹⁰⁰) ^{198,199}	77	
MIL-101(Cr)	TPA	0.45 ⁱ	0.4		(ThS-hi ¹⁰⁰) ^{102,196,198,203,249–252}	37	
+POM incorporated	TPA	0.42 ⁱ	0.5				37
MIL-101(Al)-NH ₂	NH ₂ -TPA	0.35	0.43	1.67	rapidly degrades upon exposure to vapor	125	
MIL-101(Al)-URPh	URPh-TPA	0.40	0.36	0.83	more slowly degrades upon exposure to vapor	125	
MIL-100(Cr)	BTC	0.36 ^j	0.4	0.77	(ThS-med ¹⁰⁰) ^{114,201,255}	202	
grafted with EG	BTC	0.35 ^j	0.43	0.47			202
grafted with DEG	BTC	0.35 ^j	0.42	0.50			202
grafted with TEG	BTC	0.35 ^j	0.33	0.53			202
grafted with EN	BTC	0.35 ^j	0.37	0.42	~2% loss in q _{max} after 20 ads. cycles	202	
MIL-100(Cr) (X = F)	BTC	0.3	0.8	48 ^k	0.93	stable after 2000 ads. cycles	201
MIL-100(Cr) (X = Cl)	BTC	0.31	0.6	48–49 ^k	0.70		201
MIL-100(Cr) (X = SO ₄)	BTC	0.25	0.6	48–49 ^k	0.70		201
MIL-100(Fe)	BTC	0.35	0.79	65–40 ^h	0.82	(HK-hi ¹⁰⁰) ^{40,203,249,256,257}	203
MIL-100(Fe)	BTC	0.29	0.75	90–50 ^h	0.85	6.4% loss in Δq after 40 ads. cycles	40
MIL-100(Fe)	BTC	0.38	0.87	80–45 ^h	0.92	stable after 10 ads. cycles	197
MIL-100(Al)	BTC	0.28	0.5	80–42 ^h	0.8	6.6% loss in Δq after 40 ads. cycles	40
MIL-125(Ti)	TPA	0.25	0.36				
MIL-125(Ti)-NH ₂	NH ₂ -TPA	0.2	0.45	0.47	(LK-lo ¹⁰⁰) ^{205,258}	77	
MIL-125(Ti)-NH ₂	NH ₂ -TPA	0.19	0.35	0.51	(HK-hi ¹⁰⁰) ^{22,205,258}	77	
MIL-125(Ti)	TPA	0.35	0.30	0.45	~17% loss in q _{max} after 40 ads. cycles	22	
MIL-125(Ti)-NH ₂	NH ₂ -TPA	0.2	0.52	0.60	unstable during H ₂ O adsorption	205	
				0.67	stable in aqueous solution (48 h)	205	
CAU-1(Al)	NH ₂ -TPA	0.38	0.55				206
CAU-1(Al)-NHCH ₃	NHCH ₃ -TPA	0.48	0.40	0.64			206
CAU-1(Al)-NHCOCH ₃	NHCOCH ₃ -TPA	0.26	0.25	0.53			206
UiO-66(Zr)	TPA	0.33	0.36				
UiO-66(Zr)-NH ₂	NH ₂ -TPA	0.15	0.36	0.41	(HK-hi ¹⁰⁰) ^{104,106,212,231,256,257,259,260}	77	
UiO-66(Zr)	TPA	0.25	0.45	0.35	(HK-hi ¹⁰⁰) ^{22,62,104,231,257,261}	77	
UiO-66(Zr)-NH ₂	NH ₂ -TPA	0.16	0.36	0.52	2% loss in S _{BET} after 1 ads. cycle	231	
UiO-66(Zr)	TPA	0.25	0.5	0.57	no loss in S _{BET} after 1 ads. cycle	231	
UiO-66(Zr)-NH ₂	NH ₂ -TPA	0.15	0.45	0.77	(HK-hi ¹⁰⁰) ^{104,106,212,231,256,257,259,260}	22	
UiO-67(Zr)	BPDC	0.6	0.18	120–60 ^h	0.70	~38% loss in q _{max} after 40 ads. cycles	22
UiO-67(Zr)	BPDC	0.5	0.29	75–50 ^h	0.97	(HK-hi ¹⁰⁰) ^{104,211,259,260}	22
UiO-66(Zr)-BIPY	BIPY	0.2	0.23		>99% loss in S _{BET} after 1 cycle	104	
UiO-66(Zr)	TPA	0.34	0.43		>99% loss in S _{BET} after 1 cycle	104	
UiO-66(Zr)	TPA	0.35	0.37	0.49	slight decr. q _{max} /strong H ₂ O adsorption	212	
UiO-66(Zr)-CH ₃	CH ₃ -TPA	0.29	0.31	0.52	(HK-hi ¹⁰⁰) ^{104,106,212,231,256,257,259,260}	262	
UiO-66(Zr)-(CH ₃) ₂	(CH ₃) ₂ -TPA	0.43	0.23	0.51	stable after 1 ads. cycle	263	
UiO-66(Zr)	TPA	0.26	0.45	0.40	stable after 1 ads. cycle	263	
UiO-66(Zr)-NH ₂	NH ₂ -TPA	0.16	0.34	0.55	(HK-hi ¹⁰⁰) ^{104,106,212,231,256,257,259,260}	62	
UiO-66(Zr)-1,4-naphthyl	1,4-NDC	0.25	0.26	0.52	(HK-hi ¹⁰⁰) ^{22,62,104,231,257,261}	62	
				0.40	no loss in crystallinity after adsorption	62	

Table 1. continued

material	ligand	α^b [-]	q_{\max}^c [g g ⁻¹]	$-\Delta_{\text{ads}}H$ [kJ mol ⁻¹]	V_p^d [cm ³ g ⁻¹]	stability ^d	ref
$M_6(\mu_3\text{-O})_{4+x}(\mu_3\text{-OH})_{4-x}$							
UiO-66(Zr)-NO ₂	NO ₂ -TPA	0.18	0.37		0.42	no loss in crystallinity after adsorption	62
UiO-66(Zr)-2,5-(OMe) ₂	(OMe) ₂ -TPA	0.2	0.42		0.38	no loss in crystallinity after adsorption	62
UiO-66(Zr)-(COOH) ₂	(COOH) ₂ -TPA	0.15 ^l	0.27		0.21	no loss in q_{\max} after 2 ads. cycles	264
MOF-801(Zr)	FA	0.09	0.36	62–47 ^h	0.45	stable after 5 ads. cycles	212
MOF-802(Zr)	PZDC	0.4	0.09		<0.01	stable after 5 ads. cycles	212
MOF-804(Zr)	(OH) ₂ -TPA	0.4	0.23		0.46	unstable/strong H ₂ O ads.	212
MOF-805(Zr)	(OH) ₂ -NDC	0.31	0.33		0.48	unstable/strong H ₂ O ads.	212
MOF-806(Zr)	(OH) ₂ -BPDC	0.1	0.34		0.85	unstable/strong H ₂ O ads.	212
MOF-808(Zr)	BTC	0.3	0.59		0.84	unstable/strong H ₂ O ads.	212
MOF-841(Zr)	MTB	0.22	0.51	58–42 ^h	0.53	stable after 5 ads. cycles	212
PIZOF-2(Zr)	(OMe) ₂ -PEDB	0.75	0.68		0.67	unstable/strong H ₂ O ads.	212
DUT-67(Zr)	TDC	0.22	0.50		0.60	unstable/strong H ₂ O ads.	212
DUT-51(Zr)	DTTDC	0.63	0.55		1.08	23% reduction in q_{N_2} after 12 h in liq	213
DUT-52(Zr)	2,6-NDC	0.35	0.24		0.54		107
1DUT-84(Zr)	2,6-NDC	0.38	0.12		0.27		107
DUT-53(Hf)	2,6-NDC	0.38	0.22		0.31		107
DUT-67(Zr)	TDC	0.35	0.41		0.44	survives HCl sol. (1 mol L ⁻¹), 3 days	214
DUT-67(Hf)	TDC	0.35	0.29		0.33	survives HCl sol. (1 mol L ⁻¹), 3 days	214
DUT-68(Zr)	TDC	0.40	0.34		0.41	survives HCl sol. (1 mol L ⁻¹), 3 days	214
DUT-68(Hf)	TDC	0.38	0.29		0.34	survives HCl sol. (1 mol L ⁻¹), 3 days	214
DUT-69(Zr)	TDC	0.30	0.26		0.31	survives HCl sol. (1 mol L ⁻¹), 1 day	214
DUT-69(Hf)	TDC	0.28	0.20		0.22		214
NU-1000(Zr)	TBAPy	0.75	1.0		1.4	stable after 1 ads. cycle	215
+SALL-1	CF ₃ CO ₂ ⁻	0.80	0.9		1	stable after 1 ads. cycle	215
+SALL-3	CF ₃ (CF ₂) ₂ CO ₂ ⁻	0.80	0.7		0.8	stable after 1 ads. cycle	215
+SALL-7	CF ₃ (CF ₂) ₆ CO ₂ ⁻	0.85	0.45		0.6	stable after 1 ads. cycle	215
+SALL-9	CF ₃ (CF ₂) ₈ CO ₂ ⁻	0.85	0.35		0.6	stable after 1 ads. cycle	215
$[\text{M}(\mu_2\text{-OH})_n]$							
MIL-53(Cr)	TPA	0.15	0.1	60–40 ^p		(HK-hi ¹⁰⁰) ¹¹⁷	219
MIL-53(Al)	TPA	0.09	0.14		0.51	(HK-hi ¹⁰⁰) ^{102,117,129}	77
MIL-53(Al)-NH ₂	NH ₂ -TPA	0.08	0.04		0.37		77
MIL-53(Ga)	TPA	0.05	0.02		0.47		77
MIL-53(Ga)-NH ₂	NH ₂ -TPA		0.02				77
MIL-53(Al)	TPA	0.30	0.09			(HK-hi ¹⁰⁰) ^{102,117,129}	265
MIL-53(Fe)-(COOH) ₂	(COOH) ₂ -TPA	0.05	0.16				265
MIL-53(Al)-OH	OH-TPA	0.75	0.40				265
MIL-53(Al)-(OH) _{0.68} (NH ₂) _{0.32}	NH ₂ -/OH-TPA	0.80	0.36				266
MIL-53(Al)-(OH) _{0.53} (NH ₂) _{0.47}	NH ₂ -/OH-TPA	0.88	0.23				266
MIL-53(Al)-(OH) _{0.34} (NH ₂) _{0.66}	NH ₂ -/OH-TPA	0.02	0.11				266
MIL-53(Al)-Cl	Cl-TPA	0.18	0.14		0.32		267
MIL-53(Al)-Br	Br-TPA	0.50	0.11		0.14		267
MIL-53(Al)-CH ₃	CH ₃ -TPA	0.25	0.11		0.32		267
MIL-53(Al)-NO ₂	NO ₂ -TPA	0.10	0.12		0.34		267
MIL-53(Al)-(OH) ₂	(OH) ₂ -TPA	0.65	0.42		0.07		267
MIL-53(Al)-F	F-TPA	0.80	0.07		0.48	no reduction in hexane capacity after 1 ads. cycle	221
MIL-53(Al)-F ₂	F ₂ -TPA	0.70	0.23		0.16		268
MIL-47(V)-F	F-TPA	0.60	0.18		0.36	~50% reduction in hexane capacity after 1 ads. cycle	221
MIL-47(V)-F ₂	F ₂ -TPA	0.70	0.18		0.34		268
MIL-53(Al)-NH ₂	NH ₂ -TPA	0.02	0.09				265
MIL-53(Al) _{ionothermal}	TPA	0.15	0.08		0.36		269
MIL-53(Al)-SO ₃ H	SO ₃ H-TPA	0.45	0.45			stable over 3 ads. cycles	65
Al(OH)-(1,4-NDC)	1,4-NDC	0.45	0.16		0.22		270
DUT-4(Al)	2,6-NDC	0.65	0.52		0.79	unstable during first ads. cycle	203
MIL-68(In)	TPA	0.58	0.32		0.42		77
MIL-68(In)-NH ₂	NH ₂ -TPA	0.44	0.32		0.30		77
CAU-10(Al)-H	IPA	0.18	0.35	53.5 ^{223,h}	0.27	no capacity loss over 700 ads. cycles	225
CAU-10(Al)-H	IPA	0.18	0.38	53.5 ^{223,h}	0.28	survives liq water (18 h)	222

Table 1. continued

material	ligand	α^b [-]	q_{\max}^c [g g ⁻¹]	$-\Delta_{\text{ads}}H$ [kJ mol ⁻¹] ^d	V_p^e [cm ³ g ⁻¹]	stability ^d	ref
[M(μ_2 -OH)] _n							
CAU-10(Al)-CH ₃	CH ₃ -IPA	0.45	0.18			survives liq water (18 h)	222
CAU-10(Al)-OCH ₃	OCH ₃ -IPA	0.25	0.08			survives liq water (18 h)	222
CAU-10(Al)-NO ₂	NO ₂ -IPA	0.32	0.17	0.21		survives liq water (18 h)	222
CAU-10(Al)-NH ₂	NH ₂ -IPA	0.16	0.23			survives liq water (18 h)	222
CAU-10(Al)-OH	OH-IPA	0.16	0.30			survives liq water (18 h)	222
CAU-13(Al)	CDC	0.22	0.16	0.15			226
Al-fumarate	FA	0.27	0.45	50–42 ^b	0.48	~13% loss in Δq over 40 ads. cycles	227
[M ₂ O ₂] _n							
MOF-74(Mg)	(OH) ₂ -TPA	0.02	0.63		0.65	83% loss in S_{BET} after 1 cycle	231
MOF-74(Mg)	(OH) ₂ -TPA	0.05	0.60		0.53	unstable/strong H ₂ O ads.	212
MOF-74(Ni)	(OH) ₂ -TPA	0.05	0.51		0.49	unstable/strong H ₂ O ads.	212
MOF-74(Co)	(OH) ₂ -TPA	0.05	0.49		0.46	unstable/strong H ₂ O ads.	212
MOF-74(Ni)	(OH) ₂ -TPA	0.02	0.54			little loss in q_{CO_2} after H ₂ O ads.	230
ZIFs							
ZIF-8(Zn)	mIm				0.49	(ThS-hi ¹⁰⁰) ^{102,114,203,234,271}	235
SIM-1(Zn)	mImca	0.27	0.14		0.30		77
MAF-4(ZIF-8)	mIm				0.65	(ThS-hi ¹⁰⁰) ^{102,114,203,234,271}	235
MAF-4 _{0.76} -7 _{0.24}	mIm/mTz	0.85	0.4		0.64		235
MAF-4 _{0.49} -7 _{0.51}	mIm/mTz	0.62	0.43		0.65		235
MAF-4 _{0.23} -7 _{0.77}	mIm/mTz	0.37	0.43		0.64		235
MAF-7(Zn)	mTz	0.27	0.43		0.65		235
ZIF-71(Zn)	dcIm	— ⁱ			0.39		272
ZIF-90(Zn)	Ica	0.35 ⁱ	0.32		0.49	(Hk-med ¹⁰⁰) ²⁷¹	272
CoNIm	NIm	0.55 ^j	0.16				273
Pillared MOFs: M(II)(L _a)(L _b) _{0.5}							
DMOF(Zn)	TPA/DABCO	0.30	0.09		0.75	100% loss in S_{BET} after 90% RH	231
DMOF(Zn)-NH ₂	NH ₂ -TPA/ DABCO	0.30	0.08		0.58	100% loss in S_{BET} after 90% RH	231
DMOF(Zn)-Br	Br-TPA/DABCO	0.45	0.05		0.53	100% loss in S_{BET} after 90% RH	152
DMOF(Zn)-Cl ₂	Cl ₂ -TPA/DABCO	0.35	0.07		0.45	100% loss in S_{BET} after 90% RH	152
DMOF(Zn)-OH	OH-TPA/DABCO	0.30	0.11		0.54	100% loss in S_{BET} after 90% RH	152
DMOF(Zn)-NO ₂	NO ₂ -TPA/ DABCO	0.40	0.14		0.53	97% loss in S_{BET} after 90% RH	152
DMOF(Zn)-N	NDC/DABCO				0.57	26% loss in S_{BET} after 90% RH	152
DMOF(Zn)-A	ADC/DABCO	0.30	0.27		0.33	4% loss in S_{BET} after 90% RH	152
DMOF-TM1(Zn) (mixed linker)	TMBDC/TPA/ DABCO	0.44	0.27		0.53	30% loss in S_{BET} after 90% RH	152
DMOF-TM2(Zn)	TMBDC/DABCO	0.26	0.43		0.51	stable over 3 ads. cycles	110
DMOF-TM(Co)	TMBDC/DABCO	0.35	0.40		0.49	3.4% loss in S_{BET} after 1 cycle	157
DMOF-TM(Ni)	TMBDC/DABCO	0.45	0.40		0.48	2.5% loss in S_{BET} after 1 cycle	157
DMOF-TM(Cu)	TMBDC/DABCO	0.55	0.42		0.46	4.9% loss in S_{BET} after 1 cycle	157
Cd(BTTB) ⁿ	BTTB	0.50	0.27		0.19	100% loss in S_{BET} after 90% RH	238
Zn(BTTB) ⁿ	BTTB	0.70	0.22		0.25	100% loss in S_{BET} after 90% RH	238
Zn(BTTB) (BDC) ⁿ	BTTB/TPA	0.50	0.09		0.21	50% loss in S_{BET} after 90% RH	238
Ni(BTTB) ⁿ	BTTB	0.80	0.02		0.20	no loss in S_{BET} after 90% RH	238
Co(BTTB) (BPY)	BTTB/BPY	0.30	0.01		0.40	no loss in S_{BET} after 90% RH	238
Zn(BTTB) (BPY)	BTTB/BPY	0.70	0.27		0.38	no loss in S_{BET} after 90% RH	238
Co(BTTB) (AZPY)	BTTB/AZPY	0.55	0.25		0.39	56% loss in S_{BET} after 90% RH	238
Zn(BTTB) (AZPY)		0.55	0.20		0.36	43% loss in S_{BET} after 90% RH	238
Co(BTTB) (DMBPY)	BTTB/DMBPY	0.85	0.20		0.29	0.2% loss in S_{BET} after 90% RH	157
Zn(BTTB) (DMBPY)	BTTB/DMBPY	0.85	0.22		0.27	1.2% loss in S_{BET} after 90% RH	157
Cu ₂ (pzdc) ₂ pyz	Pzdc/pyz	0.10 ⁱ	0.12				274
Cu ₂ (pzdc) ₂ bpy	Pzdc/bpy	0.09 ⁱ	0.17				274
Cu ₂ (pzdc) ₂ bpe	Pzdc/bpe	0.08 ⁱ	0.29				274
Copper-Based MOFs (Remainder)							
CuBTC	BTC	0.1	0.5		0.62	26% loss in S_{BET} after 1 cycle	156,231
CuMBTC	CH ₃ -BTC	0.30	0.18		0.50	loss of crystallinity after 90% RH	156
CuEBTC	C ₂ H ₅ -BTC	0.15	0.18		0.46	loss of crystallinity after 90% RH	156
Cu-BTC	BTC	0.15 ^m	0.54		(LK-hi ¹⁰⁰) ^{102,114,203,231,255,256,275}	96	
Cu-BTC	BTC	0.1	0.5		(LK-hi ¹⁰⁰) ^{102,114,203,231,255,256,275}	203	

Table 1. continued

material	ligand	α^b [-]	q_{\max}^c [g g ⁻¹]	$-\Delta_{\text{ads}}H$ [kJ mol ⁻¹]	V_p^d [cm ³ g ⁻¹]	stability ^e	ref
Copper-Based MOFs (Remainder)							
Cu-BTC	BTC	0.5	0.72			unstable when contacted with H ₂ O	230
Cu ₂ (dmcapz) ₂	dmcapz	0.33	0.22		0.23	reversible structural change upon adsorption	240
Cu ₂ (pmpmd) ₂ (CH ₃ OH) ₄ (opd) ₂	pmpmd/opd	0.15	0.20				276
Zinc-Based MOFs (Remainder)							
Zn-trimesate	BTC	0.10 ^f	0.2			stable after 40 cycles (hydrothermal)	241
Zn ₂ (bptc)	Bptc	0.18	0.16				277
MFU-4(Zn)	BBTA	0.25	0.55			no loss in q_{\max} after 1 ads. cycle	242
ThrZnOAc	Thr	0.25	0.15				245
AlaZnOAc	Ala	0.88	0.25				245
AlaZnCl	Ala	0.25	0.16			stable for 6 months in H ₂ O	246
AlaZnBr	Ala	0.60	0.14			stable for 6 months in H ₂ O	246
ValZnOAc	Val	0.78	0.25				245
ValZnCl	Val	0.45	0.07			stable for 6 months in H ₂ O	246
(H ₃ dab)[Zn ₂ (ox) ₃]	ox/dab	0.70	0.23				278
Zn(NDI-H)	NDI-H	0.45 ^j	0.45		0.65	survives liq water (24 h)	279
Zn(NDI-SEt)	NDI-SEt	0.41 ^j	0.25		0.39		279
Zn(NDI-SOEt)	NDI-SOEt	0.26 ^j	0.30		0.38		279
Zn(NDI-SO ₂ Et)	NDI-SO ₂ Et	0.35 ^j	0.25		0.31		279
Zn ₄ O(dmcapz) ₃	dmcapz	0.85	0.45		0.43	mild degradation after H ₂ O adsorption	243
Zn ₄ O(bfpdc) ₃ (bpy) _{0.5}	bfpdc/bpy	0.92	0.50		0.59	stable upon exposure to water (vapor)	244
Zn ₂ (bptc)	Bptc	0.18	0.16				277
Miscellaneous MOFs							
CAU-3(Al)	TPA	0.63	0.51		0.64		280
CAU-3(Al)-NH ₂	NH ₂ -TPA	0.67	0.50		0.53		280
CAU-6(Al)	NH ₂ -TPA	0.09	0.40		0.25	(LK-lo ¹⁰⁰) ²¹²	281
CALF-25(Ba)	PytPh	0.60	0.09	45 ^h		stable over 4 ads. cycles	148
ISE-1(Ni)	BTC/btre	0.15 ^o	0.18		0.51	stable over 10 ads. cycles	247
JUC-110(Cd)	THIPC	0.2	0.11			survives boiling water (10 days)	282
Ni ₈ (L1) ₆	L1	0.9	0.45		0.52	stable over 3 ads. cycles	248
Ni ₈ (L2) ₆	L2	0.8	0.63		0.52	mild degradation after H ₂ O adsorption	248
Ni ₈ (L3) ₆	L3	0.4	0.99		1.21	stable over 3 ads. cycles	248
Ni ₈ (L4) ₆	L4	0.45	0.9		0.97	stable over 3 ads. cycles	248
Ni ₈ (L5) ₆	L5	0.7	1.12		1.25	stable over 3 ads. cycles	248
Ni ₈ (L5-(CH ₃) ₂) ₆	L5-(CH ₃) ₂	0.72	0.70				248
Ni ₈ (L5-(CF ₃) ₂) ₆	L5-(CF ₃) ₂	0.85	0.86				248
([Ni(L6) ₂]·4H ₂ O) _n	L6	0.11	0.12			stable after 1 ads. cycle	283
[Cd(L'1) (Cl)](H ₂ O)	L'1	0.9	0.38				284
[Cd(L'2) (Cl)](H ₂ O)	L'2	0.1	0.09				284
[Cd ₂ (L'2) ₂ (Br) ₂](H ₂ O) ₃	L'2	0.5	0.04				284
[Cd(L'3) (Cl)](H ₂ O) ₂	L'3	0.15	0.11				284
[Cd(L7) (DMF)]	L7	0.1	0.15			stable in boiling water, 1 day	285
[Co(DPE)]·0.5DPE	DPE	0.45	0.20		0.14		286
[Dy(ox) (Bpybc)(H ₂ O)]	Ox/Bpybc	0.60	0.25				287
[PbL ₂] ₂ DMF·6H ₂ O	L	0.8	0.24				288

^aMaximum capacity (q_{\max}), relative pressure for which capacity is 50% of q_{\max} (α), pore volume (V_p), enthalpy of adsorption ($\Delta_{\text{ads}}H$), and remarks about stability are included where possible. ^b p/p_0 for which $q = 0.5q_{\max}$. Measured at 298 K unless otherwise noted. ^cBased on N₂ adsorption (at 77 K). Reported values are used where possible; otherwise these are estimated from N₂ isotherms. ^dFor entries that do not contain clear statements regarding stability, the classification of Burch et al. has been used, including the confidence expressed by the authors (hi(gh), lo(w), or med(ium)) and the references on which their verdict has been based.¹⁰⁰ ^eX = F, OH. ^fAverage value from isosteric method for $q < 0.1$ g g⁻¹. ^gp stands for partial, indicating that ~78% mol of the linkers is functionalized, and ~22% is plain TPA. ^hIsosteric heat of adsorption, calculated with eq 22. ⁱMeasured at 308 K. ^jMeasured at 293 K. ^kBased on Dubinin–Radushkevich (DR) analysis²⁸⁹ for second ($0.3 < p/p_0 < 0.4$) and third steps ($0.5 < p/p_0 < 0.7$). ^lMeasured at 303 K. ^mMeasured at 323 K. ⁿNot a pillared MOF, added for comparison with others. ^oMeasured at 313 K. ^pDetermined by microcalorimetry.

showing reversible, cluster-based adsorption, structure–water interactions should be tuned with scrutiny, in sharp contrast to mesoporous materials. For example, Castillo et al. have shown, using classical force fields, that simulating water adsorption in Cu-BTC is extremely sensitive to attributed partial charges,

responsible for electrostatic interactions between host and guest, and that subsequently considerate tuning is required to commensurate computational results with experiments.⁸² Using similar methods, without tuning, satisfying predictions were obtained for Al(OH)(1,4-ndc).⁸³ Ghosh et al. found for UiO-

66(Zr) that, employing Monte Carlo simulations⁸⁴ and classical force fields, the structure is significantly more hydrophobic in silico (using) than in reality.⁸⁵ By inducing defects via replacing an organic ligand and replacing it with OH-groups, a significantly more hydrophilic structure can be obtained, although a small hysteresis with experimental results remains.⁸⁵ Zang et al. found, in line with previously discussed results, that classical force fields cannot describe water adsorption in copper-based MOFs.⁸⁶ When employing more accurate and computationally more expensive DFT-derived force fields, at best a fair coherence with experiments is obtained.⁸⁶ This in contrast to, for example, CO₂-adsorption in nanoporous materials, which is seemingly nearly perfectly reproduced with these DFT-derived force fields.^{87,88} In the same line, Lin et al. have developed a different DFT-derived force field for CO₂-adsorption in MOF-74(Zn,Mg), showcasing accurate reproduction of adsorption measurements in silico.⁸⁹ The same protocol, however, only exhibits reasonable reproduction of water adsorption in these materials, in line with the findings of Zang et al.⁸⁹

On the basis of the preceding discussion, it seems difficult to describe with computational methods of varying complexity the experimentally determined adsorption data. This can only mean that these computational methods are not mature enough for in silico design or computational screening. This in sharp contrast with, for example, H₂ storage⁹⁰ or CO₂ capture,^{91,92} where screening methods are more precise.

For alcohols, coherence of simulated and experimentally observed adsorption is much more easily obtained, even when using classical force fields.^{80,93–96} Mechanistically speaking, when compared to water, alcohols show in general a less sharp uptake profile in MOFs due to their lower polarity,⁸⁰ and lowered repulsion from the aromatic ligands. Furthermore, seemingly chemisorption is not observed in the literature for alcohols.

In the case of ammonia, most data available in the literature come from in silico studies. Snurr et al. have elaborately discussed NH₃ adsorption in MOFs using quantum-chemistry derived force fields,^{97–99} showing that in principle a steep uptake can be achieved, at usefully low (relative) pressure, for various frameworks.⁹⁷ These studies, however, did not consider chemisorption effects and instability of the investigated MOFs toward ammonia (section 4.4), thus limiting the relevance of these adsorption predictions for performance assessment. Furthermore, there are little to no experimental adsorption measurements available to benchmark these predictions.

3. STABILITY

For application in AHP/ACs, MOF stability is of utmost importance. Degradation under prolonged exposure to the adsorptive of choice is unacceptable. Especially regarding water, this is a limiting constraint for application. Before discussing the factors that determine the differences in structural stability in detail, different levels of hydrothermal stability will be defined. Subsequently, an overview will be presented of techniques to increase stability of MOFs, be it in situ or postsynthetic, with focus on their potential use for AHP/ACs. In a recent review on water stability in MOFs, Burtch et al. conveniently defined four successive levels of stability:¹⁰⁰ thermodynamic stability (ThS), stable after long-term exposure to aqueous solutions; high kinetic stability (HK), stable after exposure to high relative humidity, decomposes after short exposure to liquid water; low kinetic stability (LK), stable after exposure to low relative

humidity only; and unstable (Uns), where any exposure to moisture will cause loss of structural integrity.

Eligibility to the thermodynamic stability level is considered after structural survival after exposure of at least 7 days to pure water and at least 1 day for boiling or basic/acidic conditions.¹⁰⁰ For the subsequent levels, proof requires significantly less stringency. Analysis of the extent of degradation, after exposure to applied conditions, should minimally consist of the retention of crystallinity (using, e.g., X-ray diffraction) and porosity (using adsorptive characterization).¹⁰⁰ In fact, the authors recommend one use the BET-analysis for this quantification specifically, but in light of our recent work on the inconsistencies that can arise when determining a specific surface area using this method,¹⁰¹ we here advocate one use adsorption capacities (at saturation) instead. This classification suits well to discriminate between different MOF structures on a qualitative level. Adhering to this classification, eligibility for AHP/ACs can only be considered for thermodynamic and high kinetic stability. As a material employed in AHP/ACs has to endure a large number of adsorption–desorption cycles, stability over many of these cycles has to be ensured in addition. Last, one should take into account that determining the relative stability of any structure is indeed a clear function of the application (conditions) envisaged. The aforementioned levels of stability are indicated, if possible, in Table 1 when no information on (cyclic) stability is reported alongside the adsorptive behavior of the listed MOFs.

Water can potentially damage metal–oxide clusters through ligand-displacement, replacing a ligand by a water molecule, or by forming a metal–hydroxide bond and a (partially) protonated ligand.¹⁰² Whether and to what extent these will occur is a function of several factors, as first explored in the pioneering work of Low et al.¹⁰² These factors can be subdivided into two main categories. First, there are factors determining whether an irreversible reaction of water within the MOF structure is thermodynamically favorable.¹⁰⁰ Second, of interest especially for structures for which water reactions are energetically favorable, there are factors that determine whether this reaction will occur (kinetics/sterics).¹⁰⁰ Note that while these factors are discussed individually, they cannot always be completely separated in reality.¹⁰³ Last, as these factors are described in the literature in sufficient detail already,^{76,100,102,103} allow us to be relatively brief in highlighting current knowledge. The factors identified in literature in the former category, determining the energetic feasibility of degradation reactions, revolve around the strength of the interaction of the inorganic cluster with the surrounding organic ligands, most often the structure's heel of Achilles, and the stability of the cluster toward water.^{100,103}

The most important aspects in controlling the hydrolytic stability considered currently are the valence of the metal ions, the nature of the metal, the filling of the coordination sphere of the inorganic cluster, and ligand pK_a. The (formal) valence of the metal ion is of importance, as MOFs that incorporate trivalent metal ions seem to be more stable than bivalent metal ions,^{100,102,103} and high stability is ascribed to tetravalent Zr/Hf-based MOFs.^{100,104–107}

As MOF coordination is perceived to be governed by Lewis acid/base chemistry,^{100,103} MOFs comprising basic ligands (e.g., imidazolate, pK_a ≈ 18–19) exhibit a higher hydrothermal stability than acidic ligands (e.g., carboxylates, pK_a ≈ 4).^{71,102,103,108–110}

Metal ions that show 6-fold coordination tend to be more stable than those that have 4-fold coordination, because denser filling of the coordination sphere makes coordination of water to the metal-ion more difficult.^{102,111}

In addition, the nature of the metal species plays an important role in stability.^{100,102,103} Comparing, for example, the relative stability of bivalent metal ions in isostructural M(BDC) (TED/DABCO)_{0.5},^{112,113} one would observe that hydrolysis occurs in the Cu-based MOF, ligand replacement of the TED ligands by water takes place for the Zn- and Co-based structures, whereas incorporation of Ni results in a relatively stable structure.^{112,113} Further, Cu-BTC shows moderate stability,^{105,114,115} whereas isoreticular Zn-BTC collapses upon solvent removal.¹¹⁶ Last, MIL-53(Cr) is more stable toward water than MIL-53(Al), and in turn more stable than isotypic MIL-47(V), which decomposes rapidly in the presence of liquid water.¹¹⁷

Not surprisingly based on the preceding discussion, MOFs of the isoreticular IRMOF-series, all comprising the Zn₄O-cluster, degrade in the presence of even low moisture concentrations.^{118,119} On the basis of various computational approaches on IRMOF-1, it was found that the critical water content for degradation is somewhere between 4% and 6% wt.^{120–122} In accordance with the stability factors discussed above, MIL-100(Cr), comprising trivalent, 6-fold coordinated, chromium clusters, was found to be completely water stable,¹¹⁴ as well as tetravalent zirconium atom-containing UiO-66.^{104,105,123}

On the basis of the preceding, one might expect MIL-101(Al)-based materials to be stable as well. Unfortunately, NH₂-MIL-101(Al) is transformed to NH₂-MIL-53(Al), the thermodynamically stable phase,¹²⁴ upon contact with liquid water.¹²⁵ The aforementioned stability of MIL-53(Al) is thought to be due to sterically more shielded one-dimensional inorganic building units in MIL-53.^{124,126,127} In addition, MIL-53(Al) slowly decomposes in liquid water (80 °C).¹¹⁷ More specifically, a γ-Al(OH)-phase is formed at the exterior of MIL-53(Al) crystals, consuming part of the MOF.¹²⁸ A maximum conversion of around 20% can be achieved,¹²⁸ forming an impermeable layer.¹²⁸ Qian et al. reported, in contrast, that MIL-53(Al) is hydrothermally stable,¹²⁹ although after closer inspection a reduction in pore volume and XRD reflections belonging to the γ-Al(OH)-phase¹²⁸ can be also observed, albeit only after 3 days.¹²⁹ As MIL-53(Al) was synthesized under different conditions, the rate of degradation might be due to differences in material quality.

Attempts have been made by researchers to enhance the water stability of MOFs, mostly by influencing kinetic factors. By preventing water molecules from entering the pores of the MOF entirely (“pore hydrophobicity”¹⁰⁰) or by hindering water molecules to cluster around the inorganic cluster (“internal hydrophobicity”¹⁰⁰), thermodynamically unstable clusters can be made stable from a kinetic perspective.

Interesting developments regarding external or pore hydrophobicity of MOF materials have been developed recently, by creating in one way or another an exterior layer impermeable to water.^{130–138} These approaches have indeed significantly increased the lifetime of the targeted MOF to ambient moisture by using the shielding exterior layer to prevent water from entering the structure entirely. Although exterior shielding in a hydrophobic matrix can potentially be extremely beneficial for using water-unstable (or hydrophilic) MOFs for, for example, gas separation in mixed matrix membranes,^{139–146} this approach obviously fails to be of use in AHP/ACs, as all

water is banned from the porous structure entirely and negligible adsorption may occur, rendering the material useless (for water as working fluid).

Interpenetrated growth of crystals, or catenation, can also result in an increased inherent water stability of MOFs, as was demonstrated for MOF-508 (Zn(BDC)(BPY)_{0.5}).¹⁴⁷ Uncatenated MOF-508, even with decorated methyl-groups, loses almost all porosity, while 2-fold interpenetrated MOF-508, without any water repellent functional groups, retains full adsorption capacity after exposure to water.¹⁴⁷ The increased stability is attributed to a higher thermodynamic stability of catenated structures and a significantly reduced water adsorption capacity.¹⁴⁷

The road most often traveled to increase hydrothermal stability is by ligand functionalization. Here, the focus again lies on making the material more hydrophobic, by utilizing organic ligands with water-repellent functionalities during MOF synthesis.^{110,135,148–169} Postfunctionalization of MOFs,^{170–173} a powerful technique to overcome the limitations of “isoreticular” synthesis in creating new MOF materials,¹⁷⁴ has been applied less frequently.^{125,175–178} Unfortunately, the downside of these two approaches is that the majority of the materials that have undergone this functionalization no longer adsorb appreciable amounts of water, as was the case for exterior shielding. Interestingly though, there are MOFs with repellent functions that nevertheless retain water adsorption after modification.^{110,148,152,156,157}

A somewhat paradoxical method to increase hydrothermal stability is the introduction of hydrophilic amine groups, as was shown for MOF-5(Zn)-NH₂ (IRMOF-3).^{73,179} The increase in stability was reasoned to be due to hydrogen-bonding interactions between hydrogen of the amine and oxygen of adjacent carboxylates.¹⁸⁰ Another reason is thought to be the creation of alternative adsorption sites on the organic ligand, which can reduce the water concentration at the inorganic cluster.¹⁸¹

A more suitable approach to enhance stability might be the (partial) exchange of metal-ions. For example, interchanging all Zn with Be in the M₄O-core of IRMOFs makes the material much more tolerant toward water, due to an increase in the activation energy barrier for hydrolysis.^{182,183} Partial ion substitution (doping)¹⁸⁴ of MOF-5(Zn) with Ni increases the water tolerance of the parent structure as well.^{185,186}

In conclusion, Burtch et al. identified the qualitative stability of over 200 structures,¹⁰⁰ of which roughly 10% exert thermodynamic stability, 60% high kinetic stability, 20% low kinetic stability, and 10% instability toward water. Currently, however, there are more than 20 000 MOF structures known,¹⁰⁰ of which the majority is based on bivalent metal ions. Although for most of these structures, information on hydrothermal stability is scarce, these have in general (hydrothermal) stability issues.^{187,188} Thus, it is highly likely that the percentage of structures that are unstable to water far exceeds 10%. As summarized concisely (*vide supra*), there are pathways that may lead to stabilization of MOFs, but the majority of these aim at avoiding any water adsorption in the structure, making them useless for the application at hand.

To end with a positive note, there exist MOF structures that show sufficient water stability for application in AHP/ACs, and of which the adsorptive behavior will be assessed in the next section. Solvothermal stability for methanol and ethanol is seemingly thought to be less of an issue for MOFs¹⁸⁹ and is henceforth not investigated in such detail in academia. Studies

concerning MOF (in)stability toward ammonia are seldom conducted. Stability will thus be discussed alongside ammonia adsorption (section 4.4), as detailed insights on degradation mechanisms seem to be mostly limited to water.

4. ADSORPTIVE PROPERTIES

In this section, a comprehensive overview of different MOF structures and their water, methanol, ethanol, and ammonia adsorption behavior is listed in Tables 1–4, respectively. For each of the individual structures, the parameter α is indicated, defined by Canivet et al.⁷⁷ as the relative pressure at which one-half of the structure is filled with a working fluid of choice. This indicator may help in differentiating materials with uptake inside and outside of the operating window. For water as adsorptive, $\alpha < 0.05$ indicates that a material would be too hydrophilic, whereas for $\alpha > 0.45$ a material is too hydrophobic. The α -value by Canivet et al.⁷⁷ is thus used to distinguish between hydrophobicity and hydrophilicity instead of the quantitative Weitkamp hydrophobicity index,¹⁹⁰ which has been employed for a variety of adsorbents.^{191–195} This as the former is more easily related to the application at hand, and the latter is more difficult to determine as it comprises measuring the coadsorption of water and toluene (or methylcyclohexane). The drawback of the chosen method is that α changes as a function of temperature (see eq 21) and should thus preferably be measured at or close to room temperature.

Furthermore, the maximum uptake of the working fluid, q_{\max} (per unit mass), listed in Tables 1–4, is invaluable for an initial assessment of feasibility. Although, for application, it is preferred to compare materials based on capacity per unit volume (section 6.5), q_{\max} does not require information on material density and is thus more easily determined. As the benchmark materials display, for water, $0.2 < q_{\max} < 0.3 \text{ g g}^{-1}$ (Figure 4) and has generally speaking a higher (crystallographic) density than MOFs (Table 6), as MOFs displaying $q_{\max} < 0.2 \text{ g g}^{-1}$ can already be deemed unsatisfactory for application.

These tables are further supplemented with the enthalpy of adsorption, $\Delta_{\text{ads}}H$, the pore volume based on N_2 adsorption, V_p , and remarks about material stability, indicated when available. In the case of water, for publications that contain no clear indication about hydro(thermal) stability, the classification of Burtch et al. has been used where possible.¹⁰⁰ The specific surface areas (BET) of these materials are ignored, because without the actual conditions used to determine these, and they are often omitted in practice, surface areas are by no means a proper indicator/comparator.¹⁰¹ The main findings from the literature will be discussed individually. For water (Table 1), tri- and tetravalent MOFs are subdivided into existing cluster configurations and discussed first, followed by bivalent zeolite-imidazolate frameworks (ZIFs) and pillared MOFs and the presumably less stable remaining bivalent Zn- and Cu-based MOFs, whereafter a set of miscellaneous structures is listed. For the remaining adsorptives, this subdivision is not explicitly made due to significantly less availability of literature.

4.1. Water Adsorption (Table 1)

Mesoporous MIL-101(Cr)¹⁹⁶ has received significant attention for application in heat pumps in the literature (confer Table 1), due to its robustness and high capacity. Indeed up to $1.6 \text{ g}_{\text{H}_2\text{O}} \text{ g}^{-1}$ can be adsorbed in MIL-101.¹⁹⁷ Unfortunately, a significant fraction of this loading is achieved at $p/p_o > 0.4$, which

decreases the material's applicability in AHP/ACs. Because of the large pore sizes of MIL-101(2.9, 3.4 nm), capillary condensation occurs at these undesirably high relative pressures, resulting in an undesired desorption hysteresis. By functionalizing (part of) the organic ligands, one can make the internal surface more hydrophilic. The addition of NO_2^{+} ,^{77,198,199} NH_2^- ,^{77,198,199} or SO_3H -groups¹⁹⁸ to MIL-101(Cr) shifts the step in adsorption to lower p/p_o , where α is highest for unfunctionalized MIL-101(Cr) and lowest for MIL-101(Cr)-SO₃H. For the amino- and nitro-functionalized MOFs, the location of the step in desorption is hardly altered. As reasoned by Canivet et al., because of the presence of hydrophilic groups, more water molecules adsorb before capillary condensation occurs, effectively reducing the actual volume to be filled during condensation and thus reducing the p/p_o required for this condensation.⁷⁷ During desorption, however, the filled volumes are very similar, resulting in desorption occurring at similar p/p_o for all functionalized and unfunctionalized materials. For MIL-101(Cr)-SO₃H, the hysteretic difference in p/p_o between the ad- and desorption branch is significantly enhanced, because water is more difficult to remove due to the strong interaction of the sulfonic groups with water. Subsequently, for adequate desorption, lower p/p_o and thus higher desorption temperature are required as compared to the other MIL-101(Cr)-based materials, highly undesired for AHP/ACs.

MIL-100(Cr),²⁰⁰ containing the same inorganic cluster as MIL-101(Cr) but trimesic acid instead of terephthalic acid as linker, contains smaller mesoporous cages (2.5, 2.9 nm) than MIL-101(Cr). These smaller cages make that the step in adsorption is beneficially shifted to lower p/p_o ($\alpha \approx 0.3$ –0.35,^{201,202} where $\alpha > 0.4$ for MIL-101), while retaining a large water capacity (up to $0.8 \text{ g}_{\text{H}_2\text{O}} \text{ g}^{-1}$).²⁰¹ Attempts to decorate MIL-100(Cr) with hydrophilic moieties have been directed toward modification of the chromium–oxide cluster via grafting with organic components²⁰² or counterion-replacement²⁰¹ and replacement of chromium with other metals.⁴⁰ Grafting the cussites in MIL-100(Cr) with either (mono, di, and tri)ethylene glycols or ethylene diamine results in a negligible decrease of α .²⁰² However, replacing fluoride-counterions with sulfate does result in an appreciable decrease in p/p_o required for adsorption ($\alpha \approx 0.25$).²⁰¹ The effect of changing from chromium to either iron or aluminum does not seem to have a clear effect on adsorption behavior (confer Figure 5).

The fact that the metal in the inorganic cluster is of little importance in these large mesoporous cavities is in line with the capillary condensation mechanism, driven by water–water interactions.⁸⁰ Both MIL-100 and MIL-101 show high water uptake capacities and decent stability (Table 1), but most of the uptake occurs at high p/p_o , limiting the applicability to small temperature lifts (section 6.5.3).

Another MOF investigated for application in adsorption-driven transformation of heat is titanium(IV)-based micro-porous MIL-125(Ti)-NH₂.²⁰⁴ Not only is the step in adsorption uptake beneficially shifted to lower p/p_o ,^{77,205} the amine-group makes the MOF more stable toward aqueous solutions,²⁰⁵ in a similar fashion as the increased stability of MOF-5 upon incorporation of amino-moieties.^{73,180} Although MIL-125(Ti)-NH₂ is thermally stable up to ~550 K, cycling between ad- (5.6 kPa H₂O, 40 °C) and desorption (5.6 kPa H₂O, 140 °C) results in a 17% decrease in maximum water loading after 40 cycles.²² As the stability of MOFs in contact with water vapor is a function of both vapor pressure and

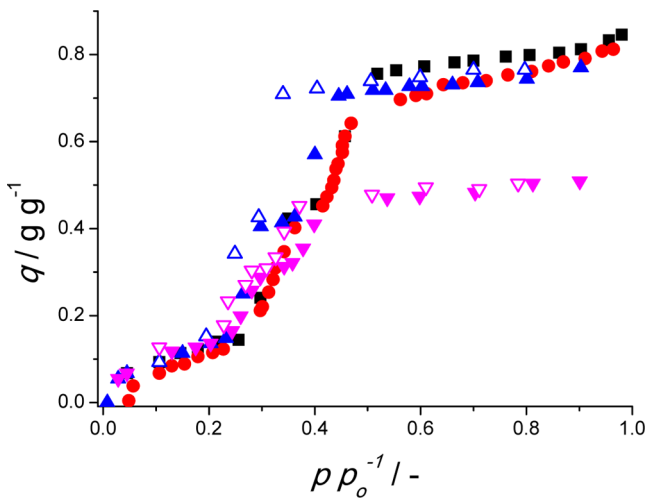


Figure 5. Adsorption isotherms for MIL-100(Fe) (blue ▲) and Al (pink ▼) materials measured at 298 K, including data from Küsgens et al. (Fe, ■)²⁰³ and Akiyama et al. (Cr, red ●).²⁰¹ Open symbols depict adsorption, while closed depict desorption. Remaining data from ref 56.

temperature,¹⁰² cycling thus between milder conditions might increase cyclic stability. On that note, given the stepwise isotherm of MIL-125(Ti)-NH₂, desorption could be operated at far lower temperatures (70–90 °C, depending on conditions). CAU-1(Al),²⁰⁶ which is isostructural to MIL-125(Ti)-NH₂ but contains μ_2 -methoxy-species instead of bridging μ_2 -oxygen, shows increased hydrophobicity, most likely due to these methoxy-species. The different postfunctionalization reactions performed on the amino-moiety increase the undesired hydrophobicity of this MOF further.

Zirconium(IV)-based UiO-66(Zr) and derivatives¹⁰⁶ have been explored for application in heat pumps.²² Of this series, especially UiO-66(Zr)-NH₂ shows interesting water adsorption behavior. As compared to MIL-125(Ti)-NH₂, cyclic stability is worse as the decrease in water capacity is significantly larger for UiO-66(Zr)-NH₂ (38% reduction in capacity over 40 cycles²²). This in contrast with previous findings, which claim that UiO-66(Zr)-NH₂ is stable when exposed to water vapor.^{104,105} The difference in stability might be due to elongated exposure to water vapor as compared to other procedures, or alternatively, due to defect chemistry. It has been demonstrated for UiO-66 and derivatives that, depending on synthesis conditions, the number of organic ligands connected to the inorganic cluster can be much lower than in a perfect crystal.^{85,207–209} More defects have a positive effect on adsorption capacity,²⁰⁷ decrease hydrophobicity,⁸⁵ but have an adverse effect on thermal stability.^{208,210} It is perfectly possible that these defects also have an adverse effect on the material's tolerance toward water, or that the thermal stability in defected UiO-66(Zr)-NH₂ is no longer sufficient. Dwelling on the latter, it has been demonstrated that the amino-group decreases the thermal stability of the UiO-66 structure.¹⁰⁴

De Coste et al. reported for UiO-67(Zr), isostructural to UiO-66(Zr) but with elongated BPDC-ligands, instability toward water vapor.¹⁰⁴ This decreased stability was claimed to be due to the torsional strain experienced in the crystalline structure of UiO-67(Zr), making it more susceptible to structural breakdown.¹⁰⁴ In a more recent publication, it was reported that the instability may be caused by surface-tension driven collapse of the structure during activation.²¹¹ When the

water present in UiO-67(Zr) is solvent-exchanged with acetone prior to thermal activation, the materials displayed no degradation.²¹¹ Others have erroneously claimed that the lower water capacity of UiO-67(Zr) as compared to UiO-66(Zr) is due to hydrophobic domains within the structure, devoid of water at saturation capacity.²² Defect chemistry is probably of less influence on UiO-67(Zr), as missing linker defects are not as frequently observed for this structure as for UiO-66(Zr).^{207,209} During cyclic operation in AHP/ACs, solvent-exchange is not an option, making UiO-67(Zr) not suitable for application (with water as adsorptive). Furukawa et al. investigated water adsorption and the stability of a set of novel MOFs incorporating the same Zr-cluster as in the UiO-series, connected by a variety of linkers,²¹² some of which show remarkable water uptake. As repeated isotherm measurements were performed separated only by brief intermediate evacuation at room temperature, no distinction can be made between intrinsic instability and strong binding of water to certain sites. For example, the authors found a strong decrease in adsorption capacity of water-stable zeolite 13X after the first cycle, because brief evacuation at room temperature is insufficient to desorb the strongly adsorbed water. This is especially relevant, as many of these novel MOFs have intrinsically a coordination number lower than 12, which means that they have coordinatively unsaturated sites, which might bind water strongly. Nonetheless, especially MOF-801(Zr) and MOF-841(Zr) show high reversibility of water adsorption with favorable S-shaped isotherms. This reversibility is also reflected in the moderate values reported for the isosteric heat of adsorption, making them excellent candidates for AHP/ACs, assuming that cyclic thermal regeneration of these materials does not cause degradation, as was the case for UiO-66(Zr) and UiO-67(Zr). Kaskel et al. reported a set of zirconium- and hafnium-based MOFs and investigated water uptake.^{107,213,214} DUT-52(Zr), DUT-53(Zr), DUT-67(Zr), and DUT-68(Zr) show interesting stepwise adsorption behavior.^{213,214} Unfortunately, for DUT-52(Zr) and DUT-53(Zr), the sorption hysteresis loop is not fully closed during desorption, losing a large part of the working capacity.²¹³ This is less of an issue for DUT-67(Zr) and DUT-68(Zr), which however have the steps in uptake at somewhat inconveniently high relative pressures ($\alpha \geq 0.35$), limiting the material to low temperature lift applications.²¹⁴ DUT-67(Hf) and DUT-68(Hf) have adsorption behavior nearly identical to that of their zirconium-counterparts.²¹⁴ The adsorption capacity, however, when expressed per unit mass of adsorbent, is lower as hafnium is a heavier element than zirconium. NU-1000(Zr) has the highest water adsorption capacity (on a weight basis) of all zirconium-based MOFs in Table 1, but the material is too hydrophobic ($\alpha = 0.75$).²¹⁵ Further, it collapses upon activation when water is present in the pores, as was the case for UiO-67(Zr).²¹¹ Using solvent-assisted ligand incorporation (SALI) post synthesis, hydrophobic organic molecules of varying length were added to unsaturated metal sites (SALI-n) to increase water-repellent behavior.²¹⁵ By adding instead hydrophilic chains, the material properties might be tuned toward application in AHP/ACs. The effect of these added ligands on the stability toward activation is unclear.

The MOFs discussed so far have in common that the inorganic cluster has a defined number of metal ions, resulting in a three-dimensional structure. There are, however, MOFs that contain polymeric metal–hydroxide or metal–oxide chains extending infinitely in one dimension. Of these, metal–

hydroxide containing MIL-53^{216,217} is arguably the most well-known, because of its reversible structural expansion upon adsorption of different guests. This effect, often referred to as “breathing”,²¹⁸ has the adverse effect that it often introduces undesired hysteretic behavior,^{77,219} despite being microporous ($d_p < D_c$ (2 nm)). The water capacity of MIL-53 and derived materials is disappointingly low and the step in uptake is at an unfeasibly high p/p_0 for AHP/ACs. Vanadium-based MIL-47,²²⁰ a rigid MOF with structure similar to that of MIL-53, is devoid of “breathing” effects and might be of interest, were it not that this structure is not stable when contacted with H_2O ¹¹⁷ and deteriorates even when decorated with fluorine-groups.²²¹

CAU-10(Al)-H,²²² another metal–hydroxide chain MOF, containing isophthalic acid and *cis*-connected AlO_6 -polyhedra that form helical chains, shows a very favorable steep uptake step at $p/p_0 = 0.18$ and a decent capacity of ~38 wt %.²²² Furthermore, the material is stable under repetitive water adsorption, has reasonably low heat of adsorption, and can be even grown directly on heat exchanger (aluminum) surfaces, making it an excellent candidate for AHP/ACs.^{223,224} Fröhlich et al. have shown that CAU-10(Al)-H does not lose any capacity over 700 adsorption cycles, showing its high stability.²²⁵ The resulting coating is stable during repetitive adsorption as well (at least 10 cycles with any loss of capacity).²²⁴ Decorating CAU-10(Al) with either hydrophilic or hydrophobic moieties introduces a significantly less favorable adsorption performance (Table 1). Replacing isophthalic acid with *trans*-1,4-cyclohexane-dicarboxylic acid (CAU-13(Al)) also yields a steep step in uptake albeit with low capacity (0.16 g g⁻¹).²²⁶ Al-fumarate, containing Al–OH chains and fumaric acid, also has a favorable isotherm for adsorption-driven reallocation of heat and cold.²²⁷ The isotherm is similar in shape and uptake to that of CAU-10(Al)-H, but the step occurs at slightly higher p/p_0 . Further, Jeremias et al. were able to grow this MOF on supports using the thermal gradient method.²²⁸ Unfortunately, the resulting material is not perfectly stable when exposed to repeated adsorption cycles, as a ~13% loss in capacity can be observed over the first 40 adsorption cycles.²²⁷ On the other hand, the coated material virtually did not show any further loss of capacity between 1500 and 4500 cycles, making the material still interesting for application.²²⁷

For MOF-74¹¹¹ (first named CPO-27²²⁹ or M/DOBDC²³⁰) materials, which can be synthesized with a variety of metal ions (Zn, Mg, Ni, or Co), water adsorption behavior is strikingly similar (for Mg, Ni, Co).^{212,230,231} Adsorption occurs primarily at very low p/p_0 , due to the irreversible adsorption of H_2O molecules on the cation-sites of the metal incorporated in the structure. The structure of MOF-74(Zn) was shown to collapse at 10% relative humidity (300 K), in line with the reported instability of many other zinc-based MOFs, as discussed previously. Dietzel et al., however, claim that the structure of Zn-based MOF-74 can be fully recovered upon dehydration.²²⁹ For MOF-74(Co), dehydration is fully reversible as well.²²⁹ Chmelik et al. showed for MOF-74(Co) that brief exposure to ambient (moist) air makes the material impermeable to any guest molecule.²³² Exposure to methanol can reverse this adverse effect.²³² The structural retention upon dehydration also holds for MOF-74(Ni). Although when oxygen is present, crystallinity is irreversibly lost, even at mild regeneration temperatures.²³³ The porosity of MOF-74(Mg) is lost irreversibly when exposed to humid air.¹⁰⁵ In any case though, high temperatures are required to desorb the water, explaining why Furukawa et al. observed a decrease in adsorption in

repeated cycles, employing only mild intermittent regeneration.²¹² The preceding again indicates that making conclusive remarks about hydrothermal stability is not always straightforward and paradoxical, or contradictory remarks may be reported in different sources.

Zeolitic imidazolate frameworks (ZIFs) are a subclass of MOFs known for excellent stability.²³⁴ ZIFs consist of imidazolate ligands that connect individual metal ions in a three-dimensional fashion. The inherent absence of metal–oxide or hydroxide groups on the inorganic cluster and the aromatic nature of imidazoles make that ZIFs are inherently hydrophobic without added functionality. Most notably, hydrophobic ZIF-8 can become increasingly hydrophilic by exchanging methyl-imidazolate ligands with methyl-triazolate ligands.²³⁵ After full ligand exchange, the material (named MAF-7) has favorable water adsorption characteristics for application in AHP/ACs, albeit that the hysteresis loop does not fully close anymore.²³⁵ As upon this functionalization only one carbon-atom in the aromatic ring of the ligand is replaced by a nitrogen-atom, no reduction in porosity and thus in adsorption capacity (based on volume) occurs, contrary to functionalization attempts performed for most dicarboxylic acid-based MOFs, where bulky functional groups often reduce the available volume for adsorption. In addition, MAF-7(Zn) has been successfully directly grown on structured zinc oxide, without the addition of any solvent, which is very beneficial for application.²³⁶ On top of that, these materials are relatively robust, as it takes multiple days to degrade these materials in boiling water.²³⁷

As mentioned, hydrothermally unstable MOFs can be modified to be more tolerant toward water (vapor). This has been demonstrated by the group of Walton in great detail for pillared MOFs.^{110,152,157,231,238} Pillared MOFs consist of metal-ions, so far all bivalent, linked together in two dimensions by one ligand and in the third dimension by a second ligand (pillars). A notable example is the DMOF²³⁹ (or DABCO-MOF) series. Without or with a variety of functional groups on the terephthalate moiety (NH₂⁻, Br⁻, Cl⁻, OH⁻, NO₂⁻, naphthyl⁻), the DMOF structure is irreversibly lost upon water adsorption.^{110,152,231} However, when all vacant positions on the terephthalic acid ligand are replaced with methyl-groups, the structure, named DMOF-TM2, is stable toward water for at least three adsorption cycles.¹¹⁰ Surprisingly, the material is not fully water repellent and adsorption of water in DMOF-TM2 contains a distinct step ($\alpha = 0.26$) with sufficient loading for application. The material becomes increasingly hydrophobic when including cobalt ($\alpha = 0.35$), nickel ($\alpha = 0.45$), or copper ($\alpha = 0.55$) ions.¹⁵⁷ Additionally, due to the flexible nature of these frameworks, there seem to be some hysteretic effects that are unfavorable for application.¹⁵⁷ Also, for other pillared MOFs, methylation may increase stability (see Table 1), but these materials are either too hydrophobic in nature or show low adsorption capacity.^{157,238}

Of all copper-based MOFs, Cu-BTC (or HKUST-1) shows highest water capacity.^{96,156,203,230,231} Unfortunately, Cu-BTC and likely other MOFs containing Cu-paddlewheel clusters are only moderately stable when subjected to water.^{156,230,231} One notable exception is Cu₂(dmcapz)₂, which seems to undergo a reversible structural transition upon water adsorption.²⁴⁰ Unfortunately, for application, the benefits of the stepwise adsorption branch are nullified by a strong, not fully closing, hysteresis loop, due to this structural transition.²⁴⁰

Table 2. MOFs Examined for Methanol Adsorption in Scientific Literature^a

material	ligand	α^b [-]	q_{\max}^c [g g ⁻¹]	$-\Delta_{\text{ads}}H$ [kJ mol ⁻¹]	V_p^c [cm ³ p g ⁻¹]	stability	ref
MIL-101(Cr)	TPA	0.25	1.15				189
MIL-53(Cr)	TPA	0.18	0.40	65–42 ^d			219
Al(OH)-(1,4-NDC)	1,4-NDC	0.05	0.16		0.22		270
ZIF-8(Zn)	mIm	0.15 ^e	0.34		0.63		272
ZIF-71(Zn)	dclm	0.25 ^e	0.27		0.39		272
ZIF-90(Zn)	Ica	0.07 ^e	0.29		0.49		272
ZIF-68(Zn)	nIm/bIm	0.25 ^f	0.28		0.44		292
MAF-4(ZIF-8)	mIm	0.18	0.40			stable in boiling methanol (7 days)	237
MAF-5(Zn)	eim	0.25	0.20			stable in boiling methanol (7 days)	237
MAF-7(Zn)	mTz	0.07	0.40			stable in boiling methanol (7 days)	237
Cu-BTC	BTC	0.05	0.60				189
Cu-BTC	BTC	0.01 ^f	0.55				96
Cu ₄ (ppmmd) ₂ (CH ₃ OH) ₄ (opd) ₂	ppmmd/opd	0.55	0.50				276
Cu ₂ (dmcapz) ₂	dmcapz	0.05	0.19		0.23	reversible structural change upon adsorption	240
Cu ₄ O(OH) ₂ (Me ₂ trzpb) ₄	Me ₂ trzpb	0.18	0.45		0.58		293
Cu ₂ (pzdc) ₂ (dpyg)	Pzdc/dpyg	0.30	0.11				294
MAF-2(Cu)	etz	0.05	0.16				295
Zn(BDC)(TED) _{0.5}	TPA/TED	0.15 ^g	0.50				94
Zn(BDC)(TED) _{0.5}	TPA/TED	0.14	0.50	60–41 ^h			290
Zn ₂ (BDC) ₂ (dabco)	BDC/dabco	0.01	0.21				291
Zn ₂ (NDC) ₂ (dabco)	1,4-NDC/dabco	<0.01	0.16				291
Zn ₅ O ₂ (bpdc) ₄	bpdc	0.10	0.15				296
ThrZnOAc	Thr	0.10	0.15				245
AlaZnOAc	Ala	0.15	0.12				245
ValZnOAc	Val	0.5	0.06				245
(H ₂ dab)[Zn ₂ (ox) ₃] ₃	ox/dab	0.35	0.32				278
Zn ₂ (bptc)	Bptc	<0.01	0.10		0.15		277
Zn(tbip)	Tbip	0.30	0.11		0.13		297
Co(pybz) ₂	pybz	0.05	0.23				298
CoDPE	DPE	0.50	0.11		0.14		286
Co ₃ (fa) ₆	FA	0.04 ^g	0.10		0.14		299
JUC-110(Cd)	THIPC	<0.01	0.06				282
Cd(4-btapa) ₂ (NO ₃) ₂	4-btapa	0.50	0.10				74
[Cd(L7) (DMF)]	L7	<0.01	0.11				285
Mn-formate	FA	0.08	0.14				300
([Ni(L6) ₂]·4H ₂ O) _n	L6	0.22	0.13			stable after 1 measurement	283
[Dy(ox) (Bpybc)(H ₂ O)]	Ox/Bpybc	0.80	0.10				287
([Eu(CAM) (HCAM) ₂ Mn ₂ (H ₂ O) ₄]) _n	(H)CAM	<0.01	0.26				301

^aMaximum capacity (q_{\max}), relative pressure for which capacity is 50% of q_{\max} (α), pore volume (V_p), enthalpy of adsorption ($\Delta_{\text{ads}}H$), and remarks about stability are included where possible. ^b p/p_0 for which $q = 0.5q_{\max}$ measured at 298 K unless otherwise mentioned. ^cBased on N₂ adsorption (at 77 K). Reported values are used where possible. Otherwise these are estimated from N₂ isotherms. ^dDetermined by microcalorimetry. ^eMeasured at 308 K. ^fMeasured at 323 K. ^gMeasured at 303 K. ^hIsosteric heat of adsorption, calculated with eq 22.

Zn-based MOFs often exhibit limited hydrothermal stability. There are, however, notable exceptions. Zn-trimesate, containing zinc-oxide clusters, shows an exceptionally high hydrothermal.²⁴¹ Even after 40 adsorption–desorption cycles, its water adsorption capacity, on itself somewhat low for application (20% wt), is retained.²⁴¹ MFU-4(Zn), containing a rare Zn₅Cl₄-based cluster, exhibits a peculiar linear water adsorption isotherm with a capacity of 0.55 g_{H₂O} g⁻¹ ($\alpha = 0.25$) and no loss in capacity after water adsorption.²⁴² Although a linear isotherm, as rare as it is, is better suited for application in AHP/ACs than Type-I isotherms, a stepwise isotherm is still preferred. Zn₄O(dmcapz)₃, which has the same cluster as water-unstable IRMOFs, shows sufficient adsorption capacity and remarkable water stability, due to the dmcapz-ligand.²⁴³

However, the material is too hydrophobic for application. Another method of increasing stability of MOFs with the Zn₄O-cluster is by fluorination of the organic ligand.²⁴⁴ Unfortunately, the reported Zn-based MOF is extremely hydrophobic ($\alpha = 0.9$), due to addition of these fluorine-groups.²⁴⁴ The amino-acid derived Zn-based MOFs reported by Kundu et al. were found to be stable as well,^{245,246} but also their adsorption characteristics are not very appealing for AHP/ACs.

ISE-1(Ni), arguably the first MOF specifically designed for application in AHP/ACs, has only a marginal water capacity (0.18 g g⁻¹) and is seemingly devoid of stepwise uptake.²⁴⁷ It is however stable upon repeated adsorption cycles.¹⁰² A set of isostructural Ni-based MOFs with increasing ligand length has

Table 3. MOFs Examined for Ethanol Adsorption in Scientific Literature^a

material	ligand	α^b [-]	q_{\max} [g g ⁻¹]	$-\Delta_{\text{ads}}H$ [kJ mol ⁻¹]	V_p^c [cm ³ g ⁻¹]	stability	ref
MIL-100(Cr)	BTC	0.1	0.6				302
MIL-100(Fe)	TPA	0.08	0.34		0.46		304
MIL-101(Cr)	TPA	0.18	1.1			stable over 20 ads. cycles	302
MIL-53(Cr)	TPA	0.18	0.36	70–48 ^d			219
UiO(bipy)	bipy	0.05 ^e	0.70		1.05	stable over 1 ads. cycle	303
ZIF-8(Zn)	mIm	0.07 ^f	0.28		0.63		272
ZIF-71(Zn)	dcIm	0.13 ^f	0.28		0.39		272
ZIF-90(Zn)	Ica	0.04 ^f	0.28		0.49		272
ZIF-68(Zn)	nIm/bIm	0.05 ^g	0.26		0.44		292
Cu-BTC	BTC	<0.01 ^g	0.57				96
MAF-2(Cu)	etz	0.05	0.25				295
Zn(BDC)(TED) _{0.5}	TPA/TED	0.09	0.4	66–41 ^h			290
(H ₂ dab)[Zn ₂ (ox) ₃]	ox/dab	0.45	0.26				278
Zn ₂ (BDC) ₂ (dabco)	BDC/dabco	0.01	0.33				291
Zn ₂ (NDC) ₂ (dabco)	1,4-NDC/dabco	<0.01	0.20				291
[Co(L) (DPE)]·0.5DPE	DPE				0.14		286
Co ₃ (fa) ₆	FA	<0.01 ⁱ	0.11		0.14		299
JUC-110(Cd)	THIPC						282
[Cd(L7) (DMF)]	L7	<0.01	0.06			stable in boiling ethanol, 1 day	285
([Ni(L6) ₂]·4H ₂ O) _n	L6	0.09	0.07			stable after 1 measurement	283
[Dy(ox) (Bpybc)(H ₂ O)]	Ox/Bpybc						287
([Eu(CAM) (HCAM) ₂ Mn ₂ (H ₂ O) ₄]) _n	(H)CAM	<0.01	0.26				301

^aMaximum capacity (q_{\max}), relative pressure for which capacity is 50% of q_{\max} (α), pore volume (V_p), enthalpy of adsorption ($\Delta_{\text{ads}}H$), and remarks about stability are included where possible. ^b p/p_0 for which $q = 0.5q_{\max}$ measured at 298 K unless otherwise mentioned. ^cBased on N₂ adsorption (at 77 K). Reported values are used where possible. Otherwise these are estimated from N₂ isotherms. ^dDetermined by microcalorimetry. ^eMeasured at 293 K. ^fMeasured at 308 K. ^gMeasured at 323 K. ^hIsosteric heat of adsorption, calculated with eq 22. ⁱMeasured at 303 K.

been reported by Padial et al.²⁴⁸ Unfortunately, this set of materials shows a clear trade-off between capacity and hydrophobicity, as the increase in capacity coincides with an increase in α . They are seemingly stable though, as was the case for ISE-1(Ni). The remaining MOFs in the miscellaneous section of Table 1 either are too hydrophobic or hydrophilic or show a low capacity.

As a general observation, for MOFs of which water adsorption is reported in multiple literature sources, both α and uptake capacity seem to vary. The latter is mostly due to variation in material quality. The former however can be caused by a variety of reasons; for example, measurements are conducted differently (static, under flow, etc.). In some isotherms, condensation effects start occurring already at $p/p_0 \approx 0.9$, implying that the p_0 value might be inaccurate. Furthermore, as water adsorption measurements are generally relatively time-consuming, there is a large fluctuation in the concentration of data points in reported isotherms, making that stepwise uptake is shown in various resolutions. Also, minor shifts in α are to be expected as a function of measurement temperature (eq 21). In addition, as indicated by Ghosh et al., also a shift in uptake might be observed due to defects.⁸⁵ One should take this into consideration when browsing through the different entries of the same structure in Table 1.

4.2. Methanol Adsorption (Table 2)

Not surprisingly, for MIL-101(Cr), one of the most reported MOFs in literature, methanol adsorption has been investigated.¹⁸⁹ The isotherm is nearly linear and the high saturation capacity is reached at $p/p_0 \approx 0.4$, making the material suitable for application in AHP/ACs.¹⁸⁹ MIL-53(Cr) shows a clear step in the desired relative pressure range.²¹⁹ Unfortunately, this step comprises only part of the (moderate) adsorption capacity.

Furthermore, the enthalpy of adsorption is relatively high as compared to the enthalpy of evaporation of methanol.

Both hydrophobic ZIF-8 and ZIF-71 and hydrophilic ZIF-91 show decent uptake of methanol in a narrow relative pressure range,²⁷² indicating that water adsorption is more sensitive to the interior decoration of the pore space than is the case for alcohols. By exchanging methyl-imidazolate ligands (ZIF-8 or MAF-4(Zn)) with methyl-triazolate ligands to form (MAF-7(Zn)), the step in adsorption can be tuned to lower relative pressures,²³⁷ as was shown for water adsorption.²³⁵

Cu-BTC displays a fair capacity for methanol, but adsorption occurs at low relative pressures, making regeneration energetically costly.⁹⁶ Cu₂(dmcapz)₂ shows a very favorable step in adsorption, making it potentially interesting for application.²⁴⁰ However, this steep adsorption step is due to a structural transition, and requires high temperatures to be reversed. Therefore, under isothermal conditions, hysteresis during desorption does not fully close. Cu₄O(OH)₂(Me₂trzpb)₄ also shows high methanol capacity but suffers from a large desorption hysteresis as well. DABCO (TED)-based MOF Zn(BDC)(TED)_{0.5}, notoriously unstable in the presence of water, shows a good uptake of methanol at relevant relative pressures and only has a mild hysteresis.²⁹⁰ Enthalpy of adsorption is in the same order of magnitude as MIL-53(Cr). The instability though might be the reason why others indicate inferior adsorption properties for seemingly the same compound.²⁹¹ Most of the remaining MOFs in Table 2 suffer from either unfavorable adsorption behavior or unsatisfactory capacity.

4.3. Ethanol Adsorption (Table 3)

MIL-101(Cr) shows adsorption behavior that can be described as the combination of two Type I isotherms, one at low and

Table 4. MOFs Examined for Ammonia Adsorption in Scientific Literature^a

material	ligand	α^b [-]	q_{\max}^c [g g ⁻¹]	$-\Delta_{\text{ads}}H$ [kJ mol ⁻¹]	V_p^d [cm ³ g ⁻¹]	stability	ref
UiO-66(Zr)-A	(NH ₂) _{0.67} ⁻ /(NH ₃ ⁺ Cl ⁻) _{0.33} ⁻ TPA	<0.01	0.10 ^d			stable/reversible adsorption	314
UiO-66(Zr)-B	(NH ₃ ⁺ Cl ⁻) _{0.30} ⁻ /(hma) _{0.50} ⁻ /(azi) _{0.20} ⁻ TPA	<0.01	0.11 ^d			stable/reversible adsorption	314
UiO-66(Zr)-C	(NH ₃ ⁺ Cl ⁻) _{0.33} ⁻ /(hma) _{0.11} ⁻ /(azi) _{0.56} ⁻ TPA	0.01	0.15 ^d			stable/reversible adsorption	314
UiO-66(Zr)-NH ₂	NH ₂ -TPA	— ^e	0.06 ^f		0.46		306
UiO-66(Zr)	TPA		0.03 ^g				315
UiO-66(Zr)-NH ₂	NH ₂ -TPA		0.06 ^g				315
UiO-66(Zr)-NO ₂	NO ₂ -TPA		0.03 ^g				315
UiO-66(Zr)-OH	OH-TPA		0.10 ^f				315
UiO-66(Zr)-(OH) ₂	(OH) ₂ -TPA		0.04 ^f				315
UiO-66(Zr)-SO ₃ H	SO ₃ H-TPA		0.04 ^f				315
UiO-66(Zr)-(COOH) ₂	(COOH) ₂ -TPA		0.05 ^f				315
DMOF(Zn)	TPA/DABCO		<0.01 ^g				315
DMOF(Zn)-A	ADC/DABCO		<0.01 ^g				315
DMOF(Zn)-TM2	TMBDC/DABCO		<0.01 ^g				315
Zn(BTTB)	BTTB		0.08 ^g				315
Cu(BTB)	BTB		0.04 ^g				315
MOF-74(Zn)	(OH) ₂ -TPA		0.09 ^h		0.39		308
MOF-74(Zn)	(OH) ₂ -TPA	— ^e	0.06 ^g		0.28		305
MOF-74(Ni)	(OH) ₂ -TPA	— ^e	0.04 ^g		0.31		305
MOF-74(Mg)	(OH) ₂ -TPA	— ^e	0.13 ^g		0.56		305
MOF-74(Co)	(OH) ₂ -TPA	— ^e	0.10 ^g		0.45		305
Cu-BTC	BTC	— ⁱ	0.11 ^d	85–65 ^j		strong loss in q_{\max} after 1 ads. cycle	311
MOF-199(Cu)	BTC		0.09 ^h		0.75		308
MOF-5(Zn)	TPA	<0.01	0.20 ^d		1.39	complete loss of porosity	309
MOF-5(Zn)	TPA		<0.01 ^h		1.22		308
MOF-177(Zn)	BTB	0.01	0.20 ^d		1.63	complete loss of porosity	309
MOF-177(Zn)	BTB		0.04 ^h		1.59		308
MOF-05(Zn)-OH	2,6-NDC-4,8-(OH) ₂ /BTB	<0.01	0.28 ^d		2.01	severe loss of crystallinity	310
DUT-6(Zn)	2,6-NDC/BTB	<0.01	0.21 ^d			severe loss of crystallinity	310
IRMOF-3(Zn)	NH ₂ -TPA		0.11 ^h		1.07		308
IRMOF-62(Zn)	dacba		0.02 ^h		0.99		308

^aMaximum capacity (q_{\max}), relative pressure for which capacity is 50% of q_{\max} (α), pore volume (V_p), enthalpy of adsorption ($\Delta_{\text{ads}}H$), and remarks about stability are included where possible. ^b p/p_0 for which $q = 0.5q_{\max}$, measured at 298 K unless noted otherwise. ^cBased on N₂ adsorption (at 77 K). Reported values are used where possible. Otherwise these are estimated from N₂ isotherms. ^dMeasured until $p/p_0 \approx 0.11$ ($p \approx 1.2$ bar). ^eMeasured at 293 K. ^fDynamic adsorption capacity determined from breakthrough experiments with 2000 mg m⁻³ NH₃ in inert carrier. ^gDynamic adsorption capacity determined from breakthrough experiments with ~1000 mg m⁻³ NH₃ in inert carrier. ^hDynamic adsorption capacity determined from breakthrough experiments with ~1% NH₃ in inert carrier. ⁱMeasured at 313 K. ^jIsosteric heat of adsorption, calculated with eq 22.

one at intermediate relative pressure, and an outstanding capacity.³⁰² Furthermore, it has been shown that for at least 20 adsorption/desorption cycles of ethanol, MIL-101(Cr) remains stable.³⁰² The Type I isotherm at low relative pressure unfortunately means that relatively high desorption temperature is required for full regeneration. MIL-100(Cr) shows uptake at lower relative pressures, at the expense of lower capacity.³⁰² Ethanol adsorption in MIL-53(Cr) shows very similar isotherm shape and step location, as was found for methanol.²¹⁹ As was the case for methanol, the enthalpy of adsorption for ethanol is somewhat high, as compared to the enthalpy of evaporation for this structure.²¹⁹ Bipyridyl-based UiO exhibits high ethanol capacity, albeit at a low relative pressure ($\alpha = 0.05$).³⁰³ The structure was deemed stable, as after ethanol adsorption and after soaking the material in water or methanol the structure does not show degradation in the X-ray diffraction pattern.³⁰³ This is in shear contrast with DeCoste et al., who reported that the bipyridyl-moiety makes

the resulting UiO-derivative unstable toward methanol exposure.¹⁰⁴

The aforementioned family of ZIFs showed a steep uptake at somewhat lower relative pressures than for methanol.²⁷² The same was found for ethanol adsorption in Cu-BTC,⁹⁶ but, like for methanol, the uptake is located at undesirably low relative pressures. Zn(BDC)(TED)_{0.5}, as was found for methanol, shows a step-like uptake of ethanol with a good capacity.²⁹⁰ Most of the remaining MOFs in Table 3 suffer from either unfavorable adsorption behavior or unsatisfactory capacity.

4.4. Ammonia Adsorption (Table 4)

The availability of ammonia adsorption data in the literature, see Table 4, is quite limited, and the research scope for this adsorptive is entirely different. Investigations are tailored toward the capture of toxic gaseous compounds,^{305–307} explaining why in many cases only (trace) ammonia adsorption capacities from breakthrough experiments, where NH₃ is diluted to concentrations down to 1000 mg m⁻³,^{305,306,308} are

presented. It is clear that, from these data, assessment for AHP/ACs would be difficult. MOF stability toward ammonia seems to be at least a similar issue as was found for water. All Zn_4O -cluster based MOFs under study seem to degrade completely upon contact with ammonia.^{309,310} Also, HKUST-1 seems to completely degrade during NH_3 adsorption.³¹¹ Although, according to Borfecchia et al., NH_3 adsorption on dry HKUST-1 only results in strong chemisorption of ammonia on Cu(II), distorting the framework, but without loss of crystallinity.³¹² Only in the simultaneous presence of water and ammonia should a strong detrimental effect on the structure be observed.³¹² In contrast, MIL-100(Fe) is more stable toward ammonia, as after breakthrough experiments with ammonia under dry or humid conditions, no significant loss in porosity can be observed from breakthrough experiments, employing MOF-carbon composites.³¹³ UiO-66(Zr), postfunctionalized with various combinations of exotic side groups, also seems to show reversible adsorption (up to $p/p_0 \approx 0.12$), indicated by the apparent closed hysteresis loop.³¹⁴ This actually indicates another issue with the assessment of ammonia for AHP/ACs. As many standard setups can only measure up to roughly 1.2 bar, yielding a relative pressure of ~ 0.12 at room temperature, only a small part of the ammonia isotherm is commonly reported. This is especially troublesome as the application window is $0.15 < p/p_0 < 0.55$ for ammonia (section 1). Therefore, the volume that could be filled with ammonia (liquid density of ammonia is $\sim 0.77 \text{ g mL}^{-1}$ at STP) is significantly smaller than the reported pore volume in all entries of Table 4. Therefore, in this study, ammonia is disregarded as potential working fluid, and future measurements should be conducted, for NH_3 -tolerant MOFs, at higher relative pressures (e.g., by decreasing measurement temperature).

5. MOF EVALUATION AND SELECTION

When regarding water as adsorptive, stability is more of an issue than for alcohols. Nonetheless, a vast amount of information on water adsorption in MOFs is available, and a lot of attention has been devoted to the development of MOFs for AHP/AC applications with water as working fluid (arguably the first being ISE-1(Ni) developed by Henninger et al.²⁴⁷). The interest is also reflected in a number of patent applications. Chang and co-workers were among the first to have patents granted for the application of MIL-100(Fe) and MIL-101(Fe) in AHP/ACs.^{316–320} Others have filed patents as well, although often specific structures are not targeted, but instead the aim is to cover a broad range of different possible structures.^{321–325} Not surprisingly, thus there are indeed MOFs that have been shown to be (relatively) stable under cyclic water adsorption. In order of increasing stability, these are Al-fumarate,²²⁷ MIL-100(Fe),⁴⁰ MIL-101(Cr),²⁵⁰ and CAU-10(Al)-H.²²⁵ It is noted here that of these MOFs both Al-fumarate and MIL-100(Fe) are commercialized by BASF and Sigma-Aldrich and are produced on a large scale already.^{326–328} In addition, there are MOFs that, at least, have not been shown to be unstable under several adsorption cycles. Of these, DMOF-TM2(Zn),¹¹⁰ MOF-801(Zr),²¹² and MOF-841(Zr)²¹² have interesting adsorption behavior. The former, due to the absence of information on enthalpy of adsorption, will not be considered further in section 6 of this work. The latter two, MOF-801(Zr) and MOF-841(Zr), comprise the same Zr-cluster as UiO-66²¹² that was demonstrated to degrade under cyclic operations.²² Whether this might also hold for MOF-801(Zr) and MOF-841(Zr), which contain the same cluster, is unclear, and for the

time being, these structures are assumed stable for the further purposes of this work. Adsorption isotherms of these interesting materials, selected for the performance assessment in section 6, are shown in Figure 6.

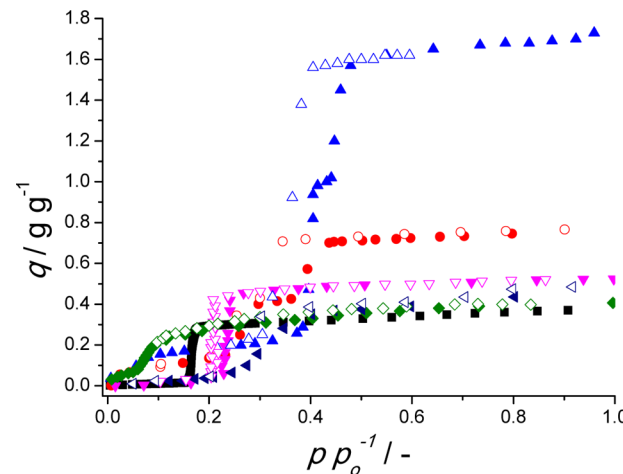


Figure 6. Water adsorption isotherms (298 K) for CAU-10(Al)-H (■), MIL-100(Fe) (red ●), MIL-101(Cr) (blue ▲), Al-fumarate (purple left-facing ▲), MOF-841(Zr) (pink ▼), and MOF-801(Zr) (green ◆). From own exp.²²³ and lit. sources.^{40,80,212,227}

Methanol (Table 2) or ethanol (Table 3) adsorption in MOFs, when compared to that of water, is far less reported. Where for previous generations of MOFs, methanol was the polar adsorptive of choice, in more recent works water seems to be preferred. This pivot in adsorption, loosely coinciding with the highly appreciated work of Küsgens et al. in 2009,²⁰³ makes that for a few MOF structures, the adsorption behavior is analyzed of both working fluids. Furthermore, information on stability is limited, and will be assumed less of an issue than for water or ammonia. Two structures were found to have at least moderate suitability for application in AHP/ACs when alcohols are employed as working fluid, MIL-53(Cr)²¹⁹ and Zn(BDC)-(TED)_{0.5},²⁹⁰ for both of which the adsorption enthalpy was reported as a function of loading. The latter is a must for detailed performance characterization (section 6.4). The seemingly most favorable isotherm for methanol is that of ZIF-71(Zn), although no information about adsorption enthalpy or desorption hysteresis could be retrieved.²⁷² The isotherms of these materials, selected for the performance assessment in section 6, are shown in Figure 7.

Both MIL-53(Cr) and Zn(BDC)(TED)_{0.5} show undesirable hysteresis, unexpected on the basis of pore size alone. As can be seen from Table 5, the critical diameter is significantly higher than the pore sizes of these materials.

This is likely caused by the flexibility of these frameworks. It is often observed that “breathing” behavior induced by adsorption of various guest molecules coincides with hysteresis in microporous materials,^{329–359} unexpected on the basis of pore size alone. For most materials, of which alcohol and water adsorption is known, α decreases for adsorptives in the order of water > methanol > ethanol, in line with increased size, and thus confinement effect, when strong flexibility effects and enhanced hydrophobicity are absent. Compare, for example, the locations of the step in uptake for water, methanol, and ethanol of MIL-100(Cr) ($\alpha = 0.45–0.48$, $\alpha = 0.25$, and $\alpha = 0.18$, respectively). This means that for alcohols, MOFs with

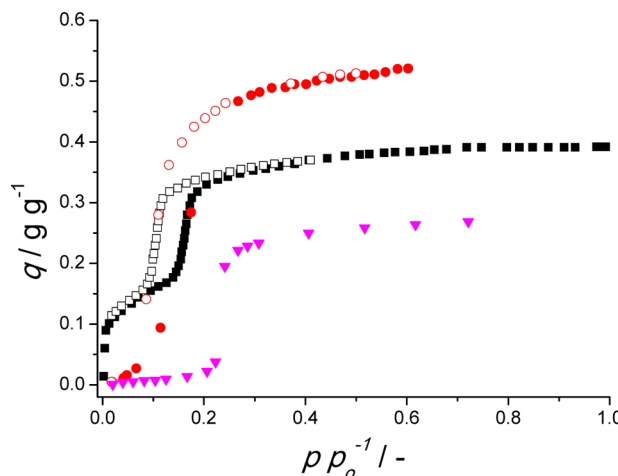


Figure 7. Methanol adsorption isotherms for MIL-53(Cr) (■), Zn(BDC) (TED)_{0.5} (red ●), and ZIF-71(Zn) (pink ▼). From lit. sources.^{219,272,290}

Table 5. Molecule Size, Sigma, Critical Temperature, and Critical Diameter (at 298 K) of Working Fluids, Calculated According to Equation 1

vapor	σ/nm	T_c/K^{35}	D_c/nm
water	0.28	647.1	2.1
methanol	0.36	512.6	3.5
ethanol	0.45	513.9	4.3
ammonia	0.29	405.7	4.4

larger pore sizes could be used than for water. MIL-101, which has a large portion of uptake for water at an undesirably high α , has the uptake of methanol almost completely at $\alpha < 0.3$. Advantageously, and in line with values for D_c (Table 5), there

is no notable hysteresis loop for methanol in MIL-101(Cr). Unfortunately, due to the lower polarity of methanol, the shape of the initial part of the isotherm ($\alpha < 0.1$) has become IUPAC Type I,^{360,361} where for water this part ($\alpha < 0.3$) was more like Type III/V.^{360,361} This means that either a high desorption temperature should be exerted for full regeneration, or the working capacity will be lowered as compared to the adsorption capacity. The number of viable MOF–alcohol working pairs is low in comparison to water-based working pairs, for which there are interesting candidates available already. However, the feasibility to employ larger pore sizes without introducing hysteresis and the decreased issues with stability can trigger further investigation. For the time being, however, the current assessment is somewhat limited due to the lack of information on uptake behavior and adsorption enthalpies. The reader is reminded last that, for ammonia adsorption, no suitable candidates were found at all.

6. PERFORMANCE ASSESSMENT

MOFs with suitable adsorption characteristics and devoid of instability issues were identified in previous sections. In the following sections, MOF performance will be compared to selected benchmark materials to further elucidate the possible benefits of using MOFs for the application at hand. To do so, a more detailed understanding of an ideal heat pump cycle is required (section 6.2). On the basis of this cycle, the governing equations of the thermodynamic model can subsequently be described (section 6.3). This model requires some thermodynamic properties as input. Their determination and/or estimation is briefly mentioned (section 6.4), followed by a detailed discussion of the results (section 6.5).

6.1. Selected Working Pairs

The MOFs that show promise for application in adsorption-driven allocation of heat and cold are listed in Table 6. Of these

Table 6. Selected MOFs and Benchmark Materials for Performance Assessment in Section 6 of This Review^a

material	pore structure	$d_{\text{window}}/\text{\AA}^b$	$d_{\text{pore}}/\text{\AA}^b$	$\rho_c/\text{g mL}^{-1c}$	$\langle -\Delta_{\text{ads}}H \rangle / \text{kJ mol}^{-1d}$	$W_{\text{sat}}/\text{mL mL}^{-1e}$	ref
MOFs							
CAU-10(Al)-H	1-D	5.6		1.15	53.5	0.43	212,222,223
MIL-101(Cr)	3-D	12, 15	27, 34	0.48	45.5	0.82	80,196,370
MIL-100(Fe)	3-D	5, 9	24, 29	0.72	50.6	0.55	40,200
Al-fumarate	1-D			1.24	42.8 ^f	0.59	227,371
MOF-841(Zr)	3-D	9.2	13.3	1.05	50.4	0.55	212
MOF-801(Zr)	3-D	4.8, 5.6, 7.4	8	1.59	58.4	0.63	212
MIL-53(Cr)	1-D, flexible	7–13		1.50 ^{np} –1.14 ^{lp}	51.5 ^{MeOH}	0.56 ^{lp}	77,219
Zn(BDC)(DABCO) _{0.5}	3-D, flexible	3.2, 4.8, 7.5 ^{lp}	3.2, 4.8, 7.5 ^{lp}	1.42 ^{np} –1.35 ^{lp}	42.8 ^{MeOH}	0.89 ^{lp}	290,372
Benchmarks							
AQSOA-Z01	1-D	7.4	8.3	1.75 ^g	56.1	0.42	373,374
AQSOA-Z02	3-D	3.7	7.4	1.43	57.0	0.45	373,375
AQSOA-Z05	1-D	7.4	8.3	1.75	52.6	0.39	373,374
silica gel	3-D, irregular			0.72 ^{bd}	55.7	0.22 ^{bd}	362
activated carbon	3-D, irregular	<6, 8, 12 ^{N2}		2.17 rd	43.0 ^{MeOH}	1.05 rd	364,365

^aPore structure, window and pore size, crystal density, loading averaged enthalpy of adsorption, and saturation volume adsorbed, per volume of adsorbent, are indicated where meaningful. ^bAs reported, unless noted otherwise. ^cCrystal density, determined from crystallographic structure, unless noted otherwise. ^dAverage enthalpy of adsorption, as calculated with eq 24, over the loading range for which the enthalpy (or else isosteric heat) of adsorption is determined. Value is for water as adsorptive, unless noted otherwise. ^eSaturation capacity (in g g⁻¹) is converted using the crystal density of the material, where possible, and liquid density of the working fluid. ^fThe reported isosteric heat of adsorption at higher loadings²²⁷ becomes lower than the evaporation enthalpy of water, yielding this unphysically low average. ^gAQSOA-Z01 is a partially Fe-exchanged AlPO₄-S material. However, the fraction of iron is not accurately reported and is thus neglected in the density calculations. bd is the bulk density. rd is the real density. np is the narrow pore configuration. lp is the large pore configuration. N₂ was derived from the pore-size distribution of the N₂ physisorption isotherm (at 77 K).

materials, pore and window size and crystallographic density are indicated when known. Most MOFs are combined with water as working fluid. Only MIL-53(Cr) and Zn(BDC)-(DABCO)_{0.5} are suitable candidates when methanol is employed. The list is completed with selected or benchmark materials.

For water as working fluid, these are commercially applied AQSOA-Z01⁴⁶ and -Z05,⁴⁵ both AlPO₄-S-based zeotypes (Z01 is partially iron-exchanged) with the AFI-structure, AQSOA-Z02, based on the SAPO-34 zeotype (CHA-structure), and silica gel (Grade 40, Davidson).³⁶²

For methanol as working fluid, research in academia has focused primarily on various activated carbons.^{363–369} Here, G32-H has been selected as reference, as it shows a good working capacity under varying working conditions and has been properly characterized for AHP/ACs.³⁶⁴ These materials will be subjected in this section to a thorough thermodynamics-based comparison to critically assess the feasibility of MOFs. In addition to the structural parameters in Table 6, the loading-averaged enthalpy change upon adsorption has also been listed, as this is a proper comparator for the adsorption energetics of different working pairs (eq 24), in addition to the volumetric saturation capacity (W_{sat}).

From Table 6, it can be concluded that the selected MOFs have a greater variety in pore sizes than the benchmark materials. Furthermore, in general, the average enthalpy of adsorption is lower for MOFs than for benchmark materials (for water). This is a primary indication that employing MOFs might energetically be more efficient as less energy is required for regeneration (desorption, section 6.3). Additionally, it appears that larger pore sizes lead to lower average enthalpies of adsorption for water as working fluid. This can be easily rationalized. For a larger pore size, there are larger voids within a structure. This in turn means that, on average, water molecules interact more with other water molecules than with the pore surface for these larger pores. This results in an enthalpy of adsorption that is closer to the evaporation enthalpy of water. Last, the crystallographic density of MOFs is lower than benchmark zeotypes, especially for large pore size structures. This is important in comparing different materials. It is customary to present adsorption capacities of porous materials per unit mass of material, but this results in a skewed evaluation, as the volume of material required to trap a certain amount of working fluid is a more important parameter. Hence, the crystallographic density is used to convert to amount adsorbed on a volumetric basis as has been done for the water isotherms of selected MOFs (Figure 6) in Figure 8.

Clearly, the adsorption capacities of interesting materials vary less in magnitude when compared per unit volume of material. We advocate here the latter basis of comparison (per unit volume), as the volume of adsorbent is important in determining the size of an AHP/AC. The main drawback of AHP/ACs traditionally is the comparably large size of these devices,³⁷⁶ and thus materials performing better per unit volume are thus highly desired. This includes household (domestic) or mobile applications, where space is only limited available. This is comparable to H₂ storage, for which the U.S. Department of Energy has formulated storage capacity targets per unit volume.^{377–379} This is especially relevant as MOFs and zeolites differ significantly in (crystallographic) density (see Table 6). In fact, one could argue that the bulk density of the material would be more appropriate to perform this conversion than the density of a (perfect) crystal. The bulk density, ρ_b ,

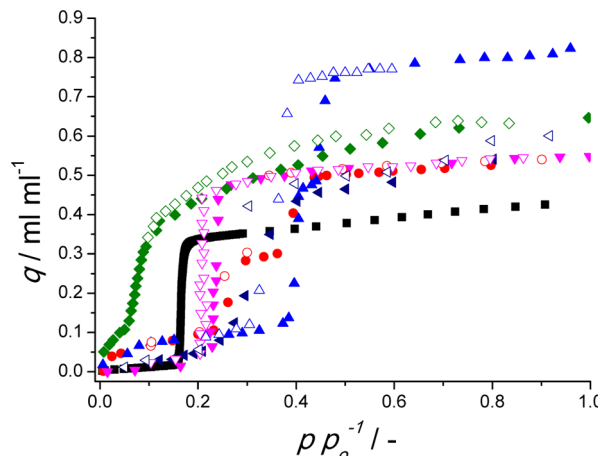


Figure 8. Adsorption isotherms for CAU-10(Al)-H (■), MIL-100(Fe) (red ●), MIL-101(Cr) (blue ▲), Al-fumarate (purple left-facing ▲), MOF-841(Zr) (pink ▼), and MOF-801(Zr) (green ◆) represented in mL of H₂O(liq) per mL of (dry) MOF. Liquid water and MOF crystal densities were used for the conversion from Figure 6.

depends on the bulk porosity, ε_b , of the sample under investigation:

$$\rho_b = \rho_c(1 - \varepsilon_b) \quad (2)$$

Note that in eq 2, it is tacitly assumed that the particle density (excluding extra-particle voids, ρ_p) is equal to that of the perfect crystal (ρ_c), which is adequate if the particles are sufficiently crystalline. Often, if not always, both the particle and the bulk density are omitted for the materials reported in section 4 of this Review. In addition, these measurements are almost exclusively performed on powder samples, of which bulk densities are likely to be different from materials applied in AHP/AC. Thus, even if the bulk density is known, the porosity is expected to be different than in actual application. With the above assumption, one could in principle estimate the bulk density with knowledge of ε_b (see eq 2). However, in actual devices, often either coatings or pellets are attached to heat exchanger surfaces and additionally when ε_b is decreased (i) bulk capacity is increased, (ii) mass transport is hampered, (iii) heat transfer is enhanced, and (iv) the actual cycle is less ideal.³⁸⁰ Thus, ε_b is both morphology-dependent and a possible tuning parameter for mass and heat transfer (which are not well-known for the MOFs discussed in this work), and it is thus very difficult to give this quantity a priori a representative value for AHP/ACs. Hence, it is clearly best to compare working capacities per volume of material ($\varepsilon_b = 0$) in the remainder of this work.

6.2. Heat Pump Cycle

An adsorption-driven heat pump cycle consists of four steps, two for adsorption and two for desorption. These steps are briefly explained with the aid of the cycle diagram (Figure 9).

In this diagram, the x-axis indeed is shown as $-1/T$, which is typically done in the literature^{30,52,381–385} to ensure both that the isosteric lines are straight (ln p versus $1/T$ ensures this) and that the lowest temperature is at the left end of the figure. Starting from a fully saturated adsorbent (point I), these four steps are consecutively.

Isosteric heating (I-II): The adsorbent is fully saturated (W_{max}) and requires regeneration or desorption of working fluid. Before working fluid can be released to the condenser,

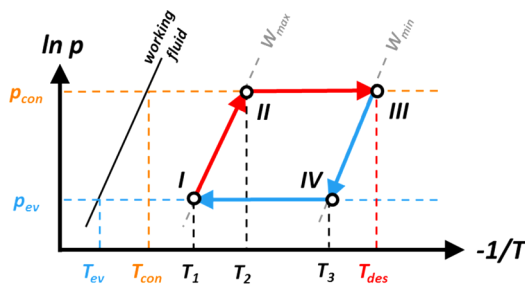


Figure 9. Isosteric cycle diagram of an adsorption heat pump cycle, including the vapor pressure of the chosen working fluid (black line), minimum and maximum isosteres, lines of equal loading, W_{\min} and W_{\max} (gray dashed lines), temperature and pressure of the evaporator (T_{ev} , p_{ev} , blue dashed lines) and condenser (T_{con} , p_{con} , orange dashed lines), desorption temperature (T_{des} , red dashed line), and intermediate cycle temperatures (T_1 , T_2 , and T_3 , black dashed line).

pressure needs to be increased from p_{ev} to p_{con} . This is realized by heating the adsorbent from T_1 to T_2 . During this stage, ideally, no working fluid is desorbed and the adsorbent vessel is disconnected from both the condenser and the evaporator.

Isobaric desorption (II–III): Adsorbent heating is continued. Because the adsorbent vessel is connected to the condenser in this stage, working fluid is allowed to desorb and no further pressure increase occurs. This process is stopped when desorption temperature (T_{des}) is reached and the adsorbent loading is minimal (W_{\min}). The desorbed working fluid ($W_{\max} - W_{\min}$) is condensed, releasing heat to the environment in the condenser (Q_{con} , Figure 1).

Isosteric cooling (III–IV): The adsorbent is regenerated and can be used for adsorption. However, first the pressure needs to be reduced to p_{ev} by cooling the vessel from T_{des} to T_3 , again isothermally and disconnected from condenser and evaporator.

Isobaric adsorption (IV–I): Cooling is continued. Because the adsorbent vessel is connected to the evaporator in this stage, working fluid is allowed to adsorb and no further pressure decrease occurs. This process is stopped when T_1 is reached and the adsorbent loading is maximal again (W_{\max}). The adsorbed working fluid ($W_{\max} - W_{\min}$) has taken up energy from the environment at a low temperature in the evaporator by its evaporation (Q_{ev} , Figure 1), while releasing heat in the adsorber at an intermediate temperature level upon adsorption.

The energy required for trajectories I–II and II–III combined is the energy required for desorption (Q_{des} , Figure 1), while the energy released during trajectories III–IV and IV–I is equal to the adsorption energy (Q_{ads} , Figure 1). For practical reasons, in most cases it is chosen to equate T_1 , often called (minimum) temperature of adsorption (T_{ads}), to the condenser temperature, T_{con} .^{52,386} The remaining temperatures and pressures used in this cycle cannot be all independently chosen. The condenser and evaporator pressure are inherently linked to their respective temperatures by the vapor–liquid equilibrium of the selected working fluid. For a given working pair, T_2 is related to T_{con} via the maximum loading isostere (W_{\max}). This means that, for a given working pair, T_2 is fixed by choosing the condenser temperature (and pressure). T_3 and T_{des} are related through the minimum loading isostere (W_{\min}), and T_3 is fixed when the evaporator temperature is selected. In summary, for a given working pair, the operational conditions are fully fixed when evaporator, condenser, and (maximum) desorption temperature are chosen. Generally speaking, one

can use this cycle for two purposes, heating or cooling, as schematically indicated in Figure 10.

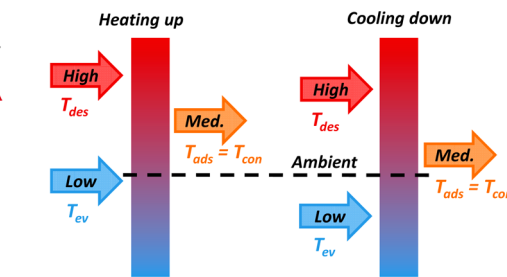


Figure 10. Modes of operation of a heat pump cycle. Heating (left) and cooling (right). Arrows indicate the flow of energy to or from the heat pump cycle (rectangle) at a high (red), medium (orange), or low (blue) temperature level. Dashed line indicates ambient temperature.

When using the cycle for heating, energy at a high temperature (used for regeneration of the sorbent) is transferred to an intermediate temperature (via condensation and adsorption). The energy taken up from the environment at ambient (low) temperature (required for evaporation) is also released at the intermediate temperature. The required energy at the ambient (low) temperature for evaporation can in principle be employed without effort, and this is the reason that a heat pump has a higher energy efficiency in transferring energy from high to medium temperatures than a simple heat exchanger.

For cooling purposes, the energy taken up by evaporation desirably occurs at a low temperature. This is why the temperature of the low level is subambient for cooling processes. The energy at high temperature, used for regeneration of the cycle, is used as input energy to generate this cooling effect. The energy rejected at the intermediate temperature level is not effectively used when cooling using this cycle. The temperatures at which the evaporator and condenser are operated depend on the actual application. The employed operational temperatures used to assess the performance of MOFs in comparison to selected benchmark materials, for different applications, are listed in Table 7 and are comparable to those used by others.^{52,55,364,381,382,385–387}

Table 7. Employed Operational Temperatures in This Work for the Four Different Applications Considered

	heat pump	refrig I	refrig II	ice making ^a
T_{ev}/K	288	283	278	268
T_{con}/K	318	303	303	298

^aWater cannot be employed as working fluid for ice making, due to freezing.

Heat pumps are considered here as a single application; cooling is subdivided into three different applications. Refrigeration (RF)-I could be used for air-conditioning purposes, whereas RF-II could be used for an actual refrigerator. Both are included (section 6.5) to highlight the effect of the minor differences in the evaporation temperature on material comparison. The desorption temperature can be independently varied to find an optimum between working capacity and energy efficiency, as will be discussed in detail (section 6.5). On a more critical note, one might argue that the evaporation temperature of the heat pump condition is at the

high end of the spectrum of commonly applied temperatures (270–288 K mostly). The choice for this somewhat high temperature (288 K) was made as most MOFs have an isotherm (Figure 6) with a step in adsorption such that the working capacity at lower temperatures will likely become negligible, as will become clear from the results (MOF-801(Zr) is the exception). This temperature however is by no means practically unfeasible.

6.3. Thermodynamic Model

Here, the necessary equations to describe the heat pump cycle from a thermodynamic perspective are presented, starting with the coefficient of performance (COP), which is the commonly adopted parameter to describe energetic efficiency.^{7,384,386} The COP is defined as the useful energy output divided by the energy required as input. For heating, this becomes

$$\text{COP}_H = \frac{-(Q_{\text{con}} + Q_{\text{ads}})}{Q_{\text{regen}}} \quad (3)$$

Here, Q_{con} is the energy released during condensation, and Q_{ads} the energy released during the adsorption stage; both have a negative value as energy is rejected from the adsorption cycle. Q_{regen} is the energy required for regeneration of adsorbent, a positive quantity as energy is added to the system. For cooling, the coefficient of performance becomes

$$\text{COP}_C = \frac{Q_{\text{ev}}}{Q_{\text{regen}}} \quad (4)$$

Here, Q_{ev} is the energy taken up in the evaporator. The energy taken up by the evaporator and released by the condenser can be calculated with knowledge of the enthalpy of evaporation, $\Delta_{\text{vap}}H$ (Figure 3), by respectively:

$$Q_{\text{ev}} = -\frac{\Delta_{\text{vap}}H(T_{\text{ev}})\rho_{\text{liq}}^{\text{wf}} m_{\text{sorbent}}\Delta W}{M_w} \quad (5)$$

$$Q_{\text{con}} = \frac{\Delta_{\text{vap}}H(T_{\text{con}})\rho_{\text{liq}}^{\text{wf}} m_{\text{sorbent}}\Delta W}{M_w} \quad (6)$$

Here, m_{sorbent} is the amount of adsorbent used in the adsorption cycle. From here, this quantity is omitted making that the quantities of energy, Q_i , are defined per unit of mass of the adsorbent used. ΔW is the working capacity, defined as the difference in working fluid between the maximum and minimum isosteres ($W_{\text{max}} - W_{\text{min}}$; see Figure 9). Note that because of the limited temperature difference between T_e and T_{con} , Q_{ev} and Q_{con} are almost equal in magnitude but opposite in sign.

The calculation of the energy required during the regeneration is more tedious as it comprises both isosteric heating (I-II) and isobaric desorption (II-III).³⁸⁶ The energy required for isosteric heating can be determined with³⁸⁶

$$Q_{\text{I-II}} = \int_{T_{\text{con}}}^{T_2} c_p^{\text{effective}}(T) dT + \int_{T_{\text{con}}}^{T_2} \rho_{\text{liq}}^{\text{wf}} W_{\text{max}} c_p^{\text{wf}}(T) dT \quad (7)$$

Here, c_p^{wf} is the heat capacity of the chosen working fluid and $c_p^{\text{effective}}$ is the effective heat capacity of the adsorbent (sorbent) and heat exchanger (hex). In fact, the heat exchanger area (~mass) can be increased to increase heat transfer, at the cost of thermodynamic efficiency, and can thus be an important

tuning parameter. As the heat and mass transport properties of MOFs are scarcely known to best of our knowledge, this tuning cannot be performed in reality. Hence, for a comparison based on intrinsic MOF properties, the mass of heat exchanger is assumed zero in the efficiency calculations, yielding thus for the bulk of this work:³⁸⁶

$$c_p^{\text{effective}}(T) = c_p^{\text{sorbent}}(T) \quad (8)$$

Note that the effect of heat exchanger mass on the effective heat capacity is envisaged in eq 25 and Figure 15. The energy required for isobaric desorption is determined with³⁸⁶

$$Q_{\text{II-III}} = \int_{T_2}^{T_{\text{des}}} c_p^{\text{effective}}(T) dT + \int_{T_2}^{T_{\text{des}}} \rho_{\text{liq}}^{\text{wf}} \frac{W_{\text{max}} + W_{\text{min}}}{2} c_p^{\text{wf}}(T) - Q_{\text{sorption}} \quad (9)$$

Q_{sorption} is the energy released during adsorption of the working fluid and can be calculated with

$$Q_{\text{sorption}} = \frac{1}{M_w} \int_{W_{\text{min}}}^{W_{\text{max}}} \rho_{\text{liq}}^{\text{wf}} \Delta_{\text{ads}}H(W) dW \quad (10)$$

Here, M_w is the molar mass of the working fluid and $\Delta_{\text{ads}}H$ the enthalpy of adsorption, which often has a significant dependence on loading (W). The estimation of $\Delta_{\text{ads}}H$ will be discussed in more detail later in this Review. Finally, combining the energy required for isosteric heating and isobaric desorption yields the total energy required for regeneration:

$$Q_{\text{regen}} = Q_{\text{I-II}} + Q_{\text{II-III}} \quad (11)$$

The energy gained during the adsorption stage is a combination of the energy gained during isosteric cooling ($Q_{\text{III-IV}}$) and isobaric adsorption ($Q_{\text{IV-I}}$):

$$Q_{\text{ads}} = Q_{\text{III-IV}} + Q_{\text{IV-I}} \quad (12)$$

The relation for the energy rejected during isosteric cooling is similar to that of isosteric heating (eq 7):

$$Q_{\text{III-IV}} = \int_{T_{\text{des}}}^{T_3} c_p^{\text{effective}}(T) dT + \int_{T_{\text{des}}}^{T_3} \rho_{\text{liq}}^{\text{wf}} W_{\text{max}} c_p^{\text{wf}}(T) dT \quad (13)$$

For isobaric adsorption, in line with eq 9, one could obtain

$$Q_{\text{IV-I}} = \int_{T_3}^{T_{\text{con}}} c_p^{\text{effective}}(T) dT + \int_{T_3}^{T_{\text{con}}} \rho_{\text{liq}}^{\text{wf}} \frac{W_{\text{max}} + W_{\text{min}}}{2} c_p^{\text{wf}}(T) + Q_{\text{sorption}} \quad (14)$$

One can observe from the above that the energy required for regeneration (Q_{regen}) will be very similar in magnitude to the energy gained during adsorption (Q_{sorption}). Furthermore, as the enthalpy of adsorption should physically be larger in absolute magnitude than the enthalpy of evaporation, Q_{con} will not be larger than Q_{sorption} . This means, for a single adsorption vessel, that

$$1 \leq \text{COP}_H \leq 2 \quad (15)$$

In fact, for $\text{COP}_H = 1$, there is no incentive to use a heat pump at all, and a simple heat exchanger should be utilized. Applying similar logic ($Q_{\text{ev}} \leq Q_{\text{regen}}$), one can conclude for cooling purposes that

$$\text{COP}_C \leq 1 \quad (16)$$

In fact, when using multiple adsorption beds, one could use parts of the energy released during adsorption of one bed for partial regeneration of another bed.^{52,386,388,389} Although this energy recovery might aid in exceeding the posed limits on the coefficient of performance (eqs 15,16) with proper design and operation, it is not taken into account in this work. This simply is because the extent of energy recovery between adsorbers is dependent on system design and can in principle be done for any working pair. Omission of any heat recovery is assumed not to modify the intrinsic material comparison aimed at in this work.

6.4. Thermodynamic Properties

The model, as presented (section 6.3) to describe the performance of a given working pair in an adsorption heat pump cycle, requires the knowledge of thermodynamic properties. First, for both working fluids (H_2O , CH_3OH), the enthalpy of evaporation and vapor pressure (see Figure 3) and heat capacity (Figure S1) are accurately known.³⁵

For the adsorbent, information on the heat capacity is also required (section 6.4.1). In addition, for each adsorbent-working fluid pair, information is needed on the loading dependence on both temperature and pressure. For this purpose, the concept of characteristic curves is conveniently adopted (section 6.4.2).^{289,386,390–392} Last, information on the enthalpy of adsorption as a function of loading is needed (section 6.4.3). The information required for the adsorbents and adsorbent-working fluid pairs is more tedious to obtain than is the case for pure fluid properties and requires proper explanation.

6.4.1. Adsorbent Heat Capacity. As highlighted above, the heat capacity of the adsorbent is necessary to assess the coefficient of performance in AHP/ACs. Mu and Walton investigated the heat capacity of MOFs in great detail in comparison with zeolites and other materials. Their results (Figure 11) indicate that for most of the materials under investigation, one could roughly state that³⁹³

$$0.6 \leq c_p^{\text{sorbent}} \leq 1.4 \left[\frac{J}{g K} \right] \quad (17)$$

Although the materials studied by Mu and Walton do not correspond with those selected in this work, their findings, which are largely in line with the heat capacities reported by Pirngruber et al.,²⁵⁵ serve as a proper indication for the unknown heat capacities. On the basis of these results, c_p^{sorbent} is assumed to be $1 J g^{-1} K^{-1}$ regardless of temperature, except for Al-fumarate ($c_p^{\text{sorbent}} \approx 1.1 J g^{-1} K^{-1}$)²²⁷ and activated carbon ($c_p^{\text{sorbent}} \approx 0.95 J g^{-1} K^{-1}$)³⁶⁴ for which the specific heat capacity is known. A small sensitivity analysis exercise can be performed, employing a simplified equation of the energy required for regeneration:

$$Q_{\text{regen}} \approx c_p^{\text{sorbent}} \Delta T - \frac{1}{M_w} \rho_{\text{liq}}^{\text{wf}} \langle \Delta_{\text{ads}} H \rangle \Delta W \quad (18)$$

With eq 18 one can estimate Q_{regen} for a heat capacity of 1.0 and $1.4 J K^{-1} g^{-1}$, as will be done for the conditions for which the influence of c_p^{sorbent} will be the highest. This means a temperature difference, ΔT , of 75 K, the largest used in the results (section 6.5), and a loading difference, ΔW , of $0.2 g g^{-1}$, the minimal value for which coefficients of performance are presented (Figure 14). Using the lowest, still physically sound,

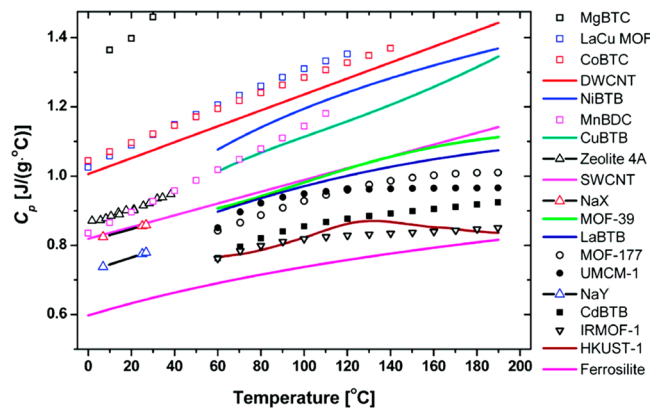


Figure 11. Specific heat capacity as a function of temperature for MOFs, coordination polymers, carbon nanotubes, zeolites, and minerals. Reprinted with permission from ref 393. Copyright 2011 American Chemical Society. Literature data included for MgBTC,³⁹⁴ LaCu MOF,³⁹⁵ CoBTC,³⁹⁶ DWCNT,³⁹⁷ MnBDC,³⁹⁸ Zeolite 4A,³⁹⁹ SWCNT,³⁹⁷ NaX,⁴⁰⁰ NaY,⁴⁰⁰ and Ferrosilite.⁴⁰¹

average adsorption enthalpy of the materials under investigation for water as working fluid ($-45.5 \text{ kJ mol}^{-1}$ for MIL-101(Cr), Table 6) indicates that a difference of $0.4 \text{ J g}^{-1} \text{ K}^{-1}$ in the used c_p^{sorbent} will result roughly only in a 5% change in Q_{regen} . For methanol, using the average adsorption enthalpy of $Zn(BDC)(DABCO)_{0.5}$ ($-42.8 \text{ kJ mol}^{-1}$, Table 6), the change in Q_{regen} will be roughly 8%. For larger adsorption enthalpies and loading differences and smaller temperature differences, these changes will become even less significant. Furthermore, the neglect of the influence of the working fluid heat capacity in eq 18 for simplicity reasons further indicates that the effect of c_p^{sorbent} on the magnitude of Q_{regen} and Q_{sorption} is exaggerated in this analysis and that thus employing a fixed sorbent heat capacity of $1.0 \text{ J g}^{-1} \text{ K}^{-1}$ for all adsorbents will not significantly affect the performance comparison of the different materials under investigation.

6.4.2. Characteristic Curve. The amount adsorbed in a porous material at equilibrium is a function of both pressure and temperature. Most often adsorption isotherms are measured for one or more given temperatures. These temperatures are frequently around room temperature (298 K), thus lower than, for example, the temperatures applied for desorption in AHP/ACs. This means that these isotherms, on which the data in sections 4 and 5 are based, cannot directly be used in the adopted model (section 6.3). To circumvent this, the concept of the characteristic curve is adopted.^{291,368,372–374} Central in this theory is the use of the Polanyi adsorption potential,^{402–404} which is the molar Gibbs free energy of adsorption with opposite sign, defined as

$$A = RT \ln \left(\frac{p_o(T)}{p} \right) \quad (19)$$

Here, p_o is the temperature-dependent vapor pressure of the adsorbate of choice. The amount adsorbed should be expressed as volume occupied by the adsorbed phase. As the density of the adsorbed phase is often not known, the liquid phase density is often used as an approximation:

$$W = \frac{q(p, T)}{\rho_{\text{liq}}^{\text{wf}}(T)} \quad (20)$$

Here, q is the mass adsorbed, W is the volume liquid adsorbed, and $\rho_{\text{liq}}^{\text{wf}}$ the liquid density of the same adsorbate. If a so-called temperature invariance of W is assumed, all measured adsorption data should collapse onto one single “characteristic curve”. In practice, this assumption can easily be verified by performing this transformation for more than one isotherm (or isobar). This results in the fact that for each amount of volume adsorbed, W , there is one value of the adsorption potential, A , and each $A-W$ combination corresponds to an isostere (e.g., W_{\max} and W_{\min} in Figure 9). Computationally, this means that each combination of pressure (p, T) can be converted to a single adsorption potential, A , for which the volume adsorbed W can be determined easily via interpolation of the characteristic curve. For a selection of MOFs and the AQSOA-series, this transformation has been performed, and the resulting curves are shown in Figure 12 (other samples in Figure S2).

Clearly, for the MOFs shown, Figure 12 (bottom), this “characteristic curve” concept works properly. The same can be said for AQSOA-Z05, Figure 12 (middle). However, for AQSOA-Z01 (Figure 12 (top)), even more for AQSOA-Z02 (Figure 12 (middle)), this concept does not perfectly hold. A clear shift in the curve toward lower adsorption potentials can be observed when temperature is increased. AQSOA-Z02, which is actually SAPO-34, displays a structural contraction upon water adsorption, reducing the unit cell volume roughly 2% at room temperature.³⁷⁵ This contraction might be different at the elevated temperatures encountered in Figure 12, which could make hydration less favorable.⁴⁰⁷

The fact that the volume adsorbed does not display temperature invariance as a function of adsorption potential makes that simple interpolation of the characteristic curve cannot be executed for AQSOA-Z01 and Z02. As for these materials isotherms are in fact measured at elevated temperatures (up to 373 K), the isotherms could in principle be used directly. To make the temperature span continuous, the isotherms are interpolated for these compounds. The details of this procedure and the effect this has on working capacity and coefficient of performance are displayed in Supporting Information S-3.

Last, as was hinted at in section 4 of this Review, the relative pressure to indicate the step in uptake, α , changes as a function of temperature of the isotherm. Using eq 19, one can derive an expression to exactly calculate the shift in α when comparing two isotherms at temperatures T_1 and T_2 , respectively, under the assumption of temperature invariance of W :

$$\alpha_2 = \alpha_1^{T_1/T_2} \quad (21)$$

Here, α_1 and α_2 are the relative pressures of the step in uptake for isotherms measured at respectively T_1 and T_2 . Clearly, this dependency of α on temperature should be considered when comparing results from different temperatures.

6.4.3. Enthalpy of Adsorption. For MIL-53(Cr) and MIL-101(Cr), $\Delta_{\text{ads}}H(W)$ is accurately known from calorimetric measurements. For the other structures, calorimetric data are not available, and thus the isosteric enthalpy of adsorption will be used. The isosteric enthalpy of adsorption can be calculated, from adsorption isotherms at two or more different temperatures, using⁴⁰⁸

$$\Delta_{\text{ads}}H_W = R \left(\frac{\partial \ln p}{\partial (1/T)} \right)_W \quad (22)$$

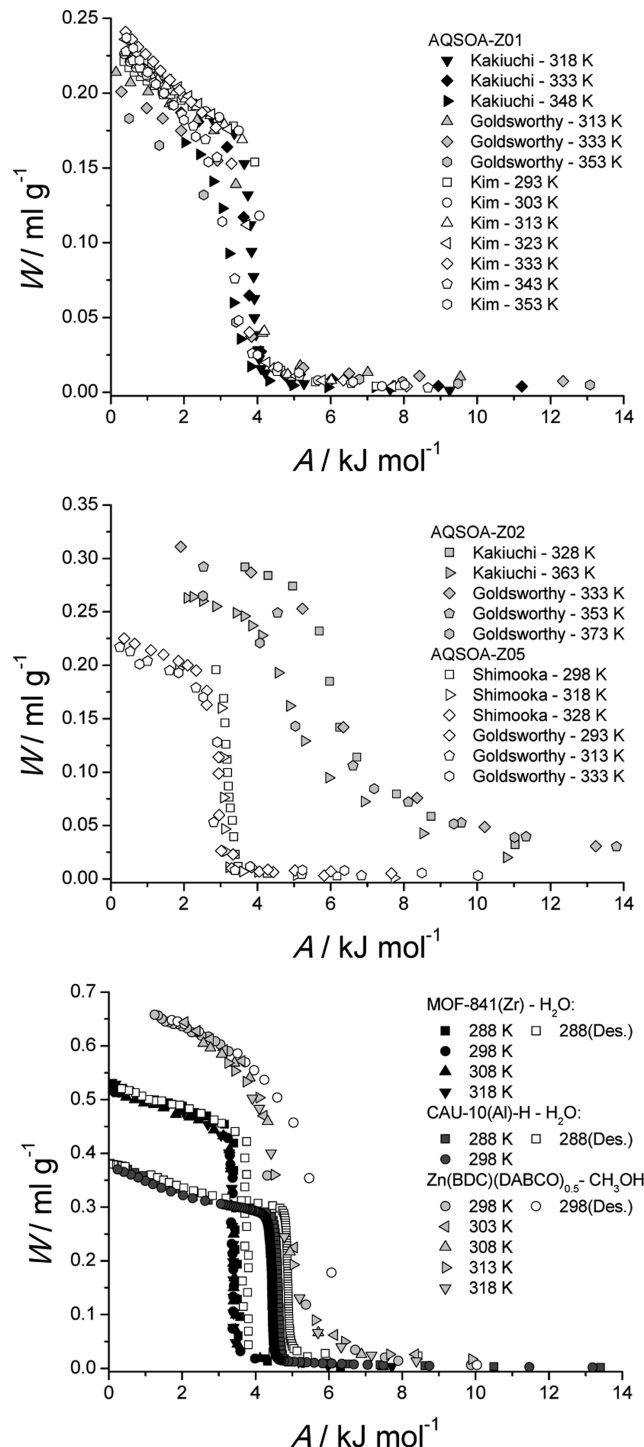


Figure 12. Characteristic curves determined using eqs 19 and 20, using adsorption isotherms from various literature sources, for AQSOA-Z01-water^{46,405,406} (top), AQSOA-Z02-water^{47,405} and AQSOA-Z05-water^{45,405} (middle), and MOF-841(Zr)-water,²¹² CAU-10(Al)-H, and Zn(BDC) (DABCO)_{0.5}-methanol²⁹⁰ (bottom).

Using this equation, it is (tacitly) assumed that adsorption is fully reversible (no chemisorption occurs), neither the internal energy of the adsorbent surface nor the adsorbent structure is altered during adsorption, and equilibrium is reached between adsorbent and adsorbate. The isosteric enthalpy of adsorption is reported alongside the isotherms at different temperatures for most adsorbents, while for others this quantity is calculated (all

are shown in the Supporting Information). It can be noticed that the maximum adsorbed volume for which $\Delta_{\text{ads}}H(W)$ is known, denoted by $W_{\max}^{\Delta H}$, is sometimes smaller than the adsorption capacity in the adsorbent (W_{\max}). In the case when $W_{\max} > W_{\max}^{\Delta H}$, it is assumed that the enthalpy of adsorption will become equal to that of evaporation, and eq 10 is expanded to include this phenomenon:

$$Q_{\text{sorption}} = \frac{\rho_{\text{liq}}^{\text{wf}}}{M_w} \int_{W_{\min}}^{W_{\max}^{\Delta H}} \Delta_{\text{ads}}H(W) \, dW + \frac{\rho_{\text{liq}}^{\text{wf}}}{M_w} (W_{\max} - W_{\max}^{\Delta H}) \Delta_{\text{vap}}H \quad (23)$$

The same can in principle be applied when $W_{\min} < W_{\min}^{\Delta H}$, although this situation occurred less frequently in this study. Last, the loading averaged enthalpy of adsorption, as reported in Table 6, is calculated using the full range of the enthalpy of adsorption as a function of adsorbed volume (from $W_{\min}^{\Delta H}$ to $W_{\max}^{\Delta H}$):

$$\langle \Delta_{\text{ads}}H \rangle = \frac{\int_{W_{\min}^{\Delta H}}^{W_{\max}^{\Delta H}} \Delta_{\text{ads}}H(W) \, dW}{W_{\max}^{\Delta H} - W_{\min}^{\Delta H}} \quad (24)$$

The loading-dependent enthalpy of adsorption, as used in this work, is shown for all materials under investigation in Figure S4.

6.5. Results and Discussion

The potential of selected MOFs for application in adsorption-driven heat pumps and chillers is assessed from a thermodynamic perspective, and compared to commercially used benchmark materials. First, the total energy storage capacity is compared (section 6.5.1), after which the performance is determined for different applications, using the operating conditions as specified in Table 7 (section 6.5.2). Additionally, the concept of temperature lift is used to further explain the potential of MOFs (section 6.5.3).

6.5.1. Capacity. From Table 6 it becomes clear that, per volume of material, most MOFs adsorb a larger volume of working fluid than commercially used sorbents (AQSOAs and silica gel). The activated carbon–methanol pair, however, even supersedes MOFs in volumetric working fluid adsorption, but one should note that the amount of energy for condensation or evaporation depends on the enthalpy of evaporation of the working fluid, which is obviously lower for methanol. The maximum energy that can be released in the condenser per cycle, Q_{con} , is when the full adsorption capacity of each material is used. This total energetic capacity, for fair comparison, is shown in Figure 13 (top). Please note that the chosen temperature here (298 K) is merely used to obtain a value for the enthalpy of evaporation and the total capacity depicted in Figure 13 is not a function of operating conditions, in contrast to the working capacity (cf., Figures 14–16).

Clearly, the activated carbon–methanol pair has a lower energy capacity, because of the lower enthalpy of evaporation of methanol. Where $\sim 2.4 \text{ kJ ml}^{-1}$ is released for water, only $\sim 0.9 \text{ kJ ml}^{-1}$ (both at 298 K) is obtained for methanol. This makes that the activated carbon–methanol pair is somewhere between MOFs and AQSOAs with regards to the volume-specific energy released/taken up. This effect further worsens the MOF–methanol pairs in comparison. Another interesting property to compare is the total amount of energy generated by adsorption,

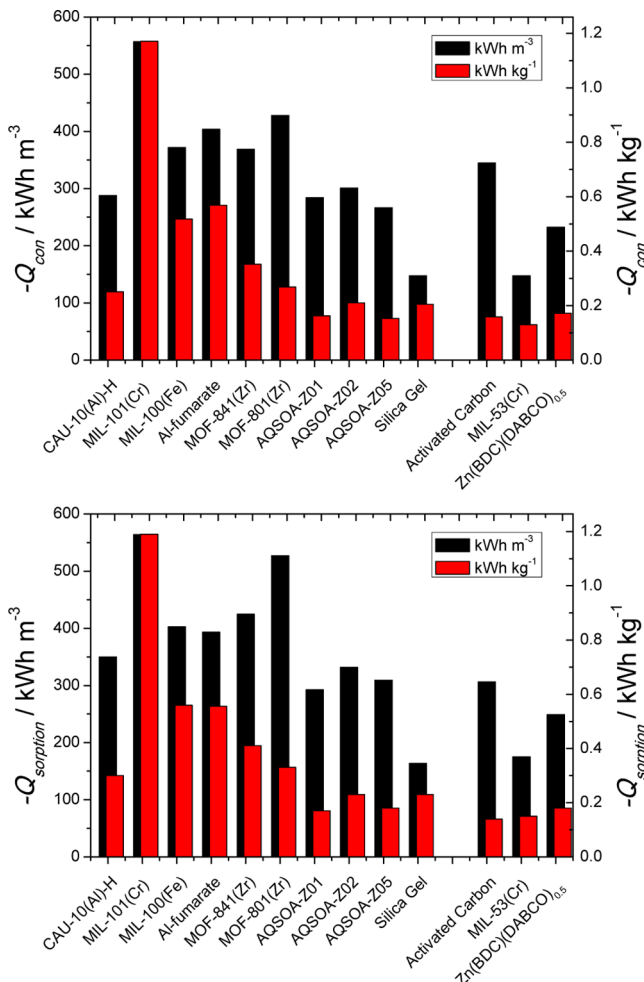


Figure 13. Total amount of energy released in the condenser (at 298 K), Q_{con} , when the full working fluid capacity is condensed (top) and total amount of energy released during adsorption, Q_{sorption} , by fully saturating the adsorbent with working fluid, both per unit MOF volume, using the densities (ρ_{p} for flexible MOFs) listed in Table 6, (black bars, left x -axis) and per unit mass (red bars, right x -axis). The last three adsorbents are calculated with methanol as working fluid; for the other water is used.

which is calculated using eq 23 from zero to saturation loading for all adsorbent-working pairs. The results are shown in Figure 13 (bottom), both per unit volume and per unit mass. In accordance with the previous discussion, mass-specific Q_{sorption} is generally found larger for MOFs than for benchmark sorbents, and methanol-based working pairs. In comparison, volumetric Q_{sorption} of the AQSOA-series is roughly equal to that of activated carbon–methanol, although Q_{con} has been found larger for the latter. This is because for the AQSOA–water working pairs the ratios of enthalpy of adsorption to evaporation are higher than for most other materials. Although this fact might be beneficial for energy storage, and this will be explored in section 7.1, this will have a negative influence on the coefficient of performance in AHP/ACs, as will be demonstrated. Further, by reporting mass-based adsorptive energy content, the comparison becomes skewed. The high mass-based uptake of MIL-101(Cr), which in fact has the lowest density among compared materials, would show vastly higher values than all other materials if performance would be reported, kWh kg^{-1} (Figure 13). When the results are

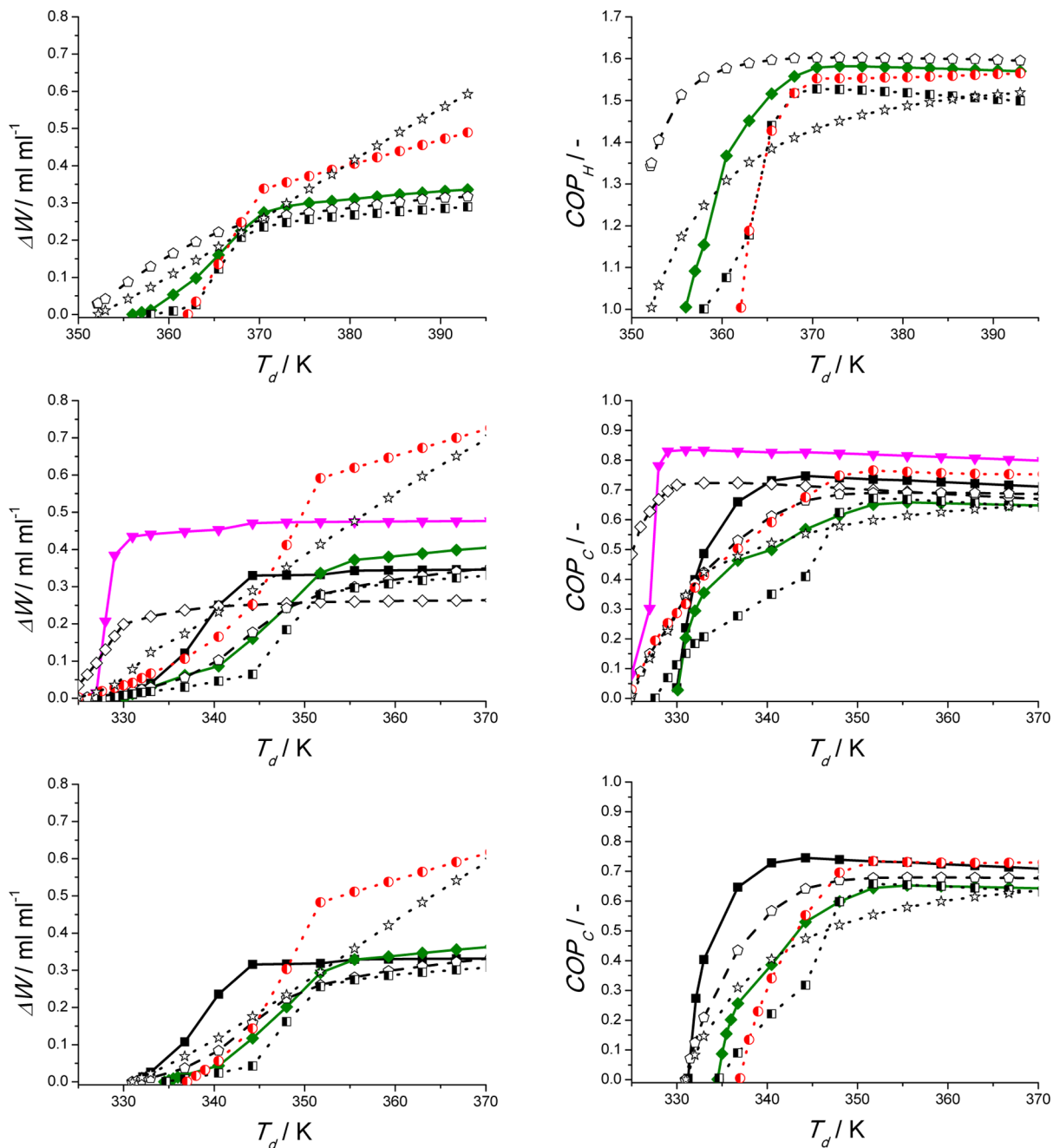


Figure 14. Working volume adsorbed per volume adsorbent, $\Delta W \rho_o$, as a function of desorption temperature, T_{des} (left), and coefficient of performance as a function of desorption temperature (right), for heat pump ($T_{\text{ev}} = 288 \text{ K}$, $T_{\text{ads}} = 318 \text{ K}$, top), refrigeration I ($T_{\text{ev}} = 283 \text{ K}$, $T_{\text{ads}} = 303 \text{ K}$, middle) and refrigeration II ($T_{\text{ev}} = 278 \text{ K}$, $T_{\text{ads}} = 303 \text{ K}$, bottom). MOF–water working pairs, CAU-10(Al)-H (■), MOF-841(Zr) (pink ▼), and MOF-801(Zr) (green ◆) with full lines. Benchmark–water pairs, AQS0A-Z01 (◇) and Z02 (□) with dashed lines. Methanol-based working pairs, MIL-53(Cr) (■), Zn(BDC) (DABCO)_{0.5} (red ●), and Activated Carbon (☆) with dotted lines.

compared on a volumetric basis, MIL-101(Cr) still exhibits the highest Q_{sorption} , but the difference with other materials is less pronounced. In conclusion, the energy content of MOFs can be larger than that of benchmark sorbents. Whether this potential can be harnessed under practical conditions will be discussed in the following section.

6.5.2. Efficiency Comparison. For heat pump application and refrigeration I and II (conditions in Table 7), both the volumetric working capacity, ΔW , and the coefficient of performance (heating for heat pump, cooling for refrigeration I and II) have been determined as a function of desorption temperature, T_{des} . For materials that show suitable uptake

under applied conditions, the results are shown in Figure 14, while for those that do not show suitable uptake, the results are shown in Figure S5. In addition, because of limited MOFs that can operate under ice-making conditions (using methanol), results for this application are shown in Figure S6.

For heat pump conditions, Figure 14 (top), employing water as working fluid, it becomes apparent that AQS0A-Z02 can be operated with lower desorption temperatures than MOF-801(Zr). Above 373 K, ΔW is almost equal for both components ($\sim 0.3 \text{ mL mL}^{-1}$), and the same holds for COP_H (~ 0.7). Activated carbon–methanol shows higher ΔW , especially at elevated desorption temperatures, but because

methanol has a lower evaporation enthalpy, the net condensable/evaporable energy per cycle is lower, as at 393 K activated carbon G32-H still contains methanol. Increasing temperature might still thus improve performance. However, as reported by Hu et al., methanol undergoes thermal decomposition at higher temperatures, and thus increasing temperature over 403 K is not very practical.⁴⁰⁹ In comparison, for $366 \text{ K} \leq T_{\text{des}} \leq 380 \text{ K}$, Zn(BDC)(DABCO)_{0.5} has a larger ΔW and a greater efficiency than activated carbon, both employing methanol. MIL-53(Cr), however, because only part of its methanol capacity is used, shows a lower uptake. In addition, both MOF–methanol pairs show little to no release of working fluid for $T_{\text{des}} \geq 370 \text{ K}$, mitigating the need to go to higher desorption temperatures. Because the adsorption potential for the adsorbed (maximum capacity) state is already quite high ($A_{\text{ads}} = 4.6 \text{ kJ mol}^{-1}$), many adsorbents do not contain significant adsorbed working fluid volume, making that a negligible working capacity is obtained regardless of desorption strategy. By decreasing the evaporator temperature further, thus increasing A_{ads} (eq 19), even more structures become useless, as during the adsorption stage the materials are hardly loaded with working fluid.

For refrigeration I, Figure 14 (middle), especially MOF-841(Zr) stands out. Saturation capacity is reached at conveniently low desorption temperatures ($T_{\text{des}} \approx 333 \text{ K}$) so that either waste or solar energy can be efficiently utilized. As compared to AQSOA-Z01, which requires a similar desorption temperature, ΔW is almost doubled (0.48 versus 0.26 mL mL⁻¹) and its efficiency is higher (COP_H of 0.83 and 0.72, respectively). The higher efficiency can be explained by the (average) enthalpy of adsorption, being -50.4 and $-56.1 \text{ kJ mol}^{-1}$ for MOF-841(Zr) and AQSOA-Z01, respectively (Figure 6). This in turn can be attributed to the higher porosity of the former, as per unit volume less adsorption sites are present, meaning that water interacts more with water in this particular structure than it would in AQSOA-Z01. In contrast thus to the heat pump conditions, for refrigeration I clearly there are MOFs that outperform benchmark materials with respect to both (energetic) capacity and thermodynamic efficiency. This difference can be attributed to the lower adsorption potential of the adsorption stage ($A_{\text{ads}} = 3.1 \text{ kJ mol}^{-1}$) for Refrigeration I, which allows structures with higher α -values to be practically utilized.

When higher desorption temperatures can be utilized, also CAU-10(Al)-H ($T_{\text{des}} \approx 345 \text{ K}$) or MOF-801(Zr) ($T_{\text{des}} \approx 355 \text{ K}$) show higher capacity than, and efficiency similar to, those of benchmark materials AQSOA-Z01 and Z02, respectively. This is of particular interest because the organic ligands used for these materials, isophthalic acid⁴¹⁰ for CAU-10(Al)-H and fumaric acid⁴¹¹ for MOF-801(Zr), are already produced on an industrial scale. In contrast, 4,4',4'',4'''-methanetetracyclotetraenoic acid (MTB), the ligand used to synthesize MOF-841(Zr), is not produced on any commercial scale, to the best of our knowledge.

For refrigeration II, Figure 14 (bottom), the lower evaporator temperature (278 K instead of 283 K) or higher adsorption potential of the adsorption stage ($A_{\text{ads}} = 4.0$ instead of 3.1 kJ mol^{-1}) makes that MOF-841(Zr) and AQSOA-Z01 can no longer be utilized. CAU-10(Al)-H is under these conditions the best performing adsorbent, followed by MOF-801(Zr) AQSOA-Z02.

For ice-making conditions, the discussion can be brief. Activated carbon outperforms the two MOF–methanol

working pairs (see Figure S6) over the whole range of desorption temperatures; only for $T_{\text{des}} \approx 345 \text{ K}$ does Zn(BDC)(DABCO)_{0.5} have a capacity similar to that of the activated carbon. So, on the basis of these results, there is no clear incentive to use MOF–methanol working pairs for this specific application. From Figure 14 one can observe that an increase in COP is often observed at lower T_{des} than is the case for ΔW . This can be reasoned by the small effect of the effective heat capacity. The heat capacity of the heat exchange surface is ignored in this evaluation, as this generates better intrinsic adsorbent performance comparison. As the heat capacity of the adsorbent has a small influence (section 6.4.1) on the total energy balance, any nonzero ΔW constitutes already a Q_{regen} (and $Q_{\text{desorption}}$) with a magnitude in the same order as $Q_{\text{ev}}/Q_{\text{con}}$. This yields as a result that directly a coefficient of performance can be observed, while the (volumetric) working capacity might be still negligibly small. This is thus a direct effect of ignoring the heat capacity of the heat conduction surface (see eq 8). The influence of heat exchanger (hex) on effective heat capacity can be written as³⁸⁶

$$c_p^{\text{effective}}(T) = c_p^{\text{adsorbent}}(T) + \frac{m_{\text{hex}}}{m_{\text{adsorbent}}} c_p^{\text{hex}}(T) \quad (25)$$

The mass of heat exchanger, m_{hex} , is defined relative to the mass of adsorbent used. For lab/pilot-scale AHP/ACs, one frequently observes a $m_{\text{hex}}/m_{\text{adsorbent}}$ ratio between 1 and 4 for benchmark materials,^{52,386,412–416} although values as high as 8 may be observed.⁴¹⁷ As heat-exchangers are commonly composed of either copper, aluminum, or stainless steel, one could rightfully assume that $0.4 < c_p^{\text{hex}} < 0.9 \text{ J g}^{-1} \text{ K}^{-1}$.³⁵ This in turn means that roughly speaking $1.4 < c_p^{\text{effective}} < 10 \text{ J g}^{-1} \text{ K}^{-1}$. To envisage the influence of the effective heat capacity, the coefficient of performance for MOF-841(Zr)-water has been calculated for increasing magnitude of $c_p^{\text{effective}}$ with the conditions of refrigeration I (Figure 14 (middle)), and shown in Figure 15. Clearly, when $c_p^{\text{effective}}$ is increased, the coefficient of performance does not increase at lower T_{des} than ΔW anymore. Furthermore, the COP decreases as relatively more energy is required for heating. The desorption temperature

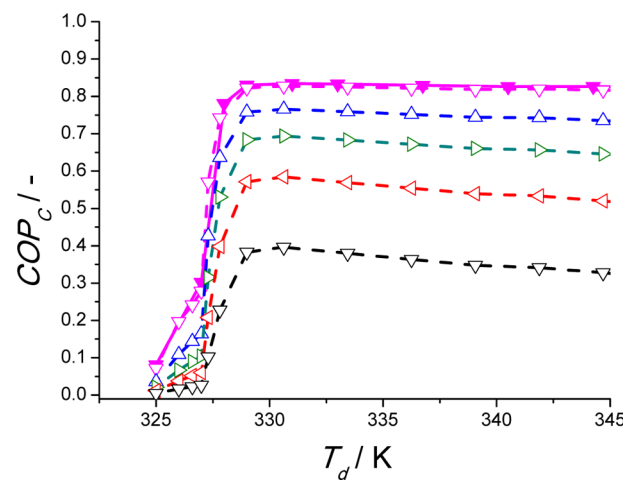


Figure 15. Coefficient of performance for cooling for MOF-841-water for conditions of refrigeration I ($T_{\text{ev}} = 283 \text{ K}$, $T_{\text{con}} = 303 \text{ K}$) with varying effective heat capacity. For $C_p^{\text{effective}} = 1$ (same as in Figure 14(middle), pink \blacktriangledown), $C_p^{\text{effective}} = 1.4$ (pink \triangledown), $C_p^{\text{effective}} = 5$ (blue \triangle), $C_p^{\text{effective}} = 10$ (green right-facing \triangle), $C_p^{\text{effective}} = 20$ (red left-facing \triangle), and $C_p^{\text{effective}} = 50$ (∇).

corresponding with the optimum COP_c is not significantly influenced by the effective heat capacity. The decrease with higher T_{des} however is stronger for larger c_p^{effective}. This is because increasing temperature does not significantly release more working fluid, but energy is nonetheless still required for a further temperature increase. This is obviously more cumbersome when c_p^{effective} is higher (more heat exchanger mass is present). The influence of c_p^{effective} on COP increases with decreasing ΔW, lower enthalpy of adsorption, and higher T_{des}, obviously. Coming back to the results shown in Figure 14, more specifically to further elucidate the effect of operational temperatures on performance, the concept of “temperature lift” will be introduced and utilized.

6.5.3. Temperature Lift. The temperature lift during the adsorption half-cycle can be defined as the difference between T_{con} and T_{ev}.³⁸⁶ During desorption, this is the difference between T_{des} and T_{con}.³⁸⁶ Here, focus is on the former, which can be interpreted as the temperature gain during adsorption for heat pumps, or the achievable decrease in temperature for cooling purposes. For a condenser temperature of 303 K and a fixed desorption temperature (373 K), the temperature of the evaporator is varied to envisage the effect of temperature lift on the energy withdrawal per volume of adsorbent per cycle. Results for all adsorbents are shown in Figure 16.

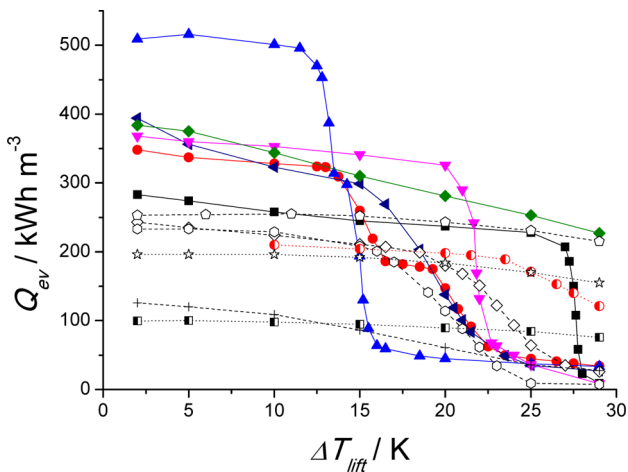


Figure 16. Energy taken up by the evaporator as a function of temperature lift during adsorption, obtained by varying T_{ev} when T_{des} = 373 K and T_{con} = 303 K. MOF–water working pairs, CAU-10(Al)-H (■), MIL-100(Fe) (red ●), MIL-101(Cr) (blue ▲), Al-fumarate (purple left-facing ▲), MOF-841(Zr) (pink ▼), and MOF-801(Zr) (green ◆) with solid lines. Benchmark–water pairs, silica gel (+), AQSOA-Z01 (◇), Z02 (○), and Z05 (○) with dashed lines. Methanol-based working pairs, MIL-53(Cr) (■), Zn(BDC) (DABCO)_{0.5} (red ●), and Activated Carbon (☆) with dotted lines.

For low temperature lifts, ΔT_{lift} ≤ 12 K, MIL-101(Cr) has the highest volumetric energy capacity (~500 kWh m⁻³). For higher required temperature lifts, 12 ≤ ΔT_{lift} ≤ 20 K, MOF-841(Zr) is the adsorbent of choice (~350 kWh m⁻³). For higher temperature lifts, CAU-10(Al)-H (20 ≤ ΔT_{lift} ≤ 26 K) or MOF-801(Zr) can be efficiently utilized (~250 and ~280 kWh m⁻³, respectively). In fact, it seems that CAU-10(Al)-H would have performance similar to that of AQSOA-Z02 over a wide range of temperature lifts. However, CAU-10(Al)-H can be regenerated at a significantly lower desorption temperature (see Figure 14) than either AQSOA-Z02 or MOF-801(Zr). To dwell on that, the required desorption temperature increases in

order of MIL-101(Cr) < MOF-841(Zr) < CAU-10(Al)-H < AQSOA-Z02 < MOF-801(Zr) (derived from Figure 14), perfectly in line with the maximum achievable temperature lift. The coefficient of performance for cooling purposes also decreases with this maximum achievable temperature lift of each material: MIL-101 (Cr, COP_c ≈ 0.89) > MOF-841 (Zr, COP_c ≈ 0.79) > CAU-10(Al)-H (COP_c ≈ 0.72) > AQSOA-Z02 (COP_c ≈ 0.69) > MOF-801 (Zr, COP_c ≈ 0.68). Thus, over a wide range of temperature lifts, MOFs can be more efficiently applied than currently available adsorbents. To allow for efficient heat removal by the evaporator, the immediate surroundings of the evaporator (e.g., the inside of a refrigerator) should have a (slightly) higher temperature, T_{ev'}. The reverse is true for the surroundings of the condenser, which should be lower than T_{con} (T_{con'}). The effective temperature lift thus, T_{ev'} - T_{con'}, is lower than that mentioned in the preceding discussion. Allowing thus for efficient heat transfer in condenser and evaporator, this will diminish part of the maximum achievable temperature lift.

The above results can be, at least qualitatively, reasoned with the aid of pore size. A larger pore size means that pores are filled at lower adsorption potential, A_{ads} (or higher α), so that the maximum temperature lift is reduced. For the same reason, the material is efficiently regenerated at lower adsorption potential of desorption, A_{des} (or lower desorption temperature). Because of the larger pore volume of structures with larger pores, the volumetric adsorption capacity is also increased (see Figure 8, Table 6), and thus also Q_{ev} per volume of material. Last, because of a larger pore volume, the average adsorption enthalpy is lower, as previously mentioned, making thermodynamic efficiency greater. This discussion is based on MOF–water working pairs, and because water is very sensitive to specific adsorption sites, this rationale cannot be quantified fully with only the pore sizes of different materials. For methanol (or other working fluids), although less data are available, it can be safely assumed that this qualitative rationale also holds. The volumetric energy density for methanol, however, has been found lower in comparison to water as working fluid, because of the lower enthalpy of evaporation.

In short, thus, for AHP/ACs, MOFs offer from the thermodynamic perspective a significant improvement of thermodynamic efficiency and released/withdrawn energy per unit volume per cycle for over a wide range of desired temperature lifts. This is because of the large variation of pore sizes and possible tuning of adsorption sites. However, heat and mass transfer, left out of the comparison in this work as this is scarcely investigated for MOFs, are also important for actual application. If the characteristic cycle times for the above-mentioned MOFs would be significantly longer than for conventional materials, application would still not be feasible. As the configuration of the employed adsorbent (powder, pellets, granules, or coatings) plays a determining role,^{51,363,418–420} dynamic studies should be performed in conjunction with shaping MOF adsorbents. As with MOFs one has the ability to employ larger pore sizes, one may expect that diffusion inside these materials is faster than more narrow pore zeolites. Unfortunately, as studies on thermal transport of MOFs are mainly limited to water-unstable MOF-5,^{421–425} it is difficult to predict a priori whether MOFs might display shorter cycle times for a given configuration. Last, as the COPs reported in this work are based on thermodynamic equilibrium, which essentially means with infinite cycle times, in reality efficiency will be lower than determined here. In fact, there is

an optimal cycle time to obtain a maximal power per unit volume ($\text{J s}^{-1} \text{m}^{-3}$) where the efficiency is maximal at infinite cycle time.⁴²⁶ Furthermore, because in an actual adsorption cycle a certain amount of working fluid is required to desorb in the isosteric heating stage to achieve the pressure increase from p_{ev} to p_{con} , the actual working capacity is reduced as compared to the ideal working capacity used in this work, and thus also the coefficient of performance. The magnitude of this decrease can be mitigated by allowing for only a small empty volume in the adsorption vessel.^{380,427} Before concluding this Review with a summary and outlook (section 8), alternative applications in which MOF adsorbents could potentially be employed are briefly discussed. All of these applications utilized water as working fluid.

7. ALTERNATIVE APPLICATIONS

Adsorption-driven allocation of heat or cold is not the only application based on the reversible ad- and desorption of a working fluid. In this section, two major alternative applications will be discussed briefly, and the potential of applying MOFs in these will be concisely assessed. These are thermochemical energy storage (section 7.1) and open cycle dehumidification for air conditioning (section 7.2).

7.1. Thermochemical Energy Storage

As mentioned in section 1, temporary energy storage is required when energy supply and demand are out of phase. Especially thermochemical storage is interesting, as it requires significantly less volume to store the same amount of energy^{18,19} as compared to systems based on latent²⁰ or sensible energy.²¹ Conceptually, sorption-based thermochemical storage follows the same cycle as a heat pump, with the exception that the adsorption and desorption processes are separated by storage time.³⁸⁶ The relevant energy is comprised by the sorption energy and the latent heat of the sorbent. As during desorption, or charging, the adsorbent is heated, this latent heat could thus also be employed, in theory, during the exothermic adsorption stage for additional energy. However, depending on system insulation and storage time, only a fraction of the sensible heat can be recovered.³⁸⁶ This contribution will be omitted here, as it constitutes only a small fraction of the total energy anyway, and the amount of stored energy will be equated to Q_{sorption} . The amount of storable energy is thus a function of operational conditions, as is the case for AHP/ACs, meaning that the volumetric storage capacity is lower than the values indicated in Figure 13 (bottom). This fact is sometimes forgotten when materials are compared, as mentioned by Stach et al.⁴²⁸ Another difference in practical operation is that relatively small temperature lifts of adsorption can be employed, down to $\sim 10 \text{ K}$,^{386,429,430} which means (see Figure 16) that the potential of MOFs can optimally be employed. For $T_{\text{con}} = 293 \text{ K}$, an often employed temperature when thermochemical storage is considered,^{430–432} and $T_{\text{ev}} = 283 \text{ K}$,³⁸⁶ sufficient for residential heating, Q_{sorption} as a function of desorption temperature can be calculated. Results are shown in Figure 17 for the more promising MOFs, based on Figures 13 and 16, and compared to inorganic salts that in combination with water or NH_3 are commonly employed for energy storage at similar desorption or driving temperatures.^{6,19,433}

Clearly, most of the inorganic salt–fluid combinations exhibit larger volumetric storage density than those of the porous adsorbents. Note that these quantities are based on the pure

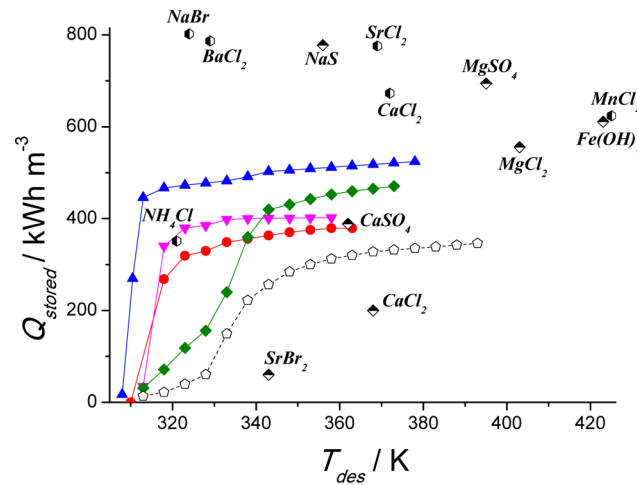


Figure 17. Storable energy density as a function of T_{des} for $T_{\text{ev}} = 283 \text{ K}$ and $T_{\text{con}} = 293 \text{ K}$. MOF–water working pairs, MIL-100(Fe) (red ●), MIL-101(Cr) (blue ▲), MOF-841(Zr) (pink ▼), and MOF-801(Zr) (green ◆) shown with solid lines. AQSOA-Z02 (◇) with dashed lines. Inorganic salts, used for comparison, in combination with water (top-shaded ◆) for SrBr_2 ,^{6,434,435} CaCl_2 ,^{6,436} CaSO_4 ,^{433,437} NaS ,^{433,438,439} MgSO_4 ,^{6,432,440} MgCl_2 ,^{6,431} and Fe(OH)_2 ,^{433,437} and in combination with NH_3 (left-shaded ◉) for NH_4Cl ,^{19,441} NaBr ,^{19,441} BaCl_2 ,^{19,441} SrCl_2 ,^{19,441} CaCl_2 ,^{19,441} and MnCl_2 ,^{19,441}

salt–solvate densities and that these salts are nonporous; some even become liquid upon hydration. Both aspects may induce transport limitations and slow the response time. Embedding these in porous solids is considered,^{442–446} decreasing the energy density. Therefore, to calculate an effective (energy) density, a bulk porosity of 50% is often assumed.^{19,431} In Figure 17, however, this has not been done (MOFs and salt–solvates are employed both with 0% porosity). As MOFs are indeed porous, a lower effective bulk porosity than 0.5 might be used in practice, making that energy densities become more in line with those of inorganic salts. As compared to especially water–salt combinations, MOFs have the advantage that lower desorption temperatures can be used, for low temperature lifts. In addition, some of these salts, MgCl_2 , display significant degradation over a few ad- and desorption cycles.⁴⁴⁷ Last, zeolites were not considered in this section, despite investigations for thermal energy storage, because these generally exhibit lower energy densities (110 and 160 kWh m^{-3} for NaX and LiX ,⁴⁴⁸ respectively) and often require higher desorption temperatures than the adsorbents presented in Figure 17.

7.2. Open Cycle Air-Conditioning

As was already mentioned (section 1), the great advantage of open system air-conditioning by desiccation^{13–16} is that water vapor can be removed directly from the ambient air, whereas the closed devices require cooling of the incoming air to temperatures below the dew point.¹⁷ The concept revolves around the direct adsorption of water vapor from ambient air, an effective way of dehumidification. The solid adsorbent is commonly coated on the internal channels of a rotating wheel, called either a sorption rotor or a desiccant wheel. Devices employing either zeolites, zeotypes, or silica gel are already commercially available.^{48,449,450} The actual operation of desiccant wheel dehumidification is more complex than the heat pump cycle, and the operating conditions depend on outside climate and season.^{13,451–453} Detailed performance

characterization of materials in open cycle desiccation is entirely different from AHP/ACs and is considered out of the scope of this Review. However, desired adsorbent properties are similar to those for AHP/ACs, sufficient stability toward water and suitable adsorptive properties. Additionally, as the adsorbent will be exposed to the ambient, fouling resistance by, for example, microbes should be considered. As a difference, the adsorption uptake is allowed to occur at higher relative α 's (or relative humidity, RH) than is the case for heat pumps.¹⁷ So, all AQSOA-materials are used for open cycle dehumidification, while AQZOA-Z05, the material with the highest α , is not used for application in AHP/ACs.⁴⁸ This means that MOFs with a high volumetric capacity (e.g., MOF-841, MIL-100, and MIL-101) can in principle be efficiently utilized for this purpose. This has been demonstrated by Seo et al., who showed that the rate mass uptake (RH = 60%) per unit mass of material, for MIL-101, is far greater than other adsorbents, including SAPO-34 (see Figure 18).²⁴⁹

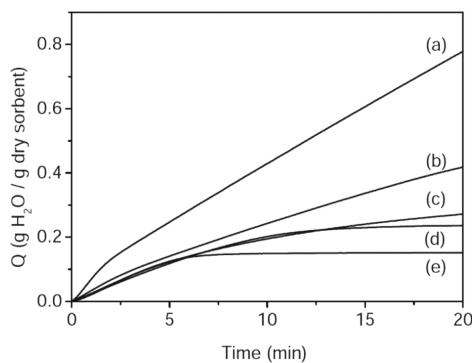


Figure 18. Water adsorption uptake profiles of adsorbent materials at 30 °C in a humid N₂ flow: (a) MIL-101(Cr), (b) MIL-100(Fe), (c) silica gel, (d) SAPO-34, and (e) NaX. Test conditions: adsorption at 30 °C, RH 60%, and flow rate of N₂, 200 mL min⁻¹. Reproduced with permission from ref 249. Copyright 2011 John Wiley and Sons.

This also clearly indicates a potential advantage of MOFs in dehumidification applications over commonly used adsorbents. Guo et al. further underlined this potential. They claimed, based on an array of different MOFs in comparison with alumina, their industrial adsorbent of choice for dehumidification, that all MOFs have superior total capacities, and some also display superior breakthrough behavior, and thus faster kinetics.⁴⁵⁴ In addition, cyclic regeneration for MOFs can be achieved with significantly less energy (lower T_{des}), all in line with preceding findings (desiccant, AHP/AC).⁴⁵⁴

8. SUMMARY AND FUTURE PERSPECTIVES

8.1. Summary

The potential of MOFs as adsorbents in adsorption-driven allocation of heat and cold has been thoroughly assessed in this Review. The adsorption mechanism of water on MOFs is known. Water initially adsorbs at specific hydrophilic sites (uncoordinated metal sites, OH-groups on inorganic clusters, or functional groups on the organic ligand). Subsequently, additional water clusters around these initially adsorbed water molecules, after which the pores are filled via volume filling ($d_p < D_c$) or capillary condensation ($d_p > D_c$). In silico prediction of water adsorption in MOFs is deemed not yet mature enough for accurate selection of MOF structures. For alcohols the adsorption mechanism is somewhat similar, although the

adsorption behavior is often devoid of steep steps in uptake. In this case, in silico prediction seems to work better, as the behavior of methanol is well described by classical force fields.

The stability of MOFs with respect to water has been researched in a plethora of communications. Various factors that (co-)determine the structural stability have been posed, of which the most important are the metal species, its valence, coordination number, and degree of filling of the coordination sphere, and the metal–ligand bond strength. Additionally, structural defects can play an important role on stability. Further, degradation reactions do not always occur in the bulk of the material. In some cases, only an exterior shell is degraded, forming an impervious layer, preserving the bulk of the material. Surface tension of water might also have adverse effects on the stability for MOFs with elongated ligands. Last, MOFs that have been claimed to be stable toward water vapor have been shown to degrade under repeated ad- and desorption cycles. The preceding highlights the complexity of influences on water stability. Nonetheless, there are MOFs that exhibit the level of hydrothermal stability required for application in AHP/ACs. Of these structures, some show the interesting stepwise water uptake behavior for this target application. These are CAU-10(Al)-H, MIL-100(Fe), MIL-101(Cr), MOF-801(Zr), MOF-841(Zr), and Al-fumarate, of which the performance is thoroughly assessed in section 6 of this Review. Especially CAU-10(Al)-H stands out with respect to stability, as no degradation was observed for over 700 adsorption cycles.²²⁵ For methanol, stability is seemingly less of an issue. However, the list of structures for which methanol adsorption has been investigated (at more than one temperature) is too limited for a proper evaluation. Only the performance of MIL-53(Cr) and Zn(BDC)(DABCO)_{0.5} could be assessed. These structures exhibit the desired stepwise uptake of methanol, although this is caused by the structural flexibility of the frameworks, making an undesired hysteresis-loop observed. Last, for ammonia, because of stability issues and subsequent limited adsorption data, no suitable candidate could be identified. Of the available adsorption data, a significant part is used for trace removal, which is characterized by very low partial pressures of working fluid, making the bulk of the retrieved studies of little use for detailed assessment.

A thermodynamic model of the ideal adsorption heat pump cycle has been adopted, with the aim to assess the performance of MOFs for adsorption-driven allocation of heat and cold on an accurate and objective manner. Per unit volume, MOFs can in total store more energy, Q_{sorption} and release more energy per cycle ($Q_{\text{ev}}/Q_{\text{con}}$) when water is the working fluid of choice. Especially the latter is desired for the application at hand. Also, especially for cooling applications, MOFs clearly have been shown to display improved capacity and thermodynamic efficiency. Over a wide range of required temperature lifts for application, MOFs display higher capacity and efficiency than benchmark materials. The specific material that has optimal performance depends on the desired temperature lift. For low temperature lifts, $\Delta T_{\text{lift}} \leq 12$ K, MIL-101(Cr) has the highest energy capacity per unit volume MOF (~ 500 kWh m⁻³). For higher required temperature lifts, $12 \leq \Delta T_{\text{lift}} \leq 20$ K, MOF-841(Zr) is the adsorbent of choice (~ 350 kWh m⁻³). For higher temperature lifts, CAU-10(Al)-H ($20 \leq \Delta T_{\text{lift}} \leq 26$ K) or MOF-801(Zr) can be efficiently utilized (~ 250 and ~ 280 kWh m⁻³, respectively). The required desorption temperature increases, for the investigated adsorbent–water pairs, in the order: MIL-101(Cr) < MOF-841(Zr) < CAU-10(Al)-H <

AQSOA-ZO2 < MOF-801(Zr). Last, thermodynamic efficiency follows the same trend: MIL-101 (Cr, COP_c ≈ 0.89) > MOF-841 (Zr, COP_c ≈ 0.79) > CAU-10(Al)-H (COP_c ≈ 0.72) > AQSOA-ZO2 (COP_c ≈ 0.69) > MOF-801 (Zr, COP_c ≈ 0.68). These trends can be directly related to the material's pore size. A larger pore size means that pores are generally filled at higher α , and thus at lower adsorption potential for adsorption, A_{ads} , meaning that the maximum temperature lift is reduced, but the material is efficiently regenerated at lower adsorption potential for desorption, A_{des} , as well. A larger pore volume leads to an increased volumetric adsorption capacity. Because of a larger pore volume, the average adsorption enthalpy is lower, resulting in a higher thermodynamic efficiency.

Furthermore, MOFs have great potential for the efficient direct dehumidification of air for air-conditioning purposes. For energy storage applications, focus should be especially on low desorption temperature applications, as MOF–water pairs are likely to be more competitive in this range. In this Review, however, no better performance with respect to commonly used inorganic salts has been identified in terms of energy storage capacity.

8.2. Future Perspectives

The focus of this Review is on the thermodynamic (“static”) properties of MOFs in relation to allocation of heat and cold, as these are most abundantly available. For successful application, however, also the dynamics of the MOF–working fluid pair are important. The latter depends heavily on the macroscopic structure of the MOF chosen in the heat exchange application. Furthermore, MOFs are commonly synthesized and characterized on the (sub)gram scale, while actual heat pumps contain adsorbent material in the order of kilograms. To help put things into perspective, seven subsequent stages are defined that will eventually lead to application.

Stage 0 – Stability: As the primary requirement, MOFs should be tolerant toward the working fluid of choice. This should be ensured before anything else.

Stage 1 – Adsorptive properties: On the basis of primary vapor adsorption measurement(s), the shape of an isotherm can be envisaged. From this the initial feasibility can be assessed.

Stage 2 – Thermodynamic efficiency and working capacity: With knowledge of the enthalpy of adsorption, preferably directly from calorimetric measurements or else calculated isosteric enthalpy (from isotherms at more than one temperature) and (crystallographic) density of a material, the efficiency and volumetric (working) capacity can be assessed as has been done extensively in section 6 of this Review.

Stage 3 – Shaping of materials: The previous stages have in common that they can be assessed on as-synthesized powders. As dynamics of heat and mass transfer (stage 4) are dependent on the chosen configuration of the employed adsorbent (e.g., pellets, granules, or coatings), shaping is in order.

Stage 4 – Heat and mass transfer of shaped materials: On the basis of the morphology chosen in stage 3, the effective heat and mass transfer rates should be determined to assess the dynamics of the MOF-working pair.

Stage 5 – Scale-up of synthesis: Previous stages can be performed on the (sub)gram scale. For actual application, the synthesis should be properly scaled up, to allow for large-scale performance testing.

Stage 6 – Large-scale evaluation of shaped systems: The performance of a large-scale system should be ensured before

commercialization. Additionally, on the basis of the performance and the results of stage 5, an economic evaluation will ultimately determine the feasibility of the MOF–working fluid combination.

This classification will help assess at which stage are MOFs combined with the working fluid of choice. Furthermore, guidelines and considerations can be posed for focus of future work.

8.2.1. Ammonia – Stage 0. Very few MOFs, if any, have been convincingly demonstrated to reversibly adsorb significant amounts of ammonia with structural retention. The number of different MOF structures for which this has been examined is far lower than for water. The cause of instability with respect to ammonia has received little attention. It is therefore not clear whether there exists a justifiable expectation for ammonia-stable MOFs. If any desire exists to employ MOF–ammonia working pairs in heat pumps, focus should be on resolving instability of MOFs toward ammonia.

8.2.2. Alcohols – Stage 2. Interesting adsorption properties have been reported for several MOFs with respect to methanol/ethanol, for ZIFs (ZIF-8, -68, -71, and -90), MIL-53(Cr), and Zn(BDC)(DABCO)_{0.5}. Of the ZIFs, little to no information on either desorption or enthalpy of adsorption is known, making practical assessment impossible. Of the latter two, the energy capacity turned out to be lower than for water–MOF pairs. Because of the higher vapor pressure of methanol and to a lesser extent ethanol, dynamics might be faster than for water, so a lower energetic capacity does not necessarily exclude a viable application. However, for most conditions, the methanol–MOF pairs exhibited lower coefficients of performance (COP) than methanol-activated carbon. Regarding the to be avoided adsorption–desorption hysteresis, alcohols require larger pore diameters than do water (3.5 nm for methanol, 4.3 nm for ethanol, and 2 nm for water). So, larger pore sizes could be used for MOF–alcohol pairs than for water, and for alcohols focus should be on exploring adsorption on additional MOF structures, especially comprising larger pore size structures to obtain more efficient alcohol-based working pairs.

8.2.3. Water – Stages 3/4. In section 6 of this Review, it has been demonstrated convincingly that water–MOF working pairs exist with higher capacity and thermodynamic efficiency than benchmark sorbents. Shaping of these materials should be focused on, in conjunction with, measurements on heat and mass transfer dynamics. For packed bed systems, heat transfer is often limiting, making coatings an optimal configuration.^{S1,418,455} Most work regarding MOF coatings has focused on the creation of thin films,^{456–461} of which the thickness is generally on the submicrometer-scale, orders of magnitude off for target application. However, there are studies focusing on creating thick MOF films (>100 μm), suited for application. These are based on direct crystallization on the surface, without the need for a physical binder material.^{223,227,228} Furthermore, MAF-4 has been grown directly from and on structured ZnO,²³⁶ and Al-based MOFs have been formed directly on and from structured alumina-supports.⁴⁶² These and other^{463,464} examples highlight the potential of direct growth of MOFs on various structured supports. Alternatively, granules or pellets^{424,465–468} can be utilized. For benchmark materials AQSOA-Z01,^{469,470} AQSOA-Z02,^{471–473} and silica gel,^{473,474} the adsorption dynamics of water have been determined and serve as a good basis for comparison.

Although there are few accounts of their large-scale synthesis,^{304,475,476} MOFs potentially offer advantages, as

environmentally benign,^{477–480} room temperature,^{481–488} and even solvent-free synthesis^{489–494} protocols have been developed. In comparison, zeolite and zeotype synthesis often requires relatively expensive sacrificial organic templates,^{495–500} as is the case for the synthesis of SAPO-34 (AQSOA-ZO2)^{501–503} and AlPO-5 (AQSOA-Z01/Z05).^{504–506}

In short, MOFs with water as working fluid show improved thermodynamic efficiency and volumetric adsorption capacity in comparison to commercially available benchmark materials for adsorption-driven allocation of heat and cold. MOF potential is further strengthened by the availability of low temperature, environmentally benign, and even solvent-free synthesis protocols and the possibility of synthesizing these materials directly on heat exchanger surfaces. MOFs thus have a bright future for application in adsorption-driven heat pumps and chillers.

ASSOCIATED CONTENT

Supporting Information

The Supporting Information is available free of charge on the ACS Publications website at DOI: [10.1021/acs.chemrev.5b00059](https://doi.org/10.1021/acs.chemrev.5b00059).

Additional calculation results, model input, and information about the employed interpolation scheme (for AQSOA-Z01 and -Z02) ([PDF](#))

AUTHOR INFORMATION

Corresponding Author

*E-mail: f.kapteijn@tudelft.nl.

Notes

The authors declare no competing financial interest.

Biographies



Martijn F. de Lange (1986) received his M.Sc. in Chemical Engineering at the Delft University of Technology in 2011 (Cum Laude), after which he started his Ph.D. at the same university under the supervision of Thijs, Freek, and Jorge, the topic being the application of metal–organic frameworks in the adsorption-driven allocation of heat and cold, using a multidisciplinary approach. During his Ph.D., he has been a visiting scientist at the Universität Leipzig (Germany), Universidad Pablo Olavide (Sevilla, Spain), and Zhejiang Normal University (Jinhua, China). He received his Ph.D. degree (Cum Laude) in 2015.



Karlijn J. F. M. Verouden (1988) obtained her bachelor in Applied Science on “Optimisation of high aspect ratio, nanoscale fillers in polymer dispersion coatings for enhanced barrier performance” in 2010 at the Fontys Hogeschool Toegepaste Natuurwetenschappen. After that she wanted to focus more on Process Engineering. She received her M.Sc. in Chemical Engineering on the topic “The applicability of MOFs in heat pumps” in 2014 at Delft University of Technology.



Thijs J. H. Vlugt (1974) received his M.Sc. degree in Chemical Engineering in 1997 at Eindhoven University of Technology (The Netherlands). In 2000, he obtained his Ph.D. degree at the University of Amsterdam with R. Krishna and Berend Smit as thesis advisors. After postdoctoral research in Mainz (Germany) and Leiden (The Netherlands), he was appointed assistant professor at Utrecht University (The Netherlands). In 2007 he moved to Delft University of Technology (The Netherlands), first as Associate Professor and later as full professor and chair Engineering Thermodynamics (2010). In 2005 he received a prestigious VIDI personal grant for research on the self-assembly on nanocrystals. He is also director of the honors program at the faculty of Mechanical, Maritime, and Materials Engineering in Delft. He has coauthored over 150 scientific publications.



Jorge Gascon (1977) received his M.Sc. in Chemistry in 2002 and his Ph.D. in Chemical Engineering in 2006, both at the University of Zaragoza (Spain). Starting as postdoc at TUDelft, he is since 2014 “Anthonie van Leeuwenhoek Professor” of Catalysis Engineering. His research interests include fundamental aspects and applications of new nanostructured materials and composites. He has coauthored over 100 publications, several patents, and has edited the book “Metal Organic Frameworks as Heterogeneous Catalysts”. He has been the recipient of the prestigious VENI (2010), VIDI (2013), and ERC Starting (2013) personal grants. Recently, he received the 2013 ExxonMobil Chemical European Science and Engineering Award.



Freek Kapteijn (1952), M.Sc. in Chemistry and Mathematics, received his Ph.D. on “Metathesis of alkenes” in 1980 at the University of Amsterdam. After postdoc positions (Coal Science) in Amsterdam and Nancy (ENSIC), he became Associate professor in Amsterdam. He moved to Delft University of Technology in 1992, became “Anthonie van Leeuwenhoek professor” in 1999, and since 2008 is chair of Catalysis Engineering, with visiting professorships at ETH Zürich, Tianjin, and Zhejiang Normal University. His research interest focuses on the interplay of catalysis and engineering, comprising structured and multifunctional catalysts, adsorption, separation, and (catalytic) membranes. He has coauthored over 500 publications in peer-reviewed journals and as book chapters.

ACKNOWLEDGMENTS

Financial support from the Advanced Dutch Energy Materials (ADEM) program of the Dutch Ministry of Economic Affairs, Agriculture and Innovation is gratefully acknowledged.

ABBREVIATIONS

MOF Terminology

CAU	Christian Albrechts University
Cus	coordinatively unsaturated site

DMOF	DABCO MOF
DUT	Dresden University of Technology
MAF	metal azolate framework
MFU	metal–organic framework Ulm University
MIL	Material Institut Lavoisier
NU	Northwestern University
PIZOF	porous interpenetrated zirconium–organic frameworks
SALI	solvent-assisted ligand exchange
UiO	University of Oslo
ZIF	zeolitic imidazolate framework

Ligands

4-btapa	1,3,5-benzene tricarboxylic acid tris-[N-(4-pyridyl)-amide]
ADC	9,10-anthracenedicarboxylic acid
Ala	alanine
Azi	aziridine
AZPY	azopyridine
BBTA	1 <i>H</i> , <i>S</i> -benzo(1,2- <i>d</i> :4,5- <i>d</i> ')bistriazole
BDC	1,4-benzene dicarboxylic acid (TPA)
bfpdc	2,2'-bistrifluoromethyl-biphenyl-4,4'-dicarboxylic acid
bIm	benzimidazole
BIPY	2,2'-bipyridine-5,5'-dicarboxylate
BPDC	4,4'-biphenyldicarboxylic acid
bpe	<i>trans</i> -1,2-bis(4-pyridyl)ethylene
bptc	4,4'-biperylene-2,6,2',6'-tetracarboxylic acid
bpy	4,4'-bipyridine
Bpybc	1,1'-bis(4-carboxybenzyl)-4,4'-bipyridine
BTB	benzene tribenzoate
BTC	1,3,5-benzene tricarboxylic acid
Btre	1,2-bis(1,2,4-triazol-4-yl)ethane
BTTB	4,4',4'',4'''-benzene-1,2,4,5-tetrayltetrabenzoic acid
CAM	chelidamic acid
CDC	<i>trans</i> -1,4-cyclohexane dicarboxylic acid
Dab	1,4-diamino-butane
DABCO	1,4-diazabicyclo[2.2.2]octane (TED)
dacba	diacetylene-1,4-bis(4-benzoic acid)
dcIm	dichloroimidazole
DMBPy	2,2'-dimethyl 4,4'-bipyridine
dmcapz	3,5-dimethyl-4-carboxypyrazole
DPE	1,2-di(4-pyridyl)ethylene
Dpyg	1,2-di(4-pyridyl)glycol
DTTDC	dithieno[3,2- <i>b</i> ;20,30- <i>d</i>]-thiophene-2,6-dicarboxylate
Eim	2-ethylimidazole
etz	3,5-diethyl-1,2,4-triazolate
FA	fumaric acid
Hma	hemiaminal
Ica	imidazole-2-carboxaldehyde
IPA	isophthalic acid (1,3-benzene dicarboxylic acid)
L	N-(4-carboxyphenyl) isonicotinamide 1-oxide
L'	2-((pyridin-4-yl)methylamino)-4-methylpentanoic acid
L''	2-(pyridin-4-yl)methylamino)-3-hydroxypropanoic acid
L'''	2-((pyridin-4-yl)methylamino)-3-hydroxybutanoic acid
L1	1 <i>H</i> -pyrazole-4-carboxylic acid
L2	4-(1 <i>H</i> -pyrazole-4-yl)benzoic acid
L3	4,4'-benzene-1,4-diylbis(1 <i>H</i> -pyrazole)
L4	4,4'-buta-1,3-diylbis(1 <i>H</i> -pyrazole)

L5	4,4'-(benzene-1,4-diyl)diethyne-2,1-diyl)bis(1 <i>H</i> -pyrazole)
L6	3,5-di(pyridine-4-yl)benzoic acid
L7	5-(4-pyridyl)-isophthalic acid
Me ₂ trzpb	4-(3,5-dimethyl-4 <i>H</i> -1,2,4-triazol-4-yl)benzoate
mIm	2-methyl-imidazole
mImca	4-methyl-5-imidazolecarboxaldehyde
MTB	4,4',4"-methanetetracyltribenzoic acid
mTz	3-methyl-1,2,4-triazole
NDC	naphthalenedicarboxylic acid
NDI	2,7-bis(3,5-dimethyl-1 <i>H</i> -pyrazol-4-yl)benzo[1mn]-[3,8]phenanthroline-1,3,6,8(2 <i>H</i> ,7 <i>H</i>)-tetraone
NIm	2-nitro-imidazole
OAc	acetoxy
opd	<i>o</i> -phthalic acid
Ox	oxalate
PEDB	4,4'-(1,4-phenylenebis(ethyne-2,1-diyl))dibenzoic acid
pmpmd	<i>N,N'</i> -bis (4-pyridylmethyl) phenyldiimide
pybz	4-(4-pyridyl)benzoate
PytPh	pyrene-1,3,6,8-tetraphosphonate
pyz	pyrazine
PZDC	1 <i>H</i> -pyrazole-3,5-dicarboxylic acid
TBAPy	,3,6,8-tetrakis(<i>p</i> -benzoic-acid)pyrene
Tbip	5- <i>tert</i> -butyl isophthalic acid
TDC	thiophene-2,5-dicarboxylic acid
TED	triethylenediamine (DABCO)
THIPC	(<i>S</i>)-4,5,6,7-tetrahydro-1 <i>H</i> -imidazo[4,5- <i>c</i>]pyridine-6-carboxylate
Thr	threonine
TMBDC	2,3,5,6-tetramethyl-1,4-benzenedicarboxylic acid
TPA	terephthalic acid (BDC)
URPh	phenylurea
Val	valine

Miscellaneous

AC	adsorption chiller
ads	adsorption
AHP	adsorption-driven heat pump
BT	obtained from breakthrough experiments
DEG	diethylene glycol
des	desorption
EG	ethylene glycol
EN	ethylenediamine
FAM Z	functional adsorbent material zeolite
HK	high kinetic stability
LK	low kinetic stability
POM	polyoxometalate
RH	relative humidity
TEG	tryethylene glycol
ThS	thermodynamic stability
Uns	unstable

List of Symbols**Latin**

A	adsorption potential, kJ mol ⁻¹
COP	coefficient of performance
<i>c_p</i>	heat capacity, J g ⁻¹ K ⁻¹ /(J mol ⁻¹ K ⁻¹)
D	diameter, nm
<i>m</i>	mass, g
<i>M_w</i>	molar mass, g mol ⁻¹
<i>p</i>	pressure, bar
<i>p/p_o</i>	relative pressure
<i>p_o</i>	saturation pressure, bar

q amount adsorbed, g g⁻¹
energy, kJ mol⁻¹ (except for Figures 13, 16, and 17 where Q's are displayed per mL of sorbent (ρ_c used for conversion))

Q gas constant, J K⁻¹ mol⁻¹

T temperature, K

V_p pore volume, mL(liq) g⁻¹

W liquid volume adsorbed, mL(liq) g⁻¹ (except for Figures 8 and 14, where *W* is displayed in mL mL⁻¹ of sorbent (ρ_c used for conversion))

Greek

α p/p_o for which $q = 0.5q_{max}$

$\Delta_{ads}H$ enthalpy of adsorption, kJ mol⁻¹

$\Delta_{vap}H$ enthalpy of evaporation, kJ mol⁻¹

ϵ porosity

ρ density, g mL⁻¹

σ molecule size, nm

Subscripts

1 of point 1 (in Figure 9)

2 of point 2 (in Figure 9)

3 of point 3 (in Figure 9)

4 of point 4 (in Figure 9)

ads adsorber

b bulk

c critical (point)

c crystal(line)

C cooling (COP)

con condenser

des desorption

ev evaporator

H heating (COP)

hex heat exchanger

liq liquid

max maximum

min minimum

regen regeneration

sat at saturation

sorbent adsorbent

sorption adsorption

W for volume *W* adsorbed

Superscripts

effective effective

hex heat exchanger

sorbent adsorbent

wf working fluid

ΔH for which $\Delta_{ads}H$ is known

REFERENCES

- (1) Isaac, M.; van Vuuren, D. P. Modeling global residential sector energy demand for heating and air conditioning in the context of climate change. *Energy Policy* **2009**, *37*, S07–S21.
- (2) International Energy Agency, World Energy Outlook. 2011, p 696; http://www.iea.org/publications/freepublications/publication/weo2011_web.pdf (accessed 17-01-2015).
- (3) Eurostat Database for Energy Statistics. <http://ec.europa.eu/eurostat/web/energy/publications> (accessed 17-01-2015).
- (4) European Commission Energy. Projected primary energy consumption in 2020 (NL); http://ec.europa.eu/energy/efficiency/eed/reporting_en.htm (accessed 17-01-2015).
- (5) Agentschap N. L. Warmte in Nederland, publ. nr. 2NECW1003; <http://www.rvov.nl/sites/default/files/Warmte%20en%20Koude%20NL%202NECW1202%20jan13.pdf> (accessed 17-01-2015).

- (6) Tatsidjodoung, P.; Le Pierrès, N.; Luo, L. A review of potential materials for thermal energy storage in building applications. *Renewable Sustainable Energy Rev.* **2013**, *18*, 327–349.
- (7) Moran, M. J.; Shapiro, H. N. *Fundamentals of Engineering Thermodynamics*, 5th ed.; Wiley: New York, 2006.
- (8) Wongsuwan, W.; Kumar, S.; Neveu, P.; Meunier, F. A review of chemical heat pump technology and applications. *Appl. Therm. Eng.* **2001**, *21*, 1489–1519.
- (9) Fadhel, M. I.; Sopian, K.; Daud, W. R. W.; Alghoul, M. A. Review on advanced of solar assisted chemical heat pump dryer for agriculture produce. *Renewable Sustainable Energy Rev.* **2011**, *15*, 1152–1168.
- (10) Wu, W.; Zhang, X.; Li, X.; Shi, W.; Wang, B. Comparisons of different working pairs and cycles on the performance of absorption heat pump for heating and domestic hot water in cold regions. *Appl. Therm. Eng.* **2012**, *48*, 349–358.
- (11) Srivastava, N. C.; Eames, I. W. A review of adsorbents and adsorbates in solid–vapour adsorption heat pump systems. *Appl. Therm. Eng.* **1998**, *18*, 707–714.
- (12) Balaras, C. A.; Grossman, G.; Henning, H.-M.; Infante Ferreira, C. A.; Podesser, E.; Wang, L.; Wiemken, E. Solar air conditioning in Europe—an overview. *Renewable Sustainable Energy Rev.* **2007**, *11*, 299–314.
- (13) Henning, H.-M. Solar assisted air conditioning of buildings - an overview. *Appl. Therm. Eng.* **2007**, *27*, 1734–1749.
- (14) Henning, H. M.; Erpenbeck, T.; Hindenburg, C.; Santamaria, I. S. The potential of solar energy use in desiccant cooling cycles. *Int. J. Refrig.* **2001**, *24*, 220–229.
- (15) Grossman, G. Solar-powered systems for cooling, dehumidification and air-conditioning. *Sol. Energy* **2002**, *72*, 53–62.
- (16) Daou, K.; Wang, R. Z.; Xia, Z. Z. Desiccant cooling air conditioning: a review. *Renewable Sustainable Energy Rev.* **2006**, *10*, 55–77.
- (17) Zheng, X.; Ge, T.; Wang, R. Recent progress on desiccant materials for solid desiccant cooling systems. *Energy* **2014**, *74*, 280–294.
- (18) Hadorn, J. Advanced storage concepts for active solar energy—IEA SHC Task 32 2003–2007. Eurosun—1st international conference on solar heating, cooling and buildings. Lisbon, 2008.
- (19) Yu, N.; Wang, R. Z.; Wang, L. W. Sorption thermal storage for solar energy. *Prog. Energy Combust. Sci.* **2013**, *39*, 489–514.
- (20) Fernandez, A.; Martínez, M.; Segarra, M.; Martorell, I.; Cabeza, L. Selection of materials with potential in sensible thermal energy storage. *Sol. Energy Mater. Sol. Cells* **2010**, *94*, 1723–1729.
- (21) Sharma, A.; Tyagi, V.; Chen, C.; Buddhi, D. Review on thermal energy storage with phase change materials and applications. *Renewable Sustainable Energy Rev.* **2009**, *13*, 318–345.
- (22) Jeremias, F.; Lozan, V.; Henninger, S. K.; Janiak, C. Programming MOFs for water sorption: Amino-functionalized MIL-125 and UiO-66 for heat transformation and heat storage applications. *Dalton Trans.* **2013**, *42*, 15967–15973.
- (23) Critoph, R.; Zhong, Y. Review of trends in solid sorption refrigeration and heat pumping technology. *Proc. Inst. Mech. Eng., Part E* **2005**, *219*, 285–300.
- (24) Waszkiewicz, S. D. Adsorption refrigeration system using zeolite and methanol. Ph.D. Thesis, University of Bristol, 2003.
- (25) Critoph, R. E. Solid sorption cycles: A short history. *Int. J. Refrig.* **2012**, *35*, 490–493.
- (26) Plank, R.; Kuprianoff, J. *die Kleinkältemaschine*; Springer-Verlag: New York, 1948.
- (27) Hulse, G. Freight car refrigeration by an adsorption system employing silica gel. *Refrig. Eng.* **1929**, *17*, 41–54.
- (28) Miller, E. The development of silica gel refrigeration. *Am. Soc. Refrig. Eng.* **1929**, *17*, 103–108.
- (29) U.N.E.P. *Handbook for the Montreal Protocol on Substances that Deplete the Ozone Layer*, 7th ed.; 2006.
- (30) Meunier, F. Solid sorption: An alternative to CFCs. *Heat Recovery Syst. CHP* **1993**, *13*, 289–295.
- (31) Meunier, F. Adsorption heat powered heat pumps. *Appl. Therm. Eng.* **2013**, *61*, 830–836.
- (32) Kanamori, M.; Hiramatsu, M.; Katsurayama, K.; Watanabe, F.; Matsuda, H.; Hasatani, M. Production of Cold Heat Energy by Alcohol/Activated Carbon Adsorption Heat Pump with a Disk-Module-Type Adsorber. *J. Chem. Eng. Jpn.* **1997**, *30*, 434–439.
- (33) Demir, H.; Mobedi, M.; Ülkü, S. A review on adsorption heat pump: Problems and solutions. *Renewable Sustainable Energy Rev.* **2008**, *12*, 2381–2403.
- (34) Saha, B.; El-Sharkawy, I.; Chakraborty, A.; Koyama, S. Study on an activated carbon fiber–ethanol adsorption chiller: Part I—system description and modelling. *Int. J. Refrig.* **2007**, *30*, 86–95.
- (35) Green, D. W.; Perry, R. H. *Perry's Chemical Engineers' Handbook*, 8th ed.; McGraw-Hill: New York, 2008.
- (36) Wang, L. W.; Wang, R. Z.; Oliveira, R. G. A review on adsorption working pairs for refrigeration. *Renewable Sustainable Energy Rev.* **2009**, *13*, 518–534.
- (37) Aristov, Y. I. Challenging offers of material science for adsorption heat transformation: A review. *Appl. Therm. Eng.* **2013**, *50*, 1610–1618.
- (38) Glaznev, I. S.; Ovoshchnikov, D. S.; Aristov, Y. I. Kinetics of water adsorption/desorption under isobaric stages of adsorption heat transformers: The effect of isobar shape. *Int. J. Heat Mass Transfer* **2009**, *52*, 1774–1777.
- (39) Okunev, B. N.; Gromov, A. P.; Aristov, Y. I. Modelling of isobaric stages of adsorption cooling cycle: An optimal shape of adsorption isobar. *Appl. Therm. Eng.* **2013**, *53*, 89–95.
- (40) Jeremias, F.; Khutia, A.; Henniger, S. K.; Janiak, C. MIL-100(Al, Fe) as water adsorbents for heat transformation purposes - A promising application. *J. Mater. Chem.* **2012**, *22*, 10148–10151.
- (41) Yonezawa, Y. M.; Masao; Oku, K.; Nakano, H.; Okumura, S.-i.; Yoshihara, M.; Sakai, A.; Morikawa, A. Adsorption refrigeration system. U.S. Patent 4881376, 1989.
- (42) Wang, R. Z.; Oliveira, R. G. Adsorption refrigeration—An efficient way to make good use of waste heat and solar energy. *Prog. Energy Combust. Sci.* **2006**, *32*, 424–458.
- (43) Invensor. <http://www.invensor.com/en/technology/cooling-system.htm> (accessed 17-01-2015).
- (44) Dawoud, B.; Hoefle, P.; Bornmann, A.; Chmielewski, S.; Marburger, C. Vacuum sorption apparatus. U.S. Patent 8544293, 2013.
- (45) Shimooka, S.; Oshima, K.; Hidaka, H.; Takewaki, T.; Kakiuchi, H.; Kodama, A.; Kubota, M.; Matsuda, H. The evaluation of direct cooling and heating desiccant device coated with FAM. *J. Chem. Eng. Jpn.* **2007**, *40*, 1330–1334.
- (46) Kakiuchi, H.; Shimooka, S.; Iwade, M.; Oshima, K.; Yamazaki, M.; Terada, S.; Watanabe, H.; Takewaki, T. Novel water vapor adsorbent FAM-Z01 and its applicability to an adsorption heat pump. *Kagaku Kogaku Ronbunshu* **2005**, *31*, 361–364.
- (47) Kakiuchi, H.; Shimooka, S.; Iwade, M.; Oshima, K.; Yamazaki, M.; Terada, S.; Watanabe, H.; Takewaki, T. Water vapor adsorbent FAM-Z02 and its applicability to adsorption heat pump. *Kagaku Kogaku Ronbunshu* **2005**, *31*, 273–277.
- (48) Mitsubishi Plastics. Zeolitic Water Vapor Adsorbent: AQSOA. http://www.aaasaveenergy.com/products/001/pdf/AQSOA_1210E.pdf (accessed 17-01-2015).
- (49) Henniger, S. K.; Munz, G.; Ratzsch, K. F.; Schossig, P. Cycle stability of sorption materials and composites for the use in heat pumps and cooling machines. *Renewable Energy* **2011**, *36*, 3043–3049.
- (50) Chen, H.; Cui, Q.; Wu, J.; Zhu, Y.; Li, Q.; Zheng, K.; Yao, H. Hydrothermal stability of SAPO-34 for refrigeration and air conditioning applications. *Mater. Res. Bull.* **2014**, *52*, 82–88.
- (51) Restuccia, G.; Freni, A.; Maggio, G. A zeolite-coated bed for air conditioning adsorption systems: parametric study of heat and mass transfer by dynamic simulation. *Appl. Therm. Eng.* **2002**, *22*, 619–630.
- (52) Pons, M.; Poyelle, F. Adsorptive machines with advanced cycles for heat pumping or cooling applications: Cycles à adsorption pour pompes à chaleur ou machines frigorifiques: figures. *Int. J. Refrig.* **1999**, *22*, 27–37.
- (53) Aristov, Y. I. Novel Materials for Adsorptive Heat Pumping and Storage: Screening and Nanotailoring of Sorption Properties. *J. Chem. Eng. Jpn.* **2007**, *40*, 1242–1251.

- (54) Aristov, Y. New family of solid sorbents for adsorptive cooling: Material scientist approach. *J. Eng. Thermophys.* **2007**, *16*, 63–72.
- (55) Henninger, S. K.; Schmidt, F. P.; Henning, H. M. Water adsorption characteristics of novel materials for heat transformation applications. *Appl. Therm. Eng.* **2010**, *30*, 1692–1702.
- (56) Janiak, C.; Henninger, S. K. Porous coordination polymers as novel sorption materials for heat transformation processes. *Chimia* **2013**, *67*, 419–424.
- (57) Kitagawa, S.; Kitaura, R.; Noro, S.-i. Functional Porous Coordination Polymers. *Angew. Chem., Int. Ed.* **2004**, *43*, 2334–2375.
- (58) Tranchemontagne, D. J.; Mendoza-Cortes, J. L.; O’Keeffe, M.; Yaghi, O. M. Secondary building units, nets and bonding in the chemistry of metal-organic frameworks. *Chem. Soc. Rev.* **2009**, *38*, 1257–1283.
- (59) Farha, O. K.; Eryazici, I.; Jeong, N. C.; Hauser, B. G.; Wilmer, C. E.; Sarjeant, A. A.; Snurr, R. Q.; Nguyen, S. T.; Yazaydin, A. O. z. r.; Hupp, J. T. Metal–Organic Framework Materials with Ultrahigh Surface Areas: Is the Sky the Limit? *J. Am. Chem. Soc.* **2012**, *134*, 15016–15021.
- (60) Furukawa, H.; Ko, N.; Go, Y. B.; Aratani, N.; Choi, S. B.; Choi, E.; Yazaydin, A. Ö.; Snurr, R. Q.; O’Keeffe, M.; Kim, J.; Yaghi, O. M. Ultrahigh Porosity in Metal-Organic Frameworks. *Science* **2010**, *329*, 424–428.
- (61) Yang, Q.; Wiersum, A. D.; Llewellyn, P. L.; Guillerm, V.; Serre, C.; Maurin, G. Functionalizing porous zirconium terephthalate UiO-66(Zr) for natural gas upgrading: a computational exploration. *Chem. Commun.* **2011**, *47*, 9603–9605.
- (62) Cmarik, G. E.; Kim, M.; Cohen, S. M.; Walton, K. S. Tuning the Adsorption Properties of UiO-66 via Ligand Functionalization. *Langmuir* **2012**, *28*, 15606–15613.
- (63) Tanabe, K. K.; Wang, Z.; Cohen, S. M. Systematic Functionalization of a Metal–Organic Framework via a Postsynthetic Modification Approach. *J. Am. Chem. Soc.* **2008**, *130*, 8508–8517.
- (64) Kim, M.; Cahill, J. F.; Su, Y.; Prather, K. A.; Cohen, S. M. Postsynthetic ligand exchange as a route to functionalization of ‘inert’ metal-organic frameworks. *Chem. Sci.* **2012**, *3*, 126–130.
- (65) Goesten, M. G.; Juan-Alcañiz, J.; Ramos-Fernandez, E. V.; Sai Sankar Gupta, K. B.; Stavitski, E.; van Bekkum, H.; Gascon, J.; Kapteijn, F. Sulfation of metal-organic frameworks: Opportunities for acid catalysis and proton conductivity. *J. Catal.* **2011**, *281*, 177–187.
- (66) Güçüyener, C.; van den Bergh, J.; Gascon, J.; Kapteijn, F. Ethane/ethene separation turned on its head: Selective ethane adsorption on the metal– organic framework ZIF-7 through a gate-opening mechanism. *J. Am. Chem. Soc.* **2010**, *132*, 17704–17706.
- (67) van den Bergh, J.; Güçüyener, C.; Pidko, E. A.; Hensen, E. J.; Gascon, J.; Kapteijn, F. Understanding the anomalous alkane selectivity of ZIF-7 in the separation of light alkane/alkene mixtures. *Chem. - Eur. J.* **2011**, *17*, 8832–8840.
- (68) Li, J.-R.; Kuppler, R. J.; Zhou, H.-C. Selective gas adsorption and separation in metal-organic frameworks. *Chem. Soc. Rev.* **2009**, *38*, 1477–1504.
- (69) Couck, S.; Denayer, J. F. M.; Baron, G. V.; Rémy, T.; Gascon, J.; Kapteijn, F. An amine-functionalized MIL-53 Metal–Organic Framework with large separation power for CO₂ and CH₄. *J. Am. Chem. Soc.* **2009**, *131*, 6326–6327.
- (70) Murray, L. J.; Dinca, M.; Long, J. R. Hydrogen storage in metal-organic frameworks. *Chem. Soc. Rev.* **2009**, *38*, 1294–1314.
- (71) Choi, H. J.; Dinca, M.; Dailly, A.; Long, J. R. Hydrogen storage in water-stable metal-organic frameworks incorporating 1,3- and 1,4-benzenedipyrazolate. *Energy Environ. Sci.* **2010**, *3*, 117–123.
- (72) Gascon, J.; Hernández-Alonso, M. D.; Almeida, A. R.; van Klink, G. P. M.; Kapteijn, F.; Mul, G. Isoreticular MOFs as Efficient Photocatalysts with Tunable Band Gap: An Operando FTIR Study of the Photoinduced Oxidation of Propylene. *ChemSusChem* **2008**, *1*, 981–983.
- (73) Gascon, J.; Aktay, U.; Hernandez-Alonso, M. D.; van Klink, G. P. M.; Kapteijn, F. Amino-based metal-organic frameworks as stable, highly active basic catalysts. *J. Catal.* **2009**, *261*, 75–87.
- (74) Hasegawa, S.; Horike, S.; Matsuda, R.; Furukawa, S.; Mochizuki, K.; Kinoshita, Y.; Kitagawa, S. Three-Dimensional Porous Coordination Polymer Functionalized with Amide Groups Based on Tridentate Ligand: Selective Sorption and Catalysis. *J. Am. Chem. Soc.* **2007**, *129*, 2607–2614.
- (75) Lee, J.; Farha, O. K.; Roberts, J.; Scheidt, K. A.; Nguyen, S. T.; Hupp, J. T. Metal-organic framework materials as catalysts. *Chem. Soc. Rev.* **2009**, *38*, 1450–1459.
- (76) Canivet, J.; Fateeva, A.; Guo, Y.; Coasne, B.; Farrusseng, D. Water adsorption in MOFs: fundamentals and applications. *Chem. Soc. Rev.* **2014**, *43*, 5594.
- (77) Canivet, J.; Bonnefoy, J.; Daniel, C.; Legrand, A.; Coasne, B.; Farrusseng, D. Structure–property relationships of water adsorption in metal–organic frameworks. *New J. Chem.* **2014**, *38*, 3102.
- (78) Coasne, B.; Gubbins, K. E.; Pellenq, R. J.-M. Temperature effect on adsorption/desorption isotherms for a simple fluid confined within various nanopores. *Adsorption* **2005**, *11*, 289–294.
- (79) Coasne, B.; Galarneau, A.; Pellenq, R. J. M.; Di Renzo, F. Adsorption, intrusion and freezing in porous silica: the view from the nanoscale. *Chem. Soc. Rev.* **2013**, *42*, 4141–4171.
- (80) De Lange, M. F.; Gutierrez-Sevillano, J.-J.; Hamad, S.; Vlugt, T. J. H.; Calero, S.; Gascon, J.; Kapteijn, F. Understanding Adsorption of Highly Polar Vapors on Mesoporous MIL-100(Cr) and MIL-101(Cr): Experiments and Molecular Simulations. *J. Phys. Chem. C* **2013**, *117*, 7613–7622.
- (81) Guillot, B. A reappraisal of what we have learnt during three decades of computer simulations on water. *J. Mol. Liq.* **2002**, *101*, 219–260.
- (82) Castillo, J. M.; Vlugt, T. J. H.; Calero, S. a. Understanding Water Adsorption in Cu–BTC Metal–Organic Frameworks. *J. Phys. Chem. C* **2008**, *112*, 15934–15939.
- (83) Paranthaman, S.; Coudert, F.-X.; Fuchs, A. H. Water adsorption in hydrophobic MOF channels. *Phys. Chem. Chem. Phys.* **2010**, *12*, 8123–8129.
- (84) Dubbeldam, D.; Torres-Knoop, A.; Walton, K. S. On the inner workings of Monte Carlo codes. *Mol. Simul.* **2013**, *39*, 1253–1292.
- (85) Ghosh, P.; Colon, Y. J.; Snurr, R. Q. Water adsorption in UiO-66: the importance of defects. *Chem. Commun.* **2014**, *50*, 11329.
- (86) Zang, J.; Nair, S.; Sholl, D. S. Prediction of Water Adsorption in Copper-Based Metal–Organic Frameworks Using Force Fields Derived from Dispersion-Corrected DFT Calculations. *J. Phys. Chem. C* **2013**, *117*, 7519–7525.
- (87) Fang, H.; Kamakoti, P.; Zang, J.; Cundy, S.; Paur, C.; Ravikovich, P. I.; Sholl, D. S. Prediction of CO₂ Adsorption Properties in Zeolites Using Force Fields Derived from Periodic Dispersion-Corrected DFT Calculations. *J. Phys. Chem. C* **2012**, *116*, 10692–10701.
- (88) Fang, H.; Kamakoti, P.; Ravikovich, P. I.; Aronson, M.; Paur, C.; Sholl, D. S. First principles derived, transferable force fields for CO₂ adsorption in Na-exchanged cationic zeolites. *Phys. Chem. Chem. Phys.* **2013**, *15*, 12882–12894.
- (89) Lin, L.-C.; Lee, K.; Gagliardi, L.; Neaton, J. B.; Smit, B. Force-Field Development from Electronic Structure Calculations with Periodic Boundary Conditions: Applications to Gaseous Adsorption and Transport in Metal–Organic Frameworks. *J. Chem. Theory Comput.* **2014**, *10*, 1477–1488.
- (90) Colón, Y. J.; Fairén-Jimenez, D.; Wilmer, C. E.; Snurr, R. Q. High-Throughput Screening of Porous Crystalline Materials for Hydrogen Storage Capacity near Room Temperature. *J. Phys. Chem. C* **2014**, *118*, 5383–5389.
- (91) Wilmer, C. E.; Snurr, R. Q. Towards rapid computational screening of metal-organic frameworks for carbon dioxide capture: Calculation of framework charges via charge equilibration. *Chem. Eng. J.* **2011**, *171*, 775–781.
- (92) Fernandez, M.; Boyd, P. G.; Daff, T. D.; Aghajani, M. Z.; Woo, T. K. Rapid and Accurate Machine Learning Recognition of High Performing Metal Organic Frameworks for CO₂ Capture. *J. Phys. Chem. Lett.* **2014**, *5*, 3056–3060.

- (93) Lively, R. P.; Dose, M. E.; Thompson, J. A.; McCool, B. A.; Chance, R. R.; Koros, W. J. Ethanol and water adsorption in methanol-derived ZIF-71. *Chem. Commun.* **2011**, *47*, 8667–8669.
- (94) Chen, Y. F.; Lee, J. Y.; Babarao, R.; Li, J.; Jiang, J. W. A Highly Hydrophobic Metal–Organic Framework Zn(BDC) (TED)0.5 for Adsorption and Separation of CH₃OH/H₂O and CO₂/CH₄: An Integrated Experimental and Simulation Study. *J. Phys. Chem. C* **2010**, *114*, 6602–6609.
- (95) Zhang, K.; Zhang, L.; Jiang, J. Adsorption of C1–C4 Alcohols in Zeolitic Imidazolate Framework-8: Effects of Force Fields, Atomic Charges, and Framework Flexibility. *J. Phys. Chem. C* **2013**, *117*, 25628–25635.
- (96) Van Assche, T. R. C.; Duerinck, T.; Gutiérrez Sevillano, J. J.; Calero, S.; Baron, G. V.; Denayer, J. F. M. High Adsorption Capacities and Two-Step Adsorption of Polar Adsorbates on Copper–Benzene-1,3,5-tricarboxylate Metal–Organic Framework. *J. Phys. Chem. C* **2013**, *117*, 18100–18111.
- (97) Yu, D.; Ghosh, P.; Snurr, R. Q. Hierarchical modeling of ammonia adsorption in functionalized metal–organic frameworks. *Dalton Trans.* **2012**, *41*, 3962–3973.
- (98) Kim, K. C.; Yu, D.; Snurr, R. Q. Computational Screening of Functional Groups for Ammonia Capture in Metal–Organic Frameworks. *Langmuir* **2013**, *29*, 1446–1456.
- (99) Ghosh, P.; Kim, K. C.; Snurr, R. Q. Modeling Water and Ammonia Adsorption in Hydrophobic Metal–Organic Frameworks: Single Components and Mixtures. *J. Phys. Chem. C* **2014**, *118*, 1102–1110.
- (100) Burtch, N. C.; Jasuja, H.; Walton, K. S. Water Stability and Adsorption in Metal–Organic Frameworks. *Chem. Rev.* **2014**, *114*, 10575–10612.
- (101) De Lange, M. F.; Vlugt, T. J. H.; Gascon, J.; Kapteijn, F. Adsorptive characterization of porous solids: Error analysis guides the way. *Microporous Mesoporous Mater.* **2014**, *200*, 199–215.
- (102) Low, J. J.; Benin, A. I.; Jakubczak, P.; Abrahamian, J. F.; Faheem, S. A.; Willis, R. R. Virtual High Throughput Screening Confirmed Experimentally: Porous Coordination Polymer Hydration. *J. Am. Chem. Soc.* **2009**, *131*, 15834–15842.
- (103) Qadir, N. u.; Said, S. A. M.; Bahaidarah, H. M. Structural stability of metal organic frameworks in aqueous media – Controlling factors and methods to improve hydrostability and hydrothermal cyclic stability. *Microporous Mesoporous Mater.* **2015**, *201*, 61–90.
- (104) DeCoste, J. B.; Peterson, G. W.; Jasuja, H.; Glover, T. G.; Huang, Y.-g.; Walton, K. S. Stability and degradation mechanisms of metal–organic frameworks containing the Zr₆O₄(OH)₄ secondary building unit. *J. Mater. Chem. A* **2013**, *1*, 5642–5650.
- (105) DeCoste, J. B.; Peterson, G. W.; Schindler, B. J.; Killops, K. L.; Browne, M. A.; Mahle, J. J. The effect of water adsorption on the structure of the carboxylate containing metal–organic frameworks Cu-BTC, Mg-MOF-74, and UiO-66. *J. Mater. Chem. A* **2013**, *1*, 11922–11932.
- (106) Cavka, J. H.; Jakobsen, S.; Olsbye, U.; Guillou, N.; Lamberti, C.; Bordiga, S.; Lillerud, K. P. A new zirconium inorganic building brick forming metal organic frameworks with exceptional stability. *J. Am. Chem. Soc.* **2008**, *130*, 13850–13851.
- (107) Bon, V.; Senkovska, I.; Weiss, M. S.; Kaskel, S. Tailoring of network dimensionality and porosity adjustment in Zr- and Hf-based MOFs. *CrystEngComm* **2013**, *15*, 9572–9577.
- (108) Li, P.; Chen, J.; Zhang, J.; Wang, X. Water Stability and Competition Effects Toward CO₂ Adsorption on Metal Organic Frameworks. *Sep. Purif. Rev.* **2015**, *44*, 19–27.
- (109) Colombo, V.; Galli, S.; Choi, H. J.; Han, G. D.; Maspero, A.; Palmisano, G.; Masciocchi, N.; Long, J. R. High thermal and chemical stability in pyrazolate-bridged metal–organic frameworks with exposed metal sites. *Chem. Sci.* **2011**, *2*, 1311–1319.
- (110) Jasuja, H.; Burtch, N. C.; Huang, Y.-g.; Cai, Y.; Walton, K. S. Kinetic Water Stability of an Isostructural Family of Zinc-Based Pillared Metal–Organic Frameworks. *Langmuir* **2013**, *29*, 633–642.
- (111) Rosi, N. L.; Kim, J.; Eddaoudi, M.; Chen, B.; O’Keeffe, M.; Yaghi, O. M. Rod Packings and Metal–Organic Frameworks Constructed from Rod-Shaped Secondary Building Units. *J. Am. Chem. Soc.* **2005**, *127*, 1504–1518.
- (112) Tan, K.; Nijem, N.; Canepa, P.; Gong, Q.; Li, J.; Thonhauser, T.; Chabal, Y. J. Stability and Hydrolyzation of Metal Organic Frameworks with Paddle-Wheel SBUs upon Hydration. *Chem. Mater.* **2012**, *24*, 3153–3167.
- (113) Chabal, Y. J.; Tan, K.; Nijem, N.; Zuluaga, S.; Gao, Y.; Li, J.; Thonhauser, T. Water Interactions in Metal Organic Frameworks. *CrystEngComm* **2015**, *17*, 247.
- (114) Cychoz, K. A.; Matzger, A. J. Water Stability of Microporous Coordination Polymers and the Adsorption of Pharmaceuticals from Water. *Langmuir* **2010**, *26*, 17198–17202.
- (115) Zhang, Z.; Yao, Z.-Z.; Xiang, S.; Chen, B. Perspective of Microporous Metal–Organic Frameworks for CO₂ Capture and Separation. *Energy Environ. Sci.* **2014**, *7*, 2868.
- (116) Bhunia, M. K.; Hughes, J. T.; Fettinger, J. C.; Navrotsky, A. Thermochemistry of Paddle Wheel MOFs: Cu-HKUST-1 and Zn-HKUST-1. *Langmuir* **2013**, *29*, 8140–8145.
- (117) Kang, J. J.; Khan, N. A.; Haque, E.; Jhung, S. H. Chemical and Thermal Stability of Isotypic Metal–Organic Frameworks: Effect of Metal Ions. *Chem. - Eur. J.* **2011**, *17*, 6437–6442.
- (118) Kaye, S. S.; Dailly, A.; Yaghi, O. M.; Long, J. R. Impact of Preparation and Handling on the Hydrogen Storage Properties of Zn₄O(1,4-benzenedicarboxylate)₃ (MOF-5). *J. Am. Chem. Soc.* **2007**, *129*, 14176–14177.
- (119) De Toni, M.; Jonchiere, R.; Pullumbi, P.; Coudert, F.-X.; Fuchs, A. H. How Can a Hydrophobic MOF be Water-Unstable? Insight into the Hydration Mechanism of IRMOFs. *ChemPhysChem* **2012**, *13*, 3497–3503.
- (120) Bellarosa, L.; Castillo, J. M.; Vlugt, T. J. H.; Calero, S.; López, N. On the mechanism behind the instability of isoreticular metal–organic frameworks (IRMOFs) in humid environments. *Chem. - Eur. J.* **2012**, *18*, 12260–12266.
- (121) Greathouse, J. A.; Allendorf, M. D. The interaction of water with MOF-5 simulated by molecular dynamics. *J. Am. Chem. Soc.* **2006**, *128*, 10678–10679.
- (122) Han, S. S.; Choi, S.-H.; van Duin, A. C. T. Molecular dynamics simulations of stability of metal–organic frameworks against H₂O using the ReaxFF reactive force field. *Chem. Commun.* **2010**, *46*, 5713–5715.
- (123) Gomes Silva, C.; Luz, I.; Llabrés i Xamena, F. X.; Corma, A.; García, H. Water Stable Zr–Benzenedicarboxylate Metal–Organic Frameworks as Photocatalysts for Hydrogen Generation. *Chem. - Eur. J.* **2010**, *16*, 11133–11138.
- (124) Stavitski, E.; Goesten, M.; Juan-Alcañiz, J.; Martinez-Joaristi, A.; Serra-Crespo, P.; Petukhov, A. V.; Gascon, J.; Kapteijn, F. Kinetic Control of Metal–Organic Framework Crystallization Investigated by Time-Resolved In Situ X-Ray Scattering. *Angew. Chem., Int. Ed.* **2011**, *50*, 9624–9628.
- (125) Wittmann, T.; Siegel, R.; Reimer, N.; Milius, W.; Stock, N.; Senker, J. Enhancing the Water Stability of Al-MIL-101-NH₂ via Postsynthetic Modification. *Chem. - Eur. J.* **2015**, *21*, 314–323.
- (126) Bauer, S.; Serre, C.; Devic, T.; Horcajada, P.; Marrot, J. r. m.; Férey, G. r.; Stock, N. High-Throughput Assisted Rationalization of the Formation of Metal Organic Frameworks in the Iron(III) Aminoterephthalate Solvothermal System. *Inorg. Chem.* **2008**, *47*, 7568–7576.
- (127) Wittmann, T.; Siegel, R.; Reimer, N.; Milius, W.; Stock, N.; Senker, J. Enhancing the Water Stability of Al-MIL-101-NH₂ via Postsynthetic Modification. *Chem. - Eur. J.* **2015**, *21*, 314–323.
- (128) Bezverkhyy, I.; Ortiz, G.; Chaplais, G.; Marichal, C.; Weber, G.; Bellat, J.-P. MIL-53(Al) under reflux in water: Formation of γ -Al(OH) shell and H₂BDC molecules intercalated into the pores. *Microporous Mesoporous Mater.* **2014**, *183*, 156–161.
- (129) Qian, X.; Yadian, B.; Wu, R.; Long, Y.; Zhou, K.; Zhu, B.; Huang, Y. Structure stability of metal–organic framework MIL-53 (Al) in aqueous solutions. *Int. J. Hydrogen Energy* **2013**, *38*, 16710–16715.
- (130) Yang, S. J.; Park, C. R. Preparation of Highly Moisture-Resistant Black-Colored Metal Organic Frameworks. *Adv. Mater.* **2012**, *24*, 4010–4013.

- (131) Gadielli, S.; Guo, Z. Postsynthesis Annealing of MOF-5 Remarkably Enhances the Framework Structural Stability and CO₂ Uptake. *Chem. Mater.* **2014**, *26*, 6333.
- (132) Wu, C.-M.; Rathi, M.; Ahrenkiel, S. P.; Koodali, R. T.; Wang, Z. Facile synthesis of MOF-5 confined in SBA-15 hybrid material with enhanced hydrostability. *Chem. Commun.* **2013**, *49*, 1223–1225.
- (133) Yang, S. J.; Choi, J. Y.; Chae, H. K.; Cho, J. H.; Nahm, K. S.; Park, C. R. Preparation and Enhanced Hydrostability and Hydrogen Storage Capacity of CNT@MOF-5 Hybrid Composite. *Chem. Mater.* **2009**, *21*, 1893–1897.
- (134) Liu, X.; Li, Y.; Ban, Y.; Peng, Y.; Jin, H.; Bux, H.; Xu, L.; Caro, J.; Yang, W. Improvement of hydrothermal stability of zeolitic imidazolate frameworks. *Chem. Commun.* **2013**, *49*, 9140–9142.
- (135) Li, T.; Chen, D.-L.; Sullivan, J. E.; Kozlowski, M. T.; Johnson, J. K.; Rosi, N. L. Systematic modulation and enhancement of CO₂: N₂ selectivity and water stability in an isoreticular series of bio-MOF-11 analogues. *Chem. Sci.* **2013**, *4*, 1746–1755.
- (136) Li, T.; Sullivan, J. E.; Rosi, N. L. Design and Preparation of a Core–Shell Metal–Organic Framework for Selective CO₂ Capture. *J. Am. Chem. Soc.* **2013**, *135*, 9984–9987.
- (137) Rao, K. P.; Higuchi, M.; Sumida, K.; Furukawa, S.; Duan, J.; Kitagawa, S. Design of Superhydrophobic Porous Coordination Polymers through the Introduction of External Surface Corrugation by the Use of an Aromatic Hydrocarbon Building Unit. *Angew. Chem.* **2014**, *126*, 8364–8369.
- (138) Decoste, J. B.; Peterson, G. W.; Smith, M. W.; Stone, C. A.; Willis, C. R. Enhanced Stability of Cu-BTC MOF via Perfluorohexane Plasma-Enhanced Chemical Vapor Deposition. *J. Am. Chem. Soc.* **2012**, *134*, 1486–1489.
- (139) Zornoza, B.; Tellez, C.; Coronas, J.; Gascon, J.; Kapteijn, F. Metal organic framework based mixed matrix membranes: an increasingly important field of research with a large application potential. *Microporous Mesoporous Mater.* **2013**, *166*, 67–78.
- (140) Zornoza, B.; Martinez-Joaristi, A.; Serra-Crespo, P.; Tellez, C.; Coronas, J.; Gascon, J.; Kapteijn, F. Functionalized flexible MOFs as fillers in mixed matrix membranes for highly selective separation of CO₂ from CH₄ at elevated pressures. *Chem. Commun.* **2011**, *47*, 9522–9524.
- (141) Nik, O. G.; Chen, X. Y.; Kaliaguine, S. Functionalized metal organic framework-polyimide mixed matrix membranes for CO₂/CH₄ separation. *J. Membr. Sci.* **2012**, *413*, 48–61.
- (142) Jeazet, H. B. T.; Staudt, C.; Janiak, C. Metal–organic frameworks in mixed-matrix membranes for gas separation. *Dalton Trans.* **2012**, *41*, 14003–14027.
- (143) Perez, E. V.; Balkus, K. J., Jr; Ferraris, J. P.; Musselman, I. H. Mixed-matrix membranes containing MOF-5 for gas separations. *J. Membr. Sci.* **2009**, *328*, 165–173.
- (144) Rodenas, T.; Luz, I.; Prieto, G.; Seoane, B.; Miro, H.; Corma, A.; Kapteijn, F.; i Xamena, F. X. L.; Gascon, J. Metal–organic framework nanosheets in polymer composite materials for gas separation. *Nat. Mater.* **2014**, *14*, 48.
- (145) Rodenas, T.; van Dalen, M.; García-Pérez, E.; Serra-Crespo, P.; Zornoza, B.; Kapteijn, F.; Gascon, J. Visualizing MOF Mixed Matrix Membranes at the Nanoscale: Towards Structure-Performance Relationships in CO₂/CH₄ Separation Over NH₂-MIL-53 (Al)@PI. *Adv. Funct. Mater.* **2014**, *24*, 249–256.
- (146) Yoo, Y.; Varela-Guerrero, V.; Jeong, H.-K. Isoreticular Metal–Organic Frameworks and Their Membranes with Enhanced Crack Resistance and Moisture Stability by Surfactant-Assisted Drying. *Langmuir* **2011**, *27*, 2652–2657.
- (147) Jasuja, H.; Walton, K. S. Effect of catenation and basicity of pillared ligands on the water stability of MOFs. *Dalton Trans.* **2013**, *42*, 15421–15426.
- (148) Taylor, J. M.; Vaidhyanathan, R.; Iremonger, S. S.; Shimizu, G. K. H. Enhancing Water Stability of Metal–Organic Frameworks via Phosphonate Monoester Linkers. *J. Am. Chem. Soc.* **2012**, *134*, 14338–14340.
- (149) Taylor, J. M.; Dawson, K. W.; Shimizu, G. K. H. A Water-Stable Metal–Organic Framework with Highly Acidic Pores for Proton-Conducting Applications. *J. Am. Chem. Soc.* **2013**, *135*, 1193–1196.
- (150) Wu, T.; Shen, L.; Luebbers, M.; Hu, C.; Chen, Q.; Ni, Z.; Masel, R. I. Enhancing the stability of metal–organic frameworks in humid air by incorporating water repellent functional groups. *Chem. Commun.* **2010**, *46*, 6120–6122.
- (151) Yang, C.; Kaipa, U.; Mather, Q. Z.; Wang, X.; Nesterov, V.; Venero, A. F.; Omary, M. A. Fluorous Metal–Organic Frameworks with Superior Adsorption and Hydrophobic Properties toward Oil Spill Cleanup and Hydrocarbon Storage. *J. Am. Chem. Soc.* **2011**, *133*, 18094–18097.
- (152) Jasuja, H.; Huang, Y.-g.; Walton, K. S. Adjusting the Stability of Metal–Organic Frameworks under Humid Conditions by Ligand Functionalization. *Langmuir* **2012**, *28*, 16874–16880.
- (153) Chen, T.-H.; Popov, I.; Zenasni, O.; Daugulis, O.; Miljančić, O. Š. Superhydrophobic perfluorinated metal–organic frameworks. *Chem. Commun.* **2013**, *49*, 6846–6848.
- (154) Serre, C. Superhydrophobicity in Highly Fluorinated Porous Metal–Organic Frameworks. *Angew. Chem., Int. Ed.* **2012**, *51*, 6048–6050.
- (155) Yang, J.; Grzech, A.; Mulder, F. M.; Dingemans, T. J. Methyl modified MOF-5: a water stable hydrogen storage material. *Chem. Commun.* **2011**, *47*, 5244–5246.
- (156) Cai, Y.; Zhang, Y.; Huang, Y.; Marder, S. R.; Walton, K. S. Impact of Alkyl-Functionalized BTC on Properties of Copper-Based Metal–Organic Frameworks. *Cryst. Growth Des.* **2012**, *12*, 3709–3713.
- (157) Jasuja, H.; Jiao, Y.; Burtch, N. C.; Huang, Y.-g.; Walton, K. S. Synthesis of Cobalt, Nickel, Copper, and Zinc-based Water Stable Pillared Metal–Organic Frameworks. *Langmuir* **2014**, *30*, 14300–14307.
- (158) Makal, T. A.; Wang, X.; Zhou, H.-C. Tuning the Moisture and Thermal Stability of Metal–Organic Frameworks through Incorporation of Pendant Hydrophobic Groups. *Cryst. Growth Des.* **2013**, *13*, 4760–4768.
- (159) Zhang, Z.; Zhao, Y.; Gong, Q.; Li, Z.; Li, J. MOFs for CO₂ capture and separation from flue gas mixtures: the effect of multifunctional sites on their adsorption capacity and selectivity. *Chem. Commun.* **2013**, *49*, 653–661.
- (160) Ma, D.; Li, Y.; Li, Z. Tuning the moisture stability of metal–organic frameworks by incorporating hydrophobic functional groups at different positions of ligands. *Chem. Commun.* **2011**, *47*, 7377–7379.
- (161) Zhang, J.-W.; Zhao, C.-C.; Zhao, Y.-P.; Xu, H.-Q.; Du, Z.-Y.; Jiang, H.-L. Metal-organic frameworks with improved moisture stability based on a phosphonate monoester: effect of auxiliary N-donor ligands on framework dimensionality. *CrystEngComm* **2014**, *16*, 6635–6644.
- (162) Im, J. H.; Ko, N.; Yang, S. J.; Park, H. J.; Kim, J.; Park, C. R. Enhanced water stability and CO₂ gas sorption properties of a methyl functionalized titanium metal-organic framework. *New J. Chem.* **2014**, *38*, 2752–2755.
- (163) Wang, J.-H.; Li, M.; Li, D. An Exceptionally Stable and Water-Resistant Metal–Organic Framework with Hydrophobic Nanospaces for Extracting Aromatic Pollutants from Water. *Chem. - Eur. J.* **2014**, *20*, 12004–12008.
- (164) Ma, D.-Y.; Li, X.; Wu, X.-G.; Chen, X.-Q.; Xu, Z.-R.; Liu, F.-D.; Huang, D.-F.; Guo, H.-F. Improving the moisture stability of a 3D zinc-organic framework by incorporating methyl groups into the auxiliary ligand: synthesis, characterization, luminescence and catalytic properties. *J. Mol. Struct.* **2015**, *1083*, 421.
- (165) Lin, Y.; Zhang, Q.; Zhao, C.; Li, H.; Kong, C.; Shen, C.; Chen, L. An exceptionally stable functionalized metal-organic framework for lithium storage. *Chem. Commun.* **2014**.
- (166) Racles, C.; Shova, S.; Cazacu, M.; Timpu, D. New highly ordered hydrophobic siloxane-based coordination polymers. *Polymer* **2013**, *54*, 6096–6104.
- (167) Xie, L.-H.; Suh, M. P. Flexible Metal–Organic Framework with Hydrophobic Pores. *Chem. - Eur. J.* **2011**, *17*, 13653–13656.
- (168) Weston, M. H.; Delaquil, A. A.; Sarjeant, A. A.; Farha, O. K.; Hupp, J. T.; Nguyen, S. T. Tuning the Hydrophobicity of Zinc

- Dipyridyl Paddlewheel Metal–Organic Frameworks for Selective Sorption. *Cryst. Growth Des.* **2013**, *13*, 2938–2942.
- (169) Lu, Z.; Xing, H.; Sun, R.; Bai, J.; Zheng, B.; Li, Y. Water Stable Metal–Organic Framework Evolutionally Formed from a Flexible Multidentate Ligand with Acylamide Groups for Selective CO₂ Adsorption. *Cryst. Growth Des.* **2012**, *12*, 1081–1084.
- (170) Farrusseng, D.; Canivet, J.; Quadrelli, A. Design of Functional Metal–Organic Frameworks by Post-Synthetic Modification. In *Metal-Organic Frameworks: Applications from Catalysis to Gas Storage*; Farrusseng, D., Ed.; Wiley-VCH Verlag GmbH & Co. KGaA: New York, 2011.
- (171) Tanabe, K. K.; Cohen, S. M. Postsynthetic modification of metal–organic frameworks—a progress report. *Chem. Soc. Rev.* **2011**, *40*, 498–519.
- (172) Cohen, S. M. Postsynthetic methods for the functionalization of metal–organic frameworks. *Chem. Rev.* **2012**, *112*, 970–1000.
- (173) Wang, Z.; Cohen, S. M. Postsynthetic modification of metal–organic frameworks. *Chem. Soc. Rev.* **2009**, *38*, 1315–1329.
- (174) Goesten, M. G.; Kapteijn, F.; Gascon, J. Fascinating chemistry or frustrating unpredictability: observations in crystal engineering of metal–organic frameworks. *CrystEngComm* **2013**, *15*, 9249–9257.
- (175) Nguyen, J. G.; Cohen, S. M. Moisture-Resistant and Superhydrophobic Metal–Organic Frameworks Obtained via Post-synthetic Modification. *J. Am. Chem. Soc.* **2010**, *132*, 4560–4561.
- (176) Aguilera-Sigalat, J.; Bradshaw, D. A colloidal water-stable MOF as a broad-range fluorescent pH sensor via post-synthetic modification. *Chem. Commun.* **2014**, *50*, 4711–4713.
- (177) Aguado, S.; Canivet, J.; Schuurman, Y.; Farrusseng, D. Tuning the activity by controlling the wettability of MOF eggshell catalysts: A quantitative structure–activity study. *J. Catal.* **2011**, *284*, 207–214.
- (178) Canivet, J.; Aguado, S.; Daniel, C.; Farrusseng, D. Engineering the Environment of a Catalytic Metal–Organic Framework by Postsynthetic Hydrophobization. *ChemCatChem* **2011**, *3*, 675–678.
- (179) Rostamnia, S.; Xin, H. Basic isoreticular metal–organic framework (IRMOF-3) porous nanomaterial as a suitable and green catalyst for selective unsymmetrical Hantzsch coupling reaction. *Appl. Organomet. Chem.* **2014**, *28*, 359–363.
- (180) Kim, D.; Lee, T. B.; Choi, S. B.; Yoon, J. H.; Kim, J.; Choi, S.-H. A density functional theory study of a series of functionalized metal–organic frameworks. *Chem. Phys. Lett.* **2006**, *420*, 256–260.
- (181) Bellarosa, L.; Gutierrez-Sevillano, J. J.; Calero, S.; Lopez, N. How ligands improve the hydrothermal stability and affect the adsorption in the IRMOF family. *Phys. Chem. Chem. Phys.* **2013**, *15*, 17696–17704.
- (182) Bellarosa, L.; Calero, S.; Lopez, N. Early stages in the degradation of metal–organic frameworks in liquid water from first-principles molecular dynamics. *Phys. Chem. Chem. Phys.* **2012**, *14*, 7240–7245.
- (183) Hausdorf, S.; Baitalow, F.; Böhle, T.; Rafaja, D.; Mertens, F. O. R. L. Main-Group and Transition-Element IRMOF Homologues. *J. Am. Chem. Soc.* **2010**, *132*, 10978–10981.
- (184) Han, Y.; Li, J.-R.; Xie, Y.; Guo, G. Substitution reactions in metal–organic frameworks and metal–organic polyhedra. *Chem. Soc. Rev.* **2014**, *43*, 5952–5981.
- (185) Li, H.; Shi, W.; Zhao, K.; Li, H.; Bing, Y.; Cheng, P. Enhanced Hydrostability in Ni-Doped MOF-5. *Inorg. Chem.* **2012**, *51*, 9200–9207.
- (186) Yang, J.-M.; Liu, Q.; Sun, W.-Y. Shape and size control and gas adsorption of Ni(II)-doped MOF-5 nano/microcrystals. *Microporous Mesoporous Mater.* **2014**, *190*, 26–31.
- (187) Devic, T.; Serre, C. High valence 3p and transition metal based MOFs. *Chem. Soc. Rev.* **2014**, *43*, 6097–6115.
- (188) Bosch, M.; Zhang, M.; Zhou, H.-C. Increasing the Stability of Metal-Organic Frameworks. *Adv. Chem.* **2014**, *2014*, 1.
- (189) Jeremias, F.; Fröhlich, D.; Janiak, C.; Henninger, S. K. Water and methanol adsorption on MOFs for cycling heat transformation processes. *New J. Chem.* **2014**, *38*, 1846–1852.
- (190) Berke, C. H.; Kiss, A.; Kleinschmit, P.; Weitkamp, J. Der Hydrophobitäts-Index: Eine neue Methode zur Charakterisierung der Oberflächeneigenschaften zeolithischer Adsorbentien. *Chem. Ing. Tech.* **1991**, *63*, 623–625.
- (191) Stelzer, J.; Paulus, M.; Hunger, M.; Weitkamp, J. Hydrophobic properties of all-silica zeolite beta. *Microporous Mesoporous Mater.* **1998**, *22*, 1–8.
- (192) Heinen, A. W.; Peters, J. A.; Bekkum, H. v. Competitive adsorption of water and toluene on modified activated carbon supports. *Appl. Catal., A* **2000**, *194–195*, 193–202.
- (193) Ketcome, N.; Grisdanurak, N.; Chiarakorn, S. Silylated rice husk MCM-41 and its binary adsorption of water-toluene mixture. *J. Porous Mater.* **2009**, *16*, 41–46.
- (194) Yonli, A. H.; Gener, I.; Mignard, S. Comparative study of the hydrophobicity of BEA, HZSM-5 and HY zeolites determined by competitive adsorption. *Microporous Mesoporous Mater.* **2010**, *132*, 37–42.
- (195) Vanoye, L.; Favre-Réguillon, A.; Munno, P.; Rodríguez, J. F.; Dupuy, S.; Pallier, S.; Pitault, I.; De Bellefon, C. Methanol dehydration over commercially available zeolites: Effect of hydrophobicity. *Catal. Today* **2013**, *215*, 239–242.
- (196) Férey, G.; Mellot-Draznieks, C.; Serre, C.; Millange, F.; Dutour, J.; Surblé, S.; Margiolaki, I. A chromium terephthalate-based solid with unusually large pore volumes and surface area. *Science* **2005**, *309*, 2040–2042.
- (197) Seo, Y. K.; Yoon, J. W.; Lee, J. S.; Hwang, Y. K.; Jun, C. H.; Chang, J. S.; Wuttke, S.; Bazin, P.; Vimont, A.; Daturi, M. Energy-Efficient Dehumidification over Hierachically Porous Metal–Organic Frameworks as Advanced Water Adsorbents. *Adv. Mater.* **2012**, *24*, 806–810.
- (198) Akiyama, G.; Matsuda, R.; Sato, H.; Hori, A.; Takata, M.; Kitagawa, S. Effect of functional groups in MIL-101 on water sorption behavior. *Microporous Mesoporous Mater.* **2012**, *157*, 89–93.
- (199) Khutia, A.; Rammelberg, H. U.; Schmidt, T.; Henninger, S.; Janiak, C. Water sorption cycle measurements on functionalized MIL-101Cr for heat transformation application. *Chem. Mater.* **2013**, *25*, 790–798.
- (200) Férey, G.; Serre, C.; Mellot-Draznieks, C.; Millange, F.; Surblé, S.; Dutour, J.; Margiolaki, I. A Hybrid Solid with Giant Pores Prepared by a Combination of Targeted Chemistry, Simulation, and Powder Diffraction. *Angew. Chem., Int. Ed.* **2004**, *43*, 6296–6301.
- (201) Akiyama, G.; Matsuda, R.; Kitagawa, S. Highly Porous and Stable Coordination Polymers as Water Sorption Materials. *Chem. Lett.* **2010**, *39*, 360–361.
- (202) Wickenheisser, M.; Jeremias, F.; Henninger, S. K.; Janiak, C. Grafting of hydrophilic ethylene glycols or ethylenediamine on coordinatively unsaturated metal sites in MIL-100(Cr) for improved water adsorption characteristics. *Inorg. Chim. Acta* **2013**, *407*, 145–152.
- (203) Küsgens, P.; Rose, M.; Senkovska, I.; Fröde, H.; Henschel, A.; Siegle, S.; Kaskel, S. Characterization of metal-organic frameworks by water adsorption. *Microporous Mesoporous Mater.* **2009**, *120*, 325–330.
- (204) Dan-Hardi, M.; Serre, C.; Frot, T.; Rozes, L.; Maurin, G.; Sanchez, C.; Férey, G. A new photoactive crystalline highly porous titanium(IV) dicarboxylate. *J. Am. Chem. Soc.* **2009**, *131*, 10857–10859.
- (205) Kim, S.-N.; Kim, J.; Kim, H.-Y.; Cho, H.-Y.; Ahn, W.-S. Adsorption/catalytic properties of MIL-125 and NH₂-MIL-125. *Catal. Today* **2013**, *204*, 85–93.
- (206) Ahnfeldt, T.; Gunzelmann, D.; Wack, J.; Senker, J.; Stock, N. Controlled modification of the inorganic and organic bricks in an Al-based MOF by direct and post-synthetic synthesis routes. *CrystEngComm* **2012**, *14*, 4126–4136.
- (207) Katz, M. J.; Brown, Z. J.; Colón, Y. J.; Siu, P. W.; Scheidt, K. A.; Snurr, R. Q.; Hupp, J. T.; Farha, O. K. A facile synthesis of UiO-66, UiO-67 and their derivatives. *Chem. Commun.* **2013**, *49*, 9449–9451.
- (208) Shearer, G. C.; Chavan, S.; Ethiraj, J.; Vitillo, J. G.; Svelle, S.; Olsbye, U.; Lamberti, C.; Bordiga, S.; Lillerud, K. P. Tuned to Perfection: Ironing Out the Defects in Metal–Organic Framework UiO-66. *Chem. Mater.* **2014**, *26*, 4068–4071.

- (209) Øien, S.; Wragg, D. S.; Reinsch, H.; Svelle, S.; Bordiga, S.; Lamberti, C.; Lillerud, K. P. Detailed Structure Analysis of Atomic Positions and Defects in Zirconium Metal–Organic Frameworks. *Cryst. Growth Des.* **2014**, *14*, 5370.
- (210) Valenzano, L.; Civalleri, B.; Chavan, S.; Bordiga, S.; Nilsen, M. H.; Jakobsen, S.; Lillerud, K. P.; Lamberti, C. Disclosing the Complex Structure of UiO-66 Metal Organic Framework: A Synergic Combination of Experiment and Theory. *Chem. Mater.* **2011**, *23*, 1700–1718.
- (211) Mondloch, J. E.; Katz, M. J.; Planas, N.; Semrouni, D.; Gagliardi, L.; Hupp, J. T.; Farha, O. K. Are Zr 6-based MOFs water stable? Linker hydrolysis vs. capillary-force-driven channel collapse. *Chem. Commun.* **2014**, *50*, 8944–8946.
- (212) Furukawa, H.; Gándara, F.; Zhang, Y.-B.; Jiang, J.; Queen, W. L.; Hudson, M. R.; Yaghi, O. M. Water Adsorption in Porous Metal–Organic Frameworks and Related Materials. *J. Am. Chem. Soc.* **2014**, *136*, 4369–4381.
- (213) Bon, V.; Senkovskyy, V.; Senkovska, I.; Kaskel, S. Zr(iv) and Hf(iv) based metal–organic frameworks with reo-topology. *Chem. Commun.* **2012**, *48*, 8407–8409.
- (214) Bon, V.; Senkovska, I.; Baburin, I. A.; Kaskel, S. Zr-and Hf-Based Metal–Organic Frameworks: Tracking Down the Polymorphism. *Cryst. Growth Des.* **2013**, *13*, 1231–1237.
- (215) Deria, P.; Mondloch, J. E.; Tylianakis, E.; Ghosh, P.; Bury, W.; Snurr, R. Q.; Hupp, J. T.; Farha, O. K. Perfluoroalkane Functionalization of NU-1000 via Solvent-Assisted Ligand Incorporation: Synthesis and CO₂ Adsorption Studies. *J. Am. Chem. Soc.* **2013**, *135*, 16801–16804.
- (216) Serre, C.; Millange, F.; Thouvenot, C.; Noguès, M.; Marsolier, G.; Louér, D.; Férey, G. Very Large Breathing Effect in the First Nanoporous Chromium(III)-Based Solids: MIL-53 or Cr^{III}(OH)_{O₂C-C₆H₄-CO₂}_{HO₂C-C₆H₄-CO₂H}_xH₂O_y. *J. Am. Chem. Soc.* **2002**, *124*, 13519–13526.
- (217) Férey, G.; Latroche, M.; Serre, C.; Millange, F.; Loiseau, T.; Percheron-Guégan, A. Hydrogen adsorption in the nanoporous metal-benzenedicarboxylate M(OH)(O₂C-C₆H₄-CO₂) (M = Al 3+, Cr3+), MIL-53. *Chem. Commun.* **2003**, *9*, 2976–2977.
- (218) Loiseau, T.; Serre, C.; Huguenard, C.; Fink, G.; Taulelle, F.; Henry, M.; Bataille, T.; Férey, G. A Rationale for the Large Breathing of the Porous Aluminum Terephthalate (MIL-53) Upon Hydration. *Chem. - Eur. J.* **2004**, *10*, 1373–1382.
- (219) Bourrelly, S.; Moulin, B. a.; Rivera, A.; Maurin, G.; Devautour-Vinot, S.; Serre, C.; Devic, T.; Horcajada, P.; Vimont, A.; Clet, G.; Daturi, M.; Lavalle, J.-C.; Loera-Serna, S.; Denoyel, R.; Llewellyn, P. L.; Férey, G. r. Explanation of the Adsorption of Polar Vapors in the Highly Flexible Metal Organic Framework MIL-53(Cr). *J. Am. Chem. Soc.* **2010**, *132*, 9488–9498.
- (220) Barthelet, K.; Marrot, J.; Riou, D.; Férey, G. A Breathing Hybrid Organic–Inorganic Solid with Very Large Pores and High Magnetic Characteristics. *Angew. Chem.* **2002**, *114*, 291–294.
- (221) Biswas, S.; Rémy, T.; Couck, S.; Denysenko, D.; Rampelberg, G.; Denayer, J. F.; Volkmer, D.; Detavernier, C.; Van Der Voort, P. Partially fluorinated MIL-47 and Al-MIL-53 frameworks: influence of functionalization on sorption and breathing properties. *Phys. Chem. Chem. Phys.* **2013**, *15*, 3552–3561.
- (222) Reinsch, H.; van der Veen, M. A.; Gil, B.; Marszalek, B.; Verbiest, T.; de Vos, D.; Stock, N. Structures, Sorption Characteristics, and Nonlinear Optical Properties of a New Series of Highly Stable Aluminum MOFs. *Chem. Mater.* **2013**, *25*, 17–26.
- (223) De Lange, M.; Ottevanger, C.; Wiegman, M.; Vlugt, T. J. H.; Gascon, J.; Kapteijn, F. Crystals for sustainability—structuring Al-based MOFs for the allocation of heat and cold. *CrystEngComm* **2015**, *17*, 281–285.
- (224) de Lange, M.; Zeng, T.; Vlugt, T. J. H.; Gascon, J.; Kapteijn, F. Manufacture of dense CAU-10-H coatings for application in adsorption driven heat pumps: optimization and characterization. *CrystEngComm* **2015**, *17*, 5911.
- (225) Frohlich, D.; Henninger, S. K.; Janiak, C. Multicycle water vapour stability of microporous breathing MOF aluminium isophthalate CAU-10-H. *Dalton Trans.* **2014**, *43*, 15300–15304.
- (226) Nielkiel, F.; Lannoeye, J.; Reinsch, H.; Munn, A. S.; Heerwig, A.; Zizak, I.; Kaskel, S.; Walton, R. I.; de Vos, D.; Llewellyn, P.; Lieb, A.; Maurin, G.; Stock, N. Conformation-Controlled Sorption Properties and Breathing of the Aliphatic Al-MOF [Al(OH) (CDC)]. *Inorg. Chem.* **2014**, *53*, 4610–4620.
- (227) Jeremias, F.; Frohlich, D.; Janiak, C.; Henninger, S. K. Advancement of sorption-based heat transformation by a metal coating of highly-stable, hydrophilic aluminium fumarate MOF. *RSC Adv.* **2014**, *4*, 24073–24082.
- (228) Jeremias, F.; Henninger, S. K.; Janiak, C. High performance metal–organic-framework coatings obtained via thermal gradient synthesis. *Chem. Commun.* **2012**, *48*, 9708–9710.
- (229) Dietzel, P. D. C.; Johnsen, R. E.; Blom, R.; Fjellvåg, H. Structural Changes and Coordinatively Unsaturated Metal Atoms on Dehydration of Honeycomb Analogous Microporous Metal–Organic Frameworks. *Chem. - Eur. J.* **2008**, *14*, 2389–2397.
- (230) Liu, J.; Wang, Y.; Benin, A. I.; Jakubczak, P.; Willis, R. R.; LeVan, M. D. CO₂/H₂O Adsorption Equilibrium and Rates on Metal–Organic Frameworks: HKUST-1 and Ni/DOBDC. *Langmuir* **2010**, *26*, 14301–14307.
- (231) Schoenecker, P. M.; Carson, C. G.; Jasuja, H.; Flemming, C. J. J.; Walton, K. S. Effect of Water Adsorption on Retention of Structure and Surface Area of Metal–Organic Frameworks. *Ind. Eng. Chem. Res.* **2012**, *51*, 6513–6519.
- (232) Chmelik, C.; Mundstock, A.; Dietzel, P. D. C.; Caro, J. Idiosyncrasies of Co₂(dhtp): In situ-annealing by methanol. *Microporous Mesoporous Mater.* **2014**, *183*, 117–123.
- (233) Dietzel, P. D. C.; Panella, B.; Hirscher, M.; Blom, R.; Fjellvag, H. Hydrogen adsorption in a nickel based coordination polymer with open metal sites in the cylindrical cavities of the desolvated framework. *Chem. Commun.* **2006**, 959–961.
- (234) Park, K. S.; Ni, Z.; Côté, A. P.; Choi, J. Y.; Huang, R.; Uribe-Romo, F. J.; Chae, H. K.; O’Keeffe, M.; Yaghi, O. M. Exceptional chemical and thermal stability of zeolitic imidazolate frameworks. *Proc. Natl. Acad. Sci. U. S. A.* **2006**, *103*, 10186–10191.
- (235) Zhang, J.-P.; Zhu, A.-X.; Lin, R.-B.; Qi, X.-L.; Chen, X.-M. Pore Surface Tailored SOD-Type Metal–Organic Zeolites. *Adv. Mater.* **2011**, *23*, 1268–1271.
- (236) Lin, J.-B.; Lin, R.-B.; Cheng, X.-N.; Zhang, J.-P.; Chen, X.-M. Solvent/additive-free synthesis of porous/zeolitic metal azolate frameworks from metal oxide/hydroxide. *Chem. Commun.* **2011**, *47*, 9185–9187.
- (237) Zhu, A.-X.; Lin, R.-B.; Qi, X.-L.; Liu, Y.; Lin, Y.-Y.; Zhang, J.-P.; Chen, X.-M. Zeolitic metal azolate frameworks (MAFs) from ZnO/Zn(OH)₂ and monoalkyl-substituted imidazoles and 1,2,4-triazoles: Efficient syntheses and properties. *Microporous Mesoporous Mater.* **2012**, *157*, 42–49.
- (238) Karra, J. R.; Jasuja, H.; Huang, Y.-G.; Walton, K. Structural Stability of BTTB-based Metal–Organic Frameworks under Humid Conditions. *J. Mater. Chem. A* **2015**, *3*, 1624.
- (239) Wang, Z.; Tanabe, K. K.; Cohen, S. M. Assessing postsynthetic modification in a series of metal–organic frameworks and the influence of framework topology on reactivity. *Inorg. Chem.* **2009**, *48*, 296–306.
- (240) Quartapelle Procopio, E.; Fukushima, T.; Barea, E.; Navarro, J. A. R.; Horike, S.; Kitagawa, S. A Soft Copper(II) Porous Coordination Polymer with Unprecedented Aqua Bridge and Selective Adsorption Properties. *Chem. - Eur. J.* **2012**, *18*, 13117–13125.
- (241) Birsá Čelić, T.; Mazaj, M.; Guillou, N.; Elkäim, E.; El Roz, M.; Thibault-Starzyk, F.; Mali, G.; Rangus, M.; Čendak, T.; Kaučič, V.; Zabukovec Logar, N. Study of Hydrothermal Stability and Water Sorption Characteristics of 3-Dimensional Zn-Based Trimesate. *J. Phys. Chem. C* **2013**, *117*, 14608–14617.
- (242) Biswas, S.; Grzywa, M.; Nayek, H. P.; Dehnen, S.; Senkovska, I.; Kaskel, S.; Volkmer, D. A cubic coordination framework constructed from benzobistriazolate ligands and zinc ions having selective gas sorption properties. *Dalton Trans.* **2009**, 6487–6495.

- (243) Montoro, C.; Linares, F.; Quartapelle Procopio, E.; Senkovska, I.; Kaskel, S.; Galli, S.; Masciocchi, N.; Barea, E.; Navarro, J. A. R. Capture of Nerve Agents and Mustard Gas Analogues by Hydrophobic Robust MOF-5 Type Metal–Organic Frameworks. *J. Am. Chem. Soc.* **2011**, *133*, 11888–11891.
- (244) Santra, A.; Senkovska, I.; Kaskel, S.; Bharadwaj, P. K. Gas Storage in a Partially Fluorinated Highly Stable Three-Dimensional Porous Metal–Organic Framework. *Inorg. Chem.* **2013**, *52*, 7358–7366.
- (245) Kundu, T.; Sahoo, S. C.; Banerjee, R. Relating pore hydrophilicity with vapour adsorption capacity in a series of amino acid based metal organic frameworks. *CrystEngComm* **2013**, *15*, 9634–9640.
- (246) Kundu, T.; Sahoo, S. C.; Saha, S.; Banerjee, R. Salt metathesis in three dimensional metal–organic frameworks (MOFs) with unprecedented hydrolytic regenerability. *Chem. Commun.* **2013**, *49*, S262–S264.
- (247) Henninger, S. K.; Habib, H. A.; Janiak, C. MOFs as Adsorbents for Low Temperature Heating and Cooling Applications. *J. Am. Chem. Soc.* **2009**, *131*, 2776–2777.
- (248) Padial, N. M.; Quartapelle Procopio, E.; Montoro, C.; López, E.; Oltra, J. E.; Colombo, V.; Maspero, A.; Masciocchi, N.; Galli, S.; Senkovska, I.; Kaskel, S.; Barea, E.; Navarro, J. A. R. Highly Hydrophobic Isoreticular Porous Metal–Organic Frameworks for the Capture of Harmful Volatile Organic Compounds. *Angew. Chem., Int. Ed.* **2013**, *52*, 8290–8294.
- (249) Seo, Y.-K.; Yoon, J. W.; Lee, J. S.; Hwang, Y. K.; Jun, C.-H.; Chang, J.-S.; Wuttke, S.; Bazin, P.; Vimont, A.; Daturi, M.; Bourrelly, S.; Llewellyn, P. L.; Horcajada, P.; Serre, C.; Férey, G. Porous Materials: Energy-Efficient Dehumidification over Hierarchically Porous Metal–Organic Frameworks as Advanced Water Adsorbents. *Adv. Mater.* **2012**, *24*, 710–710.
- (250) Ehrenmann, J.; Henninger, S. K.; Janiak, C. Water Adsorption Characteristics of MIL-101 for Heat-Transformation Applications of MOFs. *Eur. J. Inorg. Chem.* **2011**, *2011*, 471–474.
- (251) Hong, D.-Y.; Hwang, Y. K.; Serre, C.; Férey, G.; Chang, J.-S. Porous Chromium Terephthalate MIL-101 with Coordinatively Unsaturated Sites: Surface Functionalization, Encapsulation, Sorption and Catalysis. *Adv. Funct. Mater.* **2009**, *19*, 1537–1552.
- (252) Hu, Y.; Song, C.; Liao, J.; Huang, Z.; Li, G. Water stable metal–organic framework packed microcolumn for online sorptive extraction and direct analysis of naproxen and its metabolite from urine sample. *J. Chromatogr. A* **2013**, *1294*, 17–24.
- (253) Akiyama, G.; Matsuda, R.; Sato, H.; Takata, M.; Kitagawa, S. Cellulose Hydrolysis by a New Porous Coordination Polymer Decorated with Sulfonic Acid Functional Groups. *Adv. Mater.* **2011**, *23*, 3294–3297.
- (254) Juan-Alcañiz, J.; Ramos-Fernandez, E. V.; Lafont, U.; Gascon, J.; Kapteijn, F. Building MOF bottles around phosphotungstic acid ships: One-pot synthesis of bi-functional polyoxometalate-MIL-101 catalysts. *J. Catal.* **2010**, *269*, 229–241.
- (255) Pirngruber, G. D.; Hamon, L.; Bourrelly, S.; Llewellyn, P. L.; Lenoir, E.; Guillerm, V.; Serre, C.; Devic, T. A method for screening the potential of MOFs as CO₂ adsorbents in pressure swing adsorption processes. *ChemSusChem* **2012**, *5*, 762–776.
- (256) Soubeyrand-Lenoir, E.; Vagner, C.; Yoon, J. W.; Bazin, P.; Ragon, F.; Hwang, Y. K.; Serre, C.; Chang, J.-S.; Llewellyn, P. L. How Water Fosters a Remarkable 5-Fold Increase in Low-Pressure CO₂ Uptake within Mesoporous MIL-100(Fe). *J. Am. Chem. Soc.* **2012**, *134*, 10174–10181.
- (257) Cunha, D.; Ben Yahia, M.; Hall, S.; Miller, S. R.; Chevreau, H.; Elkaïm, E.; Maurin, G.; Horcajada, P.; Serre, C. Rationale of Drug Encapsulation and Release from Biocompatible Porous Metal–Organic Frameworks. *Chem. Mater.* **2013**, *25*, 2767–2776.
- (258) Vaesen, S.; Guillerm, V.; Yang, Q.; Wiersum, A. D.; Marszalek, B.; Gil, B.; Vimont, A.; Daturi, M.; Devic, T.; Llewellyn, P. L. A robust amino-functionalized titanium (IV) based MOF for improved separation of acid gases. *Chem. Commun.* **2013**, *49*, 10082–10084.
- (259) Guillerm, V.; Ragon, F.; Dan-Hardi, M.; Devic, T.; Vishnuvarthan, M.; Campo, B.; Vimont, A.; Clet, G.; Yang, Q.; Maurin, G. A series of isoreticular, highly stable, porous zirconium oxide based metal–organic frameworks. *Angew. Chem., Int. Ed.* **2012**, *51*, 9267–9271.
- (260) Yang, Q.; Guillerm, V.; Ragon, F.; Wiersum, A. D.; Llewellyn, P. L.; Zhong, C.; Devic, T.; Serre, C.; Maurin, G. CH 4 storage and CO 2 capture in highly porous zirconium oxide based metal–organic frameworks. *Chem. Commun.* **2012**, *48*, 9831–9833.
- (261) Kandiah, M.; Nilsen, M. H.; Usseglio, S.; Jakobsen, S.; Olsbye, U.; Tilset, M.; Larabi, C.; Quadrelli, E. A.; Bonino, F.; Lillerud, K. P. Synthesis and stability of tagged UiO-66 Zr-MOFs. *Chem. Mater.* **2010**, *22*, 6632–6640.
- (262) Jasuja, H.; Zang, J.; Sholl, D. S.; Walton, K. S. Rational tuning of water vapor and CO 2 adsorption in highly stable Zr-based MOFs. *J. Phys. Chem. C* **2012**, *116*, 23526–23532.
- (263) Jasuja, H.; Walton, K. S. Experimental Study of CO₂, CH₄, and Water Vapor Adsorption on a Dimethyl-Functionalized UiO-66 Framework. *J. Phys. Chem. C* **2013**, *117*, 7062–7068.
- (264) Yang, Q.; Vaesen, S.; Ragon, F.; Wiersum, A. D.; Wu, D.; Lago, A.; Devic, T.; Martineau, C.; Taulelle, F.; Llewellyn, P. L.; Jobic, H.; Zhong, C.; Serre, C.; De Weireld, G.; Maurin, G. A Water Stable Metal–Organic Framework with Optimal Features for CO₂ Capture. *Angew. Chem., Int. Ed.* **2013**, *52*, 10316–10320.
- (265) Shigematsu, A.; Yamada, T.; Kitagawa, H. Wide Control of Proton Conductivity in Porous Coordination Polymers. *J. Am. Chem. Soc.* **2011**, *133*, 2034–2036.
- (266) Yamada, T.; Shirai, Y.; Kitagawa, H. Synthesis, Water Adsorption, and Proton Conductivity of Solid-Solution-Type Metal–Organic Frameworks Al(OH)_x(bdc-OH)_{1-x}. *Chem. - Asian J.* **2014**, *9*, 1316–1320.
- (267) Biswas, S.; Ahnfeldt, T.; Stock, N. New Functionalized Flexible Al-MIL-53-X (X = -Cl, -Br, -CH₃, -NO₂, -(OH)₂) Solids: Syntheses, Characterization, Sorption, and Breathing Behavior. *Inorg. Chem.* **2011**, *50*, 9518–9526.
- (268) Biswas, S.; Couck, S.; Denysenko, D.; Bhunia, A.; Grzywa, M.; Denayer, J. F. M.; Volkmer, D.; Janiak, C.; Van Der Voort, P. Sorption and breathing properties of difluorinated MIL-47 and Al-MIL-53 frameworks. *Microporous Mesoporous Mater.* **2013**, *181*, 175–181.
- (269) Liu, J.; Zhang, F.; Zou, X.; Yu, G.; Zhao, N.; Fan, S.; Zhu, G. Environmentally friendly synthesis of highly hydrophobic and stable MIL-53 MOF nanomaterials. *Chem. Commun.* **2013**, *49*, 7430–7432.
- (270) Comotti, A.; Bracco, S.; Sozzani, P.; Horike, S.; Matsuda, R.; Chen, J.; Takata, M.; Kubota, Y.; Kitagawa, S. Nanochannels of Two Distinct Cross-Sections in a Porous Al-Based Coordination Polymer. *J. Am. Chem. Soc.* **2008**, *130*, 13664–13672.
- (271) Han, S.; Huang, Y.; Watanabe, T.; Dai, Y.; Walton, K. S.; Nair, S.; Sholl, D. S.; Meredith, J. C. High-Throughput Screening of Metal–Organic Frameworks for CO₂ Separation. *ACS Comb. Sci.* **2012**, *14*, 263–267.
- (272) Zhang, K.; Lively, R. P.; Dose, M. E.; Brown, A. J.; Zhang, C.; Chung, J.; Nair, S.; Koros, W. J.; Chance, R. R. Alcohol and water adsorption in zeolitic imidazolate frameworks. *Chem. Commun.* **2013**, *49*, 3245–3247.
- (273) Biswal, B. P.; Panda, T.; Banerjee, R. Solution mediated phase transformation (RHO to SOD) in porous Co-imidazolate based zeolitic frameworks with high water stability. *Chem. Commun.* **2012**, *48*, 11868–11870.
- (274) Kondo, A.; Daimaru, T.; Noguchi, H.; Ohba, T.; Kaneko, K.; Kanoh, H. Adsorption of water on three-dimensional pillared-layer metal organic frameworks. *J. Colloid Interface Sci.* **2007**, *314*, 422–426.
- (275) Rezk, A.; Al-Dadah, R.; Mahmoud, S.; Elsayed, A. Experimental investigation of metal organic frameworks characteristics for water adsorption chillers. *Proc. Inst. Mech. Eng., Part C* **2013**, *227*, 992–1005.
- (276) Li, G.-B.; Li, L.; Liu, J.-M.; Yang, T.; Su, C.-Y. A CdSO₄-Type 3D Metal–Organic Framework Showing Coordination Dynamics on Cu²⁺ Axial Sites: Vapochromic Response and Guest Sorption Selectivity. *Cryst. Growth Des.* **2013**, *13*, 1518–1525.

- (277) Lin, X.; Blake, A. J.; Wilson, C.; Sun, X. Z.; Champness, N. R.; George, M. W.; Hubberstey, P.; Mokaya, R.; Schröder, M. A Porous Framework Polymer Based on a Zinc(II) 4,4'-Bipyridine-2,6,2',6'-tetracarboxylate: Synthesis, Structure, and "Zeolite-Like" Behaviors. *J. Am. Chem. Soc.* **2006**, *128*, 10745–10753.
- (278) Sadakiyo, M.; Yamada, T.; Kitagawa, H. Hydroxyl Group Recognition by Hydrogen-Bonding Donor and Acceptor Sites Embedded in a Layered Metal–Organic Framework. *J. Am. Chem. Soc.* **2011**, *133*, 11050–11053.
- (279) Wade, C. R.; Corrales-Sánchez, T.; Narayan, T. C.; Dincă, M. Postsynthetic tuning of hydrophilicity in pyrazolate MOFs to modulate water adsorption properties. *Energy Environ. Sci.* **2013**, *6*, 2172–2177.
- (280) Reinsch, H.; Feyand, M.; Ahnfeldt, T.; Stock, N. CAU-3: A new family of porous MOFs with a novel Al-based brick: $[Al_2(OCH_3)_4(O_2C-X-CO_2)]$ (X = aryl). *Dalton Trans.* **2012**, *41*, 4164–4171.
- (281) Reinsch, H.; Marszalek, B.; Wack, J.; Senker, J.; Gil, B.; Stock, N. A new Al-MOF based on a unique column-shaped inorganic building unit exhibiting strongly hydrophilic sorption behaviour. *Chem. Commun.* **2012**, *48*, 9486–9488.
- (282) Borjigin, T.; Sun, F.; Zhang, J.; Cai, K.; Ren, H.; Zhu, G. A microporous metal-organic framework with high stability for GC separation of alcohols from water. *Chem. Commun.* **2012**, *48*, 7613–7615.
- (283) Hou, C.; Liu, Q.; Wang, P.; Sun, W.-Y. Porous metal–organic frameworks with high stability and selective sorption for CO₂ over N₂. *Microporous Mesoporous Mater.* **2013**, *172*, 61–66.
- (284) Kundu, T.; Sahoo, S. C.; Banerjee, R. Variable Water Adsorption in Amino Acid Derivative Based Homochiral Metal Organic Frameworks. *Cryst. Growth Des.* **2012**, *12*, 4633–4640.
- (285) Huang, Y.; Zheng, X.; Duan, J.; Liu, W.; Zhou, L.; Wang, C.; Wen, L.; Zhao, J.; Li, D. A highly stable multifunctional three-dimensional microporous framework: excellent selective sorption and visible photoluminescence. *Dalton Trans.* **2014**, *43*, 6811–6818.
- (286) Hou, C.; Liu, Q.; Okamura, T.-a.; Wang, P.; Sun, W.-Y. Dynamic porous metal-organic frameworks: synthesis, structure and sorption property. *CrystEngComm* **2012**, *14*, 8569–8576.
- (287) Sun, J.-K.; Ji, M.; Chen, C.; Wang, W.-G.; Wang, P.; Chen, R.-P.; Zhang, J. A charge-polarized porous metal-organic framework for gas chromatographic separation of alcohols from water. *Chem. Commun.* **2013**, *49*, 1624–1626.
- (288) Lin, X.-M.; Li, T.-T.; Chen, L.-F.; Zhang, L.; Su, C.-Y. Two ligand-functionalized Pb(ii) metal-organic frameworks: structures and catalytic performances. *Dalton Trans.* **2012**, *41*, 10422–10429.
- (289) Dubinin, M. M. The potential theory of adsorption of gases and vapors for adsorbents with energetically nonuniform surfaces. *Chem. Rev.* **1960**, *60*, 235–241.
- (290) Lee, J. Y.; Olson, D. H.; Pan, L.; Emge, T. J.; Li, J. Microporous Metal–Organic Frameworks with High Gas Sorption and Separation Capacity. *Adv. Funct. Mater.* **2007**, *17*, 1255–1262.
- (291) Uemura, K.; Komagawa, Y.; Yamasaki, Y.; Kita, H. Characterization of organic solvents adsorption/desorption on hydrophobic porous coordination polymers and their micro-crystals aggregation on mullite support. *Desalination* **2008**, *234*, 1–8.
- (292) Van der Perre, S.; Van Assche, T.; Bozbıyik, B.; Lannoeye, J.; De Vos, D. E.; Baron, G. V.; Denayer, J. F. M. Adsorptive Characterization of the ZIF-68 Metal-Organic Framework: A Complex Structure with Amphiphilic Properties. *Langmuir* **2014**, *30*, 8416–8424.
- (293) Lincke, J.; Lässig, D.; Moellmer, J.; Reichenbach, C.; Puls, A.; Moeller, A.; Gläser, R.; Kalies, G.; Staudt, R.; Krautscheid, H. A novel copper-based MOF material: Synthesis, characterization and adsorption studies. *Microporous Mesoporous Mater.* **2011**, *142*, 62–69.
- (294) Kitaura, R.; Fujimoto, K.; Noro, S.-i.; Kondo, M.; Kitagawa, S. A Pillared-Layer Coordination Polymer Network Displaying Hysteric Sorption: $[Cu_2(pzdc)_2(dpyg)]_n$ (pzdc= Pyrazine-2,3-dicarboxylate; dpyg = 1,2-Di(4-pyridyl)glycol). *Angew. Chem.* **2002**, *114*, 141–143.
- (295) Zhang, J.-P.; Chen, X.-M. Exceptional Framework Flexibility and Sorption Behavior of a Multifunctional Porous Cuprous Triazolate Framework. *J. Am. Chem. Soc.* **2008**, *130*, 6010–6017.
- (296) Fang, Q.-R.; Zhu, G.-S.; Jin, Z.; Xue, M.; Wei, X.; Wang, D.-J.; Qiu, S.-L. A Novel Metal–Organic Framework with the Diamondoid Topology Constructed from Pentanuclear Zinc–Carboxylate Clusters. *Cryst. Growth Des.* **2007**, *7*, 1035–1037.
- (297) Pan, L.; Parker, B.; Huang, X.; Olson, D. H.; Lee, Li. J. Zn(tbip) (H₂tbip= S-tert-Butyl Isophthalic Acid): A Highly Stable Guest-Free Microporous Metal Organic Framework with Unique Gas Separation Capability. *J. Am. Chem. Soc.* **2006**, *128*, 4180–4181.
- (298) Zeng, M.-H.; Tan, Y.-X.; He, Y.-P.; Yin, Z.; Chen, Q.; Kurmoo, M. A Porous 4-Fold-Interpenetrated Chiral Framework Exhibiting Vapochromism, Single-Crystal-to-Single-Crystal Solvent Exchange, Gas Sorption, and a Poisoning Effect. *Inorg. Chem.* **2013**, *52*, 2353–2360.
- (299) Li, K.; Olson, D. H.; Lee, J. Y.; Bi, W.; Wu, K.; Yuen, T.; Xu, Q.; Li, J. Multifunctional Microporous MOFs Exhibiting Gas/Hydrocarbon Adsorption Selectivity, Separation Capability and Three-Dimensional Magnetic Ordering. *Adv. Funct. Mater.* **2008**, *18*, 2205–2214.
- (300) Arnold, M.; Kortunov, P.; Jones, D. J.; Nedellec, Y.; Kärger, J.; Caro, J. Oriented Crystallisation on Supports and Anisotropic Mass Transport of the Metal-Organic Framework Manganese Formate. *Eur. J. Inorg. Chem.* **2007**, *2007*, 60–64.
- (301) Niu, Z.; Fang, S.; Ma, J.-G.; Zhang, X.-P.; Cheng, P. Enhancement of adsorption selectivity for MOFs under mild activation and regeneration conditions. *Chem. Commun.* **2014**, *50*, 7797–7799.
- (302) Rezk, A.; Al-Dadah, R.; Mahmoud, S.; Elsayed, A. Investigation of Ethanol/metal organic frameworks for low temperature adsorption cooling applications. *Appl. Energy* **2013**, *112*, 1025–1031.
- (303) Li, L.; Tang, S.; Wang, C.; Lv, X.; Jiang, M.; Wu, H.; Zhao, X. High gas storage capacities and stepwise adsorption in a UiO type metal-organic framework incorporating Lewis basic bipyridyl sites. *Chem. Commun.* **2014**, *50*, 2304–2307.
- (304) Seo, Y.-K.; Yoon, J. W.; Lee, J. S.; Lee, U.; Hwang, Y. K.; Jun, C.-H.; Horcajada, P.; Serre, C.; Chang, J.-S. Large scale fluorine-free synthesis of hierarchically porous iron (III) trimesate MIL-100 (Fe) with a zeolite MTN topology. *Microporous Mesoporous Mater.* **2012**, *157*, 137–145.
- (305) Grant Glover, T.; Peterson, G. W.; Schindler, B. J.; Britt, D.; Yaghi, O. MOF-74 building unit has a direct impact on toxic gas adsorption. *Chem. Eng. Sci.* **2011**, *66*, 163–170.
- (306) Peterson, G. W.; DeCoste, J. B.; Fatollahi-Fard, F.; Britt, D. K. Engineering UiO-66-NH₂ for Toxic Gas Removal. *Ind. Eng. Chem. Res.* **2014**, *53*, 701–707.
- (307) DeCoste, J. B.; Peterson, G. W. Metal–Organic Frameworks for Air Purification of Toxic Chemicals. *Chem. Rev.* **2014**, *114*, 5695.
- (308) Britt, D.; Tranchemontagne, D.; Yaghi, O. M. Metal-organic frameworks with high capacity and selectivity for harmful gases. *Proc. Natl. Acad. Sci. U. S. A.* **2008**, *105*, 11623–11627.
- (309) Saha, D.; Deng, S. Ammonia adsorption and its effects on framework stability of MOF-5 and MOF-177. *J. Colloid Interface Sci.* **2010**, *348*, 615–620.
- (310) Spanopoulos, I.; Xydiás, P.; Malliakas, C. D.; Trikalitis, P. N. A Straight Forward Route for the Development of Metal–Organic Frameworks Functionalized with Aromatic – OH Groups: Synthesis, Characterization, and Gas (N₂, Ar, H₂, CO₂, CH₄, NH₃) Sorption Properties. *Inorg. Chem.* **2013**, *52*, 855–862.
- (311) Petit, C.; Wrabetz, S.; Bandosz, T. J. Microcalorimetric insight into the analysis of the reactive adsorption of ammonia on Cu-MOF and its composite with graphite oxide. *J. Mater. Chem.* **2012**, *22*, 21443–21447.
- (312) Borfecchia, E.; Maurelli, S.; Gianolio, D.; Groppo, E.; Chiesa, M.; Bonino, F.; Lamberti, C. Insights into Adsorption of NH₃ on HKUST-1 Metal–Organic Framework: A Multitechnique Approach. *J. Phys. Chem. C* **2012**, *116*, 19839–19850.
- (313) Petit, C.; Bandosz, T. J. Synthesis, Characterization, and Ammonia Adsorption Properties of Mesoporous Metal–Organic

- Framework (MIL(Fe))—Graphite Oxide Composites: Exploring the Limits of Materials Fabrication. *Adv. Funct. Mater.* **2011**, *21*, 2108–2117.
- (314) Morris, W.; Doonan, C. J.; Yaghi, O. M. Postsynthetic Modification of a Metal–Organic Framework for Stabilization of a Hemiaminal and Ammonia Uptake. *Inorg. Chem.* **2011**, *50*, 6853–6855.
- (315) Jasuja, H.; Peterson, G. W.; Decoste, J. B.; Browne, M. A.; Walton, K. S. Evaluation of MOFs for air purification and air quality control applications: Ammonia removal from air. *Chem. Eng. Sci.* **2015**, *124*, 118.
- (316) Chang, J. S.; Jhung, S. H.; Hwang, Y. K. Adsorbent for water adsorption and desorption. U.S. Patent 8980128, 2015.
- (317) Chang, J. S.; Jhung, S. H.; Hwang, Y. K. Adsorbent for water adsorption and desorption. Korea Patent 0806586, 2008.
- (318) Chang, J. S.; Jhung, S. H.; Hwang, Y. K. Adsorbent for water adsorption and desorption. Japan Patent 5132671, 2012.
- (319) Chang, J. S.; Hwang, Y. K.; Jhung, S. H.; Hong, D. Y.; Seo, Y. K. Porous organic-inorganic hybrid materials and adsorbent comprising the same. U.S. Patent 8168813, 2012.
- (320) Chang, J. S.; Hwang, Y. K.; Jhung, S. H.; Hong, D. Y.; Seo, Y. K. Porous organic-inorganic hybrid materials and adsorbent comprising the same. Korea Patent 0803964, 2008.
- (321) Schubert, M.; Mueller, U.; Kiener, C. Porous metal organic frameworks as desiccants. U.S. Patent 2009-863339, 2009.
- (322) Kiener, C.; Müller, U.; Schubert, M.; Teich, F. Metal-organic frameworks in refrigeration/heating machines. EU Patent 2230288A2, 2010.
- (323) Baumann, T. F.; Satcher, J. H.; Farmer, J. C. Adsorption cooling system using metal organic frameworks. U.S. Patent 2012-457331, 2012.
- (324) Hahn, A.; Schmidt, F.; Henninger, S. Adsorbent, method of producing it and use in heat stores and heat pumps. EU Patent 2049549B1, 2014.
- (325) Dinca, M.; Wade, C. R. Compositions and methods comprising porous metal organic frameworks and related uses. U.S. Patent 2014-270385, 2014.
- (326) Czaja, A. U.; Trukhan, N.; Muller, U. Industrial applications of metal-organic frameworks. *Chem. Soc. Rev.* **2009**, *38*, 1284–1293.
- (327) Mueller, U.; Schubert, M.; Teich, F.; Puetter, H.; Schierlein-Arndt, K.; Pastre, J. Metal-organic frameworks-prospective industrial applications. *J. Mater. Chem.* **2006**, *16*, 626–636.
- (328) Gaab, M.; Trukhan, N.; Maurer, S.; Gummaraju, R.; Müller, U. The progression of Al-based metal-organic frameworks – From academic research to industrial production and applications. *Microporous Mesoporous Mater.* **2012**, *157*, 131–136.
- (329) Fletcher, A. J.; Thomas, K. M.; Rosseinsky, M. J. Flexibility in metal-organic framework materials: Impact on sorption properties. *J. Solid State Chem.* **2005**, *178*, 2491–2510.
- (330) Chen, B.; Ma, S.; Zapata, F.; Fronczek, F. R.; Lobkovsky, E. B.; Zhou, H.-C. Rationally Designed Micropores within a Metal–Organic Framework for Selective Sorption of Gas Molecules. *Inorg. Chem.* **2007**, *46*, 1233–1236.
- (331) Bureekaew, S.; Shimomura, S.; Kitagawa, S. Chemistry and application of flexible porous coordination polymers. *Sci. Technol. Adv. Mater.* **2008**, *9*, 014108.
- (332) Zhang, J.-P.; Kitagawa, S. Supramolecular Isomerism, Framework Flexibility, Unsaturated Metal Center, and Porous Property of Ag(I)/Cu(I) 3,3',5,5'-Tetrametyl-4,4'-Bipyrazolate. *J. Am. Chem. Soc.* **2008**, *130*, 907–917.
- (333) Thallapally, P. K.; Tian, J.; Radha Kishan, M.; Fernandez, C. A.; Dalgarno, S. J.; McGrail, P. B.; Warren, J. E.; Atwood, J. L. Flexible (Breathing) Interpenetrated Metal–Organic Frameworks for CO₂ Separation Applications. *J. Am. Chem. Soc.* **2008**, *130*, 16842–16843.
- (334) Noro, S.-i.; Tanaka, D.; Sakamoto, H.; Shimomura, S.; Kitagawa, S.; Takeda, S.; Uemura, K.; Kita, H.; Akutagawa, T.; Nakamura, T. Selective Gas Adsorption in One-Dimensional, Flexible CuII Coordination Polymers with Polar Units. *Chem. Mater.* **2009**, *21*, 3346–3355.
- (335) Wang, Z.; Cohen, S. M. Modulating Metal–Organic Frameworks To Breathe: A Postsynthetic Covalent Modification Approach. *J. Am. Chem. Soc.* **2009**, *131*, 16675–16677.
- (336) Neimark, A. V.; Coudert, F.-X.; Boutin, A.; Fuchs, A. H. Stress-Based Model for the Breathing of Metal–Organic Frameworks. *J. Phys. Chem. Lett.* **2010**, *1*, 445–449.
- (337) Couck, S.; Denayer, J. F. M.; Baron, G. V.; Rémy, T.; Gascon, J.; Kapteijn, F. An amine-functionalized MIL-53 Metal–Organic Framework with large separation power for CO₂ and CH₄. *J. Am. Chem. Soc.* **2009**, *131*, 6326–6327.
- (338) Chun, H.; Seo, J. Discrimination of Small Gas Molecules through Adsorption: Reverse Selectivity for Hydrogen in a Flexible Metal–Organic Framework. *Inorg. Chem.* **2009**, *48*, 9980–9982.
- (339) Park, H. J.; Suh, M. P. Stepwise and hysteretic sorption of N₂, O₂, CO₂, and H₂ gases in a porous metal-organic framework [Zn₂(BPnDC)₂(bpy)]. *Chem. Commun.* **2010**, *46*, 610–612.
- (340) Tanaka, D.; Henke, A.; Albrecht, K.; Moeller, M.; Nakagawa, K.; Kitagawa, S.; Groll, J. Rapid preparation of flexible porous coordination polymer nanocrystals with accelerated guest adsorption kinetics. *Nat. Chem.* **2010**, *2*, 410–416.
- (341) Shimomura, S.; Matsuda, R.; Kitagawa, S. Flexibility of Porous Coordination Polymers Strongly Linked to Selective Sorption Mechanism. *Chem. Mater.* **2010**, *22*, 4129–4131.
- (342) Mulfort, K. L.; Farha, O. K.; Malliakas, C. D.; Kanatzidis, M. G.; Hupp, J. T. An Interpenetrated Framework Material with Hysteretic CO₂ Uptake. *Chem. - Eur. J.* **2010**, *16*, 276–281.
- (343) Chen, B.; Xiang, S.; Qian, G. Metal–Organic Frameworks with Functional Pores for Recognition of Small Molecules. *Acc. Chem. Res.* **2010**, *43*, 1115–1124.
- (344) Boutin, A.; Coudert, F. o.-X.; Springuel-Huet, M.-A.; Neimark, A. V.; Férey, G. r.; Fuchs, A. H. The Behavior of Flexible MIL-53(Al) upon CH₄ and CO₂ Adsorption. *J. Phys. Chem. C* **2010**, *114*, 22237–22244.
- (345) Uemura, K.; Yamasaki, Y.; Onishi, F.; Kita, H.; Ebihara, M. Two-Step Adsorption on Jungle-Gym-Type Porous Coordination Polymers: Dependence on Hydrogen-Bonding Capability of Adsorbates, Ligand-Substituent Effect, and Temperature. *Inorg. Chem.* **2010**, *49*, 10133–10143.
- (346) Grunker, R.; Senkovska, I.; Biedermann, R.; Klein, N.; Lohe, M. R.; Muller, P.; Kaskel, S. A highly porous flexible Metal-Organic Framework with corundum topology. *Chem. Commun.* **2011**, *47*, 490–492.
- (347) Kondo, A.; Kajiro, H.; Noguchi, H.; Carlucci, L.; Proserpio, D. M.; Ciani, G.; Kato, K.; Takata, M.; Seki, H.; Sakamoto, M.; Hattori, Y.; Okino, F.; Maeda, K.; Ohba, T.; Kaneko, K.; Kanoh, H. Super Flexibility of a 2D Cu-Based Porous Coordination Framework on Gas Adsorption in Comparison with a 3D Framework of Identical Composition: Framework Dimensionality-Dependent Gas Adsorptivities. *J. Am. Chem. Soc.* **2011**, *133*, 10512–10522.
- (348) Reichenbach, C.; Kalies, G.; Lincke, J.; Lässig, D.; Krautschäid, H.; Moellmer, J.; Thommes, M. Unusual adsorption behavior of a highly flexible copper-based MOF. *Microporous Mesoporous Mater.* **2011**, *142*, 592–600.
- (349) Liu, Y.-Y.; Couck, S.; Vandichel, M.; Grzywa, M.; Leus, K.; Biswas, S.; Volkmer, D.; Gascon, J.; Kapteijn, F.; Denayer, J. F. M.; Waroquier, M.; Van Speybroeck, V.; Van Der Voort, P. New VIV-Based Metal–Organic Framework Having Framework Flexibility and High CO₂ Adsorption Capacity. *Inorg. Chem.* **2013**, *52*, 113–120.
- (350) Shigematsu, A.; Yamada, T.; Kitagawa, H. Selective Separation of Water, Methanol, and Ethanol by a Porous Coordination Polymer Built with a Flexible Tetrahedral Ligand. *J. Am. Chem. Soc.* **2012**, *134*, 13145–13147.
- (351) Mu, B.; Li, F.; Huang, Y.; Walton, K. S. Breathing effects of CO₂ adsorption on a flexible 3D lanthanide metal-organic framework. *J. Mater. Chem.* **2012**, *22*, 10172–10178.
- (352) Kanoo, P.; Matsuda, R.; Kitaura, R.; Kitagawa, S.; Maji, T. K. Topological Difference in 2D Layers Steers the Formation of Rigid and Flexible 3D Supramolecular Isomers: Impact on the Adsorption Properties. *Inorg. Chem.* **2012**, *51*, 9141–9143.

- (353) Nijem, N.; Wu, H.; Canepa, P.; Marti, A.; Balkus, K. J.; Thonhauser, T.; Li, J.; Chabal, Y. J. Tuning the Gate Opening Pressure of Metal–Organic Frameworks (MOFs) for the Selective Separation of Hydrocarbons. *J. Am. Chem. Soc.* **2012**, *134*, 15201–15204.
- (354) Klein, N.; Hoffmann, H. C.; Cadiou, A.; Getzschmann, J.; Lohe, M. R.; Paasch, S.; Heydenreich, T.; Adil, K.; Senkovska, I.; Brunner, E.; Kaskel, S. Structural flexibility and intrinsic dynamics in the M2(2,6-ndc)2(dabco) ($M = \text{Ni}, \text{Cu}, \text{Co}, \text{Zn}$) metal-organic frameworks. *J. Mater. Chem.* **2012**, *22*, 10303–10312.
- (355) Hong, D. H.; Suh, M. P. Selective CO₂ adsorption in a metal-organic framework constructed from an organic ligand with flexible joints. *Chem. Commun.* **2012**, *48*, 9168–9170.
- (356) Yang, S.; Lin, X.; Lewis, W.; Suyetin, M.; Bichoutskaia, E.; Parker, J. E.; Tang, C. C.; Allan, D. R.; Rizkallah, P. J.; Hubberstey, P.; Champness, N. R.; Mark Thomas, K.; Blake, A. J.; Schröder, M. A partially interpenetrated metal–organic framework for selective hysteretic sorption of carbon dioxide. *Nat. Mater.* **2012**, *11*, 710–716.
- (357) Han, L.; Yan, Y.; Sun, F.; Cai, K.; Borjigin, T.; Zhao, X.; Qu, F.; Zhu, G. Single- and Double-Layer Structures and Sorption Properties of Two Microporous Metal–Organic Frameworks with Flexible Tritopic Ligand. *Cryst. Growth Des.* **2013**, *13*, 1458–1463.
- (358) Liu, B.; Li, Y.; Hou, L.; Yang, G.; Wang, Y.-Y.; Shi, Q.-Z. Dynamic Zn-based metal-organic framework: stepwise adsorption, hysteretic desorption and selective carbon dioxide uptake. *J. Mater. Chem. A* **2013**, *1*, 6535–6538.
- (359) Sanda, S.; Parshamoni, S.; Konar, S. Third-Generation Breathing Metal–Organic Framework with Selective, Stepwise, Reversible, and Hysteretic Adsorption Properties. *Inorg. Chem.* **2013**, *52*, 12866–12868.
- (360) Pierotti, R.; Rouquerol, J. Reporting physisorption data for gas/solid systems with special reference to the determination of surface area and porosity. *Pure Appl. Chem.* **1985**, *57*, 603–619.
- (361) Sing, K.; Everett, D.; Haul, R.; Moscou, L.; Pierotti, R.; Rouquerol, J.; Siemieniewska, T. Reporting physisorption data for gas/solid systems. *Pure Appl. Chem.* **1982**, *54*, 2201.
- (362) Yeh, R. L.; Ghosh, T. K.; Hines, A. L. Effects of regeneration conditions on the characteristics of water vapor adsorption on silica gel. *J. Chem. Eng. Data* **1992**, *37*, 259–261.
- (363) Gordeeva, L.; Aristov, Y. Dynamic study of methanol adsorption on activated carbon ACM-35.4 for enhancing the specific cooling power of adsorptive chillers. *Appl. Energy* **2014**, *117*, 127–133.
- (364) Henninger, S. K.; Schicktanz, M.; Hügenell, P. P. C.; Sievers, H.; Henning, H. M. Evaluation of methanol adsorption on activated carbons for thermally driven chillers part I: Thermophysical characterisation. *Int. J. Refrig.* **2012**, *35*, 543–553.
- (365) Schicktanz, M.; Hügenell, P.; Henninger, S. K. Evaluation of methanol/activated carbons for thermally driven chillers, part II: The energy balance model. *Int. J. Refrig.* **2012**, *35*, 554–561.
- (366) Anyanwu, E.; Ezekwe, C. Design, construction and test run of a solid adsorption solar refrigerator using activated carbon/methanol, as adsorbent/adsorbate pair. *Energy Convers. Manage.* **2003**, *44*, 2879–2892.
- (367) Wang, L.; Wu, J.; Wang, R.; Xu, Y.; Wang, S. Experimental study of a solidified activated carbon-methanol adsorption ice maker. *Appl. Therm. Eng.* **2003**, *23*, 1453–1462.
- (368) Pons, M.; Grenier, P. Experimental data on a solar-powered ice maker using activated carbon and methanol adsorption pair. *J. Sol. Energy Eng.* **1987**, *109*, 303–310.
- (369) Cacciola, G.; Restuccia, G.; Mercadante, L. Composites of activated carbon for refrigeration adsorption machines. *Carbon* **1995**, *33*, 1205–1210.
- (370) Chang, J.-S. Porous Metal(III) Carboxylates as Multifunctional Adsorbents and Catalytic Materials. iCeMS-ERATO Symposium; July 26th, 2012.
- (371) Alvarez, E.; Guillou, N.; Martineau, C.; Bueken, B.; Van de Voorde, B.; Le Guillouzer, C.; Fabry, P.; Nouar, F.; Taulelle, F.; De Vos, D. The Structure of the Aluminum Fumarate Metal–Organic Framework A520. *Angew. Chem.* **2015**, *127*, 3735–3739.
- (372) Dybtsev, D. N.; Chun, H.; Kim, K. Rigid and Flexible: A Highly Porous Metal–Organic Framework with Unusual Guest-Dependent Dynamic Behavior. *Angew. Chem.* **2004**, *116*, 5143–5146.
- (373) International zeolite Association - Database of Zeolite Structures. <http://www.iza-structure.org/databases/> (accessed 17-01-2015).
- (374) Mora, A. J.; Fitch, A. N.; Cole, M.; Goyal, R.; Jones, R. H.; Jobic, H.; Carr, S. W. The structure of the calcined aluminophosphate ALPO₄-5 determined by high-resolution X-ray and neutron powder diffraction. *J. Mater. Chem.* **1996**, *6*, 1831–1835.
- (375) Wragg, D. S.; Johnsen, R. E.; Norby, P.; Fjellvåg, H. The adsorption of methanol and water on SAPO-34: in situ and ex situ X-ray diffraction studies. *Microporous Mesoporous Mater.* **2010**, *134*, 210–215.
- (376) IEA. *Heat Pump Centre Newsletter*, 1st ed.; IEA Heat Pump Centre, 2011.
- (377) Satyapal, S.; Petrovic, J.; Read, C.; Thomas, G.; Ordaz, G. The U.S. Department of Energy's National Hydrogen Storage Project: Progress towards meeting hydrogen-powered vehicle requirements. *Catal. Today* **2007**, *120*, 246–256.
- (378) Ahluwalia, R. K.; Peng, J. K.; Hua, T. Q. Sorbent material property requirements for on-board hydrogen storage for automotive fuel cell systems. *Int. J. Hydrogen Energy* **2015**, *40*, 6373–6390.
- (379) Niaz, S.; Manzoor, T.; Pandith, A. H. Hydrogen storage: Materials, methods and perspectives. *Renewable Sustainable Energy Rev.* **2015**, *50*, 457–469.
- (380) Wojcik, A. M. W. Structured Zeolites in Heat Pump Systems. Ph.D. Thesis, TU Delft, 2002.
- (381) Critoph, R. E. Performance limitations of adsorption cycles for solar cooling. *Sol. Energy* **1988**, *41*, 21–31.
- (382) Meunier, F.; Kaushik, S. C.; Neveu, P.; Poyelle, F. A comparative thermodynamic study of sorption systems: second law analysis. *Int. J. Refrig.* **1996**, *19*, 414–421.
- (383) Meunier, F. Solid sorption heat powered cycles for cooling and heat pumping applications. *Appl. Therm. Eng.* **1998**, *18*, 715–729.
- (384) Pons, M.; Meunier, F.; Cacciola, G.; Critoph, R. E.; Groll, M.; Puigjaner, L.; Spinner, B.; Ziegler, F. Thermodynamic based comparison of sorption systems for cooling and heat pumping: Comparaison des performances thermodynamique des systèmes de pompes à chaleur à sorption dans des applications de refroidissement et de chauffage. *Int. J. Refrig.* **1999**, *22*, 5–17.
- (385) Aristov, Y. I.; Tokarev, M. M.; Sharonov, V. E. Universal relation between the boundary temperatures of a basic cycle of sorption heat machines. *Chem. Eng. Sci.* **2008**, *63*, 2907–2912.
- (386) Nunez, T.; Henning, H.-M.; Mittelbach, W. Adsorption cycle modeling: Characterization and comparison of materials. International Sorption Heat Pump Conference, 1998.
- (387) El-Sharkawy, I. I.; Hassan, M.; Saha, B. B.; Koyama, S.; Nasr, M. M. Study on adsorption of methanol onto carbon based adsorbents. *Int. J. Refrig.* **2009**, *32*, 1579–1586.
- (388) Sun, L. M.; Feng, Y.; Pons, M. Numerical investigation of adsorptive heat pump systems with thermal wave heat regeneration under uniform-pressure conditions. *Int. J. Heat Mass Transfer* **1997**, *40*, 281–293.
- (389) Lambert, M. A.; Jones, B. J. Review of regenerative adsorption heat pumps. *J. Thermophys. Heat Transfer* **2005**, *19*, 471–485.
- (390) Dubinin, M. Physical adsorption of gases and vapors in micropores. *Prog. Surf. Membr. Sci.* **1975**, *9*, 1–70.
- (391) Agarwal, R. K.; Schwarz, J. A. Analysis of high pressure adsorption of gases on activated carbon by potential theory. *Carbon* **1988**, *26*, 873–887.
- (392) Yang, K.; Xing, B. Adsorption of organic compounds by carbon nanomaterials in aqueous phase: Polanyi theory and its application. *Chem. Rev.* **2010**, *110*, 5989–6008.
- (393) Mu, B.; Walton, K. S. Thermal Analysis and Heat Capacity Study of Metal–Organic Frameworks. *J. Phys. Chem. C* **2011**, *115*, 22748–22754.
- (394) Song, L. F.; Jiang, C. H.; Zhang, J.; Sun, L. X.; Xu, F.; Tian, Y. Q.; You, W. S.; Cao, Z.; Zhang, L.; Yang, D. W. Heat capacities and

- thermodynamic properties of MgBTC. *J. Therm. Anal. Calorim.* **2010**, *101*, 365–370.
- (395) Lv, X.-C.; Tan, Z.-C.; Gao, X.-H.; Zhang, Z.-H.; Yang, L.-N.; Zhao, J.-N.; Sun, L.-X.; Zhang, T. Synthesis and thermodynamic properties of a metal-organic framework:[LaCu₆(μ-OH)₃(Gly) im₆]₂(ClO₄)₆. *Thermochim. Acta* **2006**, *450*, 102–104.
- (396) Jiang, C. H.; Song, L. F.; Zhang, J.; Sun, L. X.; Xu, F.; Li, F.; Jiao, Q. Z.; Sun, Z. G.; Xing, Y. H.; Du, Y.; Zeng, J. L.; Cao, Z. Thermodynamic properties and heat capacities of Co (BTC)1/3 (DMF) (HCOO). *J. Therm. Anal. Calorim.* **2010**, *102*, 1087–1093.
- (397) Silva, G. G.; Musumeci, A. W.; Gomes, A. P.; Liu, J.-W.; Waclawik, E. R.; George, G. A.; Frost, R. L.; Pimenta, M. A. Characterization of commercial double-walled carbon nanotube material: composition, structure, and heat capacity. *J. Mater. Sci.* **2009**, *44*, 3498–3503.
- (398) Song, L. F.; Jiang, C. H.; Jiao, C. L.; Zhang, J.; Sun, L. X.; Xu, F.; Jiao, Q. Z.; Xing, Y. H.; Du, Y.; Cao, Z.; Huang, F. L. Heat capacities and thermodynamic properties of one manganese-based MOFs. *J. Therm. Anal. Calorim.* **2010**, *102*, 1161–1166.
- (399) Qiu, L.; Murashov, V.; White, M. A. Zeolite 4A: Heat capacity and thermodynamic properties. *Solid State Sci.* **2000**, *2*, 841–846.
- (400) Qiu, L.; Laws, P. A.; Zhan, B.-Z.; White, M. A. Thermodynamic investigations of zeolites NaX and NaY. *Can. J. Chem.* **2006**, *84*, 134–139.
- (401) Cemīč, L.; Dachs, E. Heat capacity of ferrosilite, Fe₂Si₂O₆. *Phys. Chem. Miner.* **2006**, *33*, 457–464.
- (402) Polanyi, M. *Verhandlungen der Deutschen Physikalischen Gesellschaft*; 1914; Vol. 16.
- (403) Polanyi, M. Section III. - Theories of the adsorption of gases. A general survey and some additional remarks. Introductory paper to section III. *Trans. Faraday Soc.* **1932**, *28*, 316–333.
- (404) Polanyi, M.; Verh, d. D. *Phys. Ges.* **1916**, *18*, 55. Goldmann, F.; Pblanyi, M. *Z. Phys. Chem.* **1928**, *132*, 321.
- (405) Goldsworthy, M. Measurements of water vapour sorption isotherms for RD silica gel, AQSOA-Z01, AQSOA-Z02, AQSOA-Z05 and CECA zeolite 3A. *Microporous Mesoporous Mater.* **2014**, *196*, 59–67.
- (406) Kim, Y.-D.; Thu, K.; Ng, K. C. Adsorption characteristics of water vapor on ferroaluminophosphate for desalination cycle. *Desalination* **2014**, *344*, 350–356.
- (407) Woodcock, D. A.; Lightfoot, P.; Villaescusa, L. A.; Díaz-Cabañas, M.-J.; Cambor, M. A.; Engberg, D. Negative thermal expansion in the siliceous zeolites chabazite and ITQ-4: A neutron powder diffraction study. *Chem. Mater.* **1999**, *11*, 2508–2514.
- (408) Rouquerol, F.; Rouquerol, J.; Sing, K. *Adsorption by Powders & Porous Solids*; Academic Press: London, 1999.
- (409) Hu, E. J. A study of thermal decomposition of methanol in solar powered adsorption refrigeration systems. *Sol. Energy* **1998**, *62*, 325–329.
- (410) Sheehan, R. Terephthalic Acid, Dimethyl Terephthalate, and Isophthalic Acid. *Ullmann's Encyclopedia of Industrial Chemistry*; Wiley-VCH Verlag GmbH & Co. KGaA: New York, 2000.
- (411) Lohbeck, K.; Haferkorn, H.; Fuhrmann, W.; Fedtke, N. Maleic and Fumaric Acids. *Ullmann's Encyclopedia of Industrial Chemistry*; Wiley-VCH Verlag GmbH & Co. KGaA: New York, 2000.
- (412) Freni, A.; Sapienza, A.; Glaznev, I. S.; Aristov, Y. I.; Restuccia, G. Experimental testing of a lab-scale adsorption chiller using a novel selective water sorbent “silica modified by calcium nitrate. *Int. J. Refrig.* **2012**, *35*, 518–524.
- (413) Dawoud, B.; Amer, E. H.; Gross, D. M. Experimental investigation of an adsorptive thermal energy storage. *Int. J. Energy Res.* **2007**, *31*, 135–147.
- (414) Vasta, S.; Freni, A.; Sapienza, A.; Costa, F.; Restuccia, G. Development and lab-test of a mobile adsorption air-conditioner. *Int. J. Refrig.* **2012**, *35*, 701–708.
- (415) Zhang, L. Z.; Wang, L. Performance estimation of an adsorption cooling system for automobile waste heat recovery. *Appl. Therm. Eng.* **1997**, *17*, 1127–1139.
- (416) Zhang, L. Z. Design and testing of an automobile waste heat adsorption cooling system. *Appl. Therm. Eng.* **2000**, *20*, 103–114.
- (417) Restuccia, G.; Cacciola, G. Performances of adsorption systems for ambient heating and air conditioning: Performances de systèmes à adsorption pour le chauffage et le conditionnement d'air d'ambiance. *Int. J. Refrig.* **1999**, *22*, 18–26.
- (418) Marletta, L.; Maggio, G.; Freni, A.; Ingrasciotta, M.; Restuccia, G. A non-uniform temperature non-uniform pressure dynamic model of heat and mass transfer in compact adsorbent beds. *Int. J. Heat Mass Transfer* **2002**, *45*, 3321–3330.
- (419) Fedorov, A. G.; Viskanta, R. Analysis of transient heat/mass transfer and adsorption/desorption interactions. *Int. J. Heat Mass Transfer* **1999**, *42*, 803–819.
- (420) Aristov, Y. I. Adsorption dynamics in adsorptive heat transformers: Review of new trends. *Heat Transfer Eng.* **2014**, *35*, 1014–1027.
- (421) Huang, B. L.; McGaughey, A. J. H.; Kaviany, M. Thermal conductivity of metal-organic framework 5 (MOF-5): Part I. Molecular dynamics simulations. *Int. J. Heat Mass Transfer* **2007**, *50*, 393–404.
- (422) Huang, B. L.; Ni, Z.; Millward, A.; McGaughey, A. J. H.; Uher, C.; Kaviany, M.; Yaghi, O. Thermal conductivity of a metal-organic framework (MOF-5): Part II. Measurement. *Int. J. Heat Mass Transfer* **2007**, *50*, 405–411.
- (423) Liu, D.; Purewal, J.; Yang, J.; Sudik, A.; Maurer, S.; Mueller, U.; Ni, J.; Siegel, D. MOF-5 composites exhibiting improved thermal conductivity. *Int. J. Hydrogen Energy* **2012**, *37*, 6109–6117.
- (424) Purewal, J.; Liu, D.; Yang, J.; Sudik, A.; Siegel, D.; Maurer, S.; Müller, U. Increased volumetric hydrogen uptake of MOF-5 by powder densification. *Int. J. Hydrogen Energy* **2012**, *37*, 2723–2727.
- (425) Ming, Y.; Chi, H.; Blaser, R.; Xu, C.; Yang, J.; Veenstra, M.; Gaab, M.; Müller, U.; Uher, C.; Siegel, D. J. Anisotropic thermal transport in MOF-5 composites. *Int. J. Heat Mass Transfer* **2015**, *82*, 250–258.
- (426) Chua, H.; Ng, K.; Malek, A.; Kashiwagi, T.; Akisawa, A.; Saha, B. Modeling the performance of two-bed, silica gel-water adsorption chillers. *Int. J. Refrig.* **1999**, *22*, 194–204.
- (427) Tatlier, M.; Erdem-Şenatalar, A. When do thin zeolite layers and a large void volume in the adsorber limit the performance of adsorption heat pumps? *Microporous Mesoporous Mater.* **2002**, *54*, 89–96.
- (428) Stach, H.; Mugele, J.; Jänen, J.; Weiler, E. Influence of cycle temperatures on the thermochemical heat storage densities in the systems water/microporous and water/mesoporous adsorbents. *Adsorption* **2005**, *11*, 393–404.
- (429) Mette, B.; Kerskes, H.; Drück, H.; Müller-Steinhagen, H. New highly efficient regeneration process for thermochemical energy storage. *Appl. Energy* **2013**, *109*, 352–359.
- (430) Bertsch, F.; Mette, B.; Asenbeck, S.; Kerskes, H.; Müller-Steinhagen, H. Low temperature chemical heat storage—an investigation of hydration reactions. Effstock Conference, Stockholm, 2009.
- (431) Zondag, H.; Kikkert, B.; Smidig, S.; Boer, R. d.; Bakker, M. Prototype thermochemical heat storage with open reactor system. *Appl. Energy* **2013**, *109*, 360–365.
- (432) Van Essen, V.; Zondag, H.; Gores, J. C.; Bleijendaal, L.; Bakker, M.; Schuitema, R.; Van Helden, W.; He, Z.; Rindt, C. Characterization of MgSO₄ hydrate for thermochemical seasonal heat storage. *J. Sol. Energy Eng.* **2009**, *131*, 041014.
- (433) Ding, Y.; Riffat, S. Thermochemical energy storage technologies for building applications: a state-of-the-art review. *Int. J. Low-Carbon Technol.* **2013**, *8*, 106–116.
- (434) Mauran, S.; Lahmidi, H.; Goetz, V. Solar heating and cooling by a thermochemical process. First experiments of a prototype storing 60kWh by a solid/gas reaction. *Sol. Energy* **2008**, *82*, 623–636.
- (435) Tanguy, G.; Papillon, P.; Paulus, C. Seasonal storage coupled to solar combisystem: dynamic simulations for process dimensioning. *Proceeding of Eurosun, Graz, Austria* **2010**.
- (436) Hennaut, S.; Thomas, S.; Andre, P.; Courbon, E.; Le Berigot, T.; Frère, M. Pré-dimensionnement par simulations dynamiques d'un

- réacteur de stockage thermochimique assurant l'autonomie d'un système solaire combiné. *Congrès Français de Thermique 2011-Energie Solaire et Thermique-Perpignan-24–27 Mai 2011* **2011**.
- (437) Visscher, K.; Veldhuis, J. Comparison of candidate materials for seasonal storage of solar heat through dynamic simulation of building and renewable energy system. Ninth International IBPSA Conference, Montréal, Canada, 2005.
- (438) De Boer, R.; Haije, W.; Veldhuis, J. Determination of structural, thermodynamic and phase properties in the Na₂S-H₂O system for application in a chemical heat pump. *Thermochim. Acta* **2002**, *395*, 3–19.
- (439) Boer, R. d.; Haije, W.; Veldhuis, J.; Smeding, S. Solid-sorption cooling with integrated thermal storage—the SWEAT prototype. Proceedings of the 3rd International Heat Powered Cycles Conference (HPC 2004), Larnaca, Cyprus, 2004.
- (440) van Essen, V.; Bleijendaal, L.; Kikkert, B.; Zondag, H.; Bakker, M.; Bach, P. Development of a compact heat storage system based on salt hydrates. Proceedings of the EUROSUN, 2010.
- (441) Li, T.; Wang, R.; Kiplagat, J. K. A target-oriented solid-gas thermochemical sorption heat transformer for integrated energy storage and energy upgrade. *AIChE J.* **2013**, *59*, 1334–1347.
- (442) Aristov, Y. I.; Restuccia, G.; Tokarev, M. M.; Cacciola, G. Selective Water Sorbents for Multiple Applications, 10. Energy Storage Ability. *React. Kinet. Catal. Lett.* **2000**, *69*, 345–353.
- (443) Zhu, D.; Wu, H.; Wang, S. Experimental study on composite silica gel supported CaCl₂ sorbent for low grade heat storage. *Int. J. Therm. Sci.* **2006**, *45*, 804–813.
- (444) Wu, H.; Wang, S.; Zhu, D. Effects of impregnating variables on dynamic sorption characteristics and storage properties of composite sorbent for solar heat storage. *Sol. Energy* **2007**, *81*, 864–871.
- (445) Jabbari-Hichri, A.; Bennici, S.; Auroux, A. Water sorption heats on silica-alumina-based composites for interseasonal heat storage. *J. Therm. Anal. Calorim.* **2014**, *118*, 1111–1118.
- (446) Liu, H.; Nagano, K.; Togawa, J. A composite material made of mesoporous siliceous shale impregnated with lithium chloride for an open sorption thermal energy storage system. *Sol. Energy* **2015**, *111*, 186–200.
- (447) Opel, O.; Rammelberg, H.; Gérard, M.; Ruck, W. Thermochemical Storage Materials Research-TGA/DSC-Hydration Studies. Proceedings of the International Conference for Sustainable Energy Storage, 2011.
- (448) Jänen, J.; Ackermann, D.; Stach, H.; Brösicke, W. Studies of the water adsorption on Zeolites and modified mesoporous materials for seasonal storage of solar heat. *Sol. Energy* **2004**, *76*, 339–344.
- (449) Munters, HoneyCombe Wheels & Desiccant Options (product leaflet). <http://webdh.munters.com/webdh/BrochureUploads/Brochure-%20Wheel%20and%20Desiccant%20options.pdf> (accessed 17-01-2015).
- (450) Klingenburg, New development Sorption rotor Hugo (product leaflet). <http://www.klingenburg-usa.com/news/hugo.html> (accessed 17-01-2015).
- (451) Kanoglu, M.; Özdiç ÇarpInlologlu, M.; Yıldırılm, M. Energy and exergy analyses of an experimental open-cycle desiccant cooling system. *Appl. Therm. Eng.* **2004**, *24*, 919–932.
- (452) Zhang, X. J.; Dai, Y. J.; Wang, R. Z. A simulation study of heat and mass transfer in a honeycombed rotary desiccant dehumidifier. *Appl. Therm. Eng.* **2003**, *23*, 989–1003.
- (453) Wang, W.; Wu, L.; Li, Z.; Fang, Y.; Ding, J.; Xiao, J. An Overview of Adsorbents in the Rotary Desiccant Dehumidifier for Air Dehumidification. *Drying Technol.* **2013**, *31*, 1334–1345.
- (454) Guo, P.; Wong-Foy, A. G.; Matzger, A. J. Microporous Coordination Polymers as Efficient Sorbents for Air Dehumidification. *Langmuir* **2014**, *30*, 1921–1925.
- (455) Kolios, G.; Frauhammer, J.; Eigenberger, G. Efficient reactor concepts for coupling of endothermic and exothermic reactions. *Chem. Eng. Sci.* **2002**, *57*, 1505–1510.
- (456) Zacher, D.; Shekhah, O.; Woll, C.; Fischer, R. A. Thin films of metal-organic frameworks. *Chem. Soc. Rev.* **2009**, *38*, 1418–1429.
- (457) Bétard, A. I.; Fischer, R. A. Metal–Organic Framework Thin Films: From Fundamentals to Applications. *Chem. Rev.* **2012**, *112*, 1055.
- (458) Shekhah, O.; Cadiou, A.; Eddaoudi, M. Fabrication and non-covalent modification of highly oriented thin films of a zeolite-like metal–organic framework (ZMOF) with rho topology. *CrystEngComm* **2015**, *17*, 290–294.
- (459) Keitz, B. K.; Yu, C. J.; Long, J. R.; Ameloot, R. Lithographic Deposition of Patterned Metal–Organic Framework Coatings Using a Photobase Generator. *Angew. Chem., Int. Ed.* **2014**, *53*, 5561–5565.
- (460) Witters, D.; Vermeir, S.; Puers, R.; Sels, B. F.; De Vos, D. E.; Lammertyn, J.; Ameloot, R. Miniaturized Layer-by-Layer Deposition of Metal–Organic Framework Coatings through Digital Microfluidics. *Chem. Mater.* **2013**, *25*, 1021–1023.
- (461) Zhao, J.; Gong, B.; Nunn, W. T.; Lemaire, P. C.; Stevens, E. C.; Sidi, F. I.; Williams, P. S.; Oldham, C. J.; Walls, H. J.; Shepherd, S. D. Conformal and highly adsorptive metal–organic framework thin films via layer-by-layer growth on ALD-coated fiber mats. *J. Mater. Chem. A* **2015**, *3*, 1458.
- (462) Reboul, J.; Furukawa, S.; Horike, N.; Tsotsalas, M.; Hirai, K.; Uehara, H.; Kondo, M.; Louvain, N.; Sakata, O.; Kitagawa, S. Mesoscopic architectures of porous coordination polymers fabricated by pseudomorphic replication. *Nat. Mater.* **2012**, *11*, 717–723.
- (463) Ramos-Fernandez, E. V.; Garcia-Domingos, M.; Juan-Alcañiz, J.; Gascon, J.; Kapteijn, F. MOFs meet monoliths: Hierarchical structuring metal organic framework catalysts. *Appl. Catal., A* **2011**, *391*, 261–267.
- (464) Gascon, J.; Aguado, S.; Kapteijn, F. Manufacture of dense coatings of Cu₃(BTC)₂ (HKUST-1) on α -alumina. *Microporous Mesoporous Mater.* **2008**, *113*, 132–138.
- (465) Dailly, A.; Poirier, E. Evaluation of an industrial pilot scale densified MOF-177 adsorbent as an on-board hydrogen storage medium. *Energy Environ. Sci.* **2011**, *4*, 3527–3534.
- (466) Remy, T.; Peter, S. A.; Van der Perre, S.; Valvakens, P.; De Vos, D. E.; Baron, G. V.; Denayer, J. F. Selective Dynamic CO₂ Separations on Mg-MOF-74 at Low Pressures: A Detailed Comparison with 13X. *J. Phys. Chem. C* **2013**, *117*, 9301–9310.
- (467) Arnold, L.; Averlant, G.; Marx, S.; Weickert, M.; Müller, U.; Mertel, J.; Horch, C.; Peksa, M.; Stallmach, F. Metal Organic Frameworks for Natural Gas Storage in Vehicles. *Chem. Ing. Tech.* **2013**, *85*, 1726–1733.
- (468) Schell, J.; Casas, N.; Blom, R.; Spjelkavik, A. I.; Andersen, A.; Cavka, J. H.; Mazzotti, M. MCM-41, MOF and UiO-67/MCM-41 adsorbents for pre-combustion CO₂ capture by PSA: adsorption equilibria. *Adsorption* **2012**, *18*, 213–227.
- (469) Sapienza, A.; Glaznev, I. S.; Santamaría, S.; Freni, A.; Aristov, Y. I. Adsorption chilling driven by low temperature heat: New adsorbent and cycle optimization. *Appl. Therm. Eng.* **2012**, *32*, 141–146.
- (470) Myat, A.; Kim Choon, N.; Thu, K.; Kim, Y.-D. Experimental investigation on the optimal performance of Zeolite–water adsorption chiller. *Appl. Energy* **2013**, *102*, 582–590.
- (471) Santamaría, S.; Sapienza, A.; Fazzica, A.; Freni, A.; Girnik, I. S.; Aristov, Y. I. Water adsorption dynamics on representative pieces of real adsorbents for adsorptive chillers. *Appl. Energy* **2014**, *134*, 11–19.
- (472) Fazzica, A.; Füldner, G.; Sapienza, A.; Freni, A.; Schnabel, L. Experimental and theoretical analysis of the kinetic performance of an adsorbent coating composition for use in adsorption chillers and heat pumps. *Appl. Therm. Eng.* **2014**, *73*, 1022–1031.
- (473) Glaznev, I.; Ovoshchnikov, D.; Aristov, Y. Effect of Residual Gas on Water Adsorption Dynamics Under Typical Conditions of an Adsorption Chiller. *Heat Transfer Eng.* **2010**, *31*, 924–930.
- (474) Aristov, Y. I.; Glaznev, I. S.; Girnik, I. S. Optimization of adsorption dynamics in adsorptive chillers: Loose grains configuration. *Energy* **2012**, *46*, 484–492.
- (475) Ragon, F.; Horcajada, P.; Chevreau, H.; Hwang, Y. K.; Lee, U.-H.; Miller, S. R.; Devic, T.; Chang, J.-S.; Serre, C. In Situ Energy-Dispersive X-ray Diffraction for the Synthesis Optimization and Scale-up of the Porous Zirconium Terephthalate UiO-66. *Inorg. Chem.* **2014**, *53*, 2491–2500.

- (476) Marquez, A. G.; Horcajada, P.; Grosso, D.; Ferey, G.; Serre, C.; Sanchez, C.; Boissiere, C. Green scalable aerosol synthesis of porous metal–organic frameworks. *Chem. Commun.* **2013**, *49*, 3848–3850.
- (477) Agostoni, V.; Horcajada, P.; Rodriguez-Ruiz, V.; Willaime, H.; Couvreur, P.; Serre, C.; Gref, R. ‘Green’fluorine-free mesoporous iron (III) trimesate nanoparticles for drug delivery. *Green Mater.* **2013**, *1*, 209–217.
- (478) Zhang, F.; Shi, J.; Jin, Y.; Fu, Y.; Zhong, Y.; Zhu, W. Facile synthesis of MIL-100(Fe) under HF-free conditions and its application in the acetalization of aldehydes with diols. *Chem. Eng. J.* **2015**, *259*, 183–190.
- (479) Garcia Marquez, A.; Horcajada, P.; Grosso, D.; Ferey, G.; Serre, C.; Sanchez, C.; Boissiere, C. Green scalable aerosol synthesis of porous metal-organic frameworks. *Chem. Commun.* **2013**, *49*, 3848–3850.
- (480) García Márquez, A.; Demessence, A.; Platero-Prats, A. E.; Heurtaux, D.; Horcajada, P.; Serre, C.; Chang, J.-S.; Férey, G.; de la Peña-O’Shea, V. A.; Boissière, C.; Grosso, D.; Sanchez, C. Green Microwave Synthesis of MIL-100(Al, Cr, Fe) Nanoparticles for Thin-Film Elaboration. *Eur. J. Inorg. Chem.* **2012**, *2012*, 5165–5174.
- (481) Mao, Y.; Li, J.; Cao, W.; Ying, Y.; Sun, L.; Peng, X. Pressure-assisted synthesis of HKUST-1 thin film on polymer hollow fiber at room temperature toward gas separation. *ACS Appl. Mater. Interfaces* **2014**, *6*, 4473–4479.
- (482) Motakef-Kazemi, N.; Shojaosadati, S. A.; Morsali, A. In situ synthesis of a drug-loaded MOF at room temperature. *Microporous Mesoporous Mater.* **2014**, *186*, 73–79.
- (483) Díaz-García, M.; Mayoral, Á.; Díaz, I.; Sánchez-Sánchez, M. Nanoscaled M-MOF-74 Materials Prepared at Room Temperature. *Cryst. Growth Des.* **2014**, *14*, 2479–2487.
- (484) Zahn, G.; Schulze, H. A.; Lippke, J.; König, S.; Sazama, U.; Fröba, M.; Behrens, P. A Water-Born Zr-Based Porous Coordination Polymer: Modulated Synthesis of Zr-fumarate MOF. *Microporous Mesoporous Mater.* **2015**, *203*, 186.
- (485) Nordin, N.; Ismail, A.; Mustafa, A.; Goh, P.; Rana, D.; Matsura, T. Aqueous room temperature synthesis of zeolitic imidazole framework 8 (ZIF-8) with various concentrations of triethylamine. *RSC Adv.* **2014**, *4*, 33292–33300.
- (486) Bustamante, E. L.; Fernández, J. L.; Zamaro, J. M. Influence of the solvent in the synthesis of zeolitic imidazolate framework-8 (ZIF-8) nanocrystals at room temperature. *J. Colloid Interface Sci.* **2014**, *424*, 37–43.
- (487) Tranchemontagne, D. J.; Hunt, J. R.; Yaghi, O. M. Room temperature synthesis of metal-organic frameworks: MOF-5, MOF-74, MOF-177, MOF-199, and IRMOF-0. *Tetrahedron* **2008**, *64*, 8553–8557.
- (488) Cravillon, J.; Münzer, S.; Lohmeier, S.-J.; Feldhoff, A.; Huber, K.; Wiebcke, M. Rapid room-temperature synthesis and characterization of nanocrystals of a prototypical zeolitic imidazolate framework. *Chem. Mater.* **2009**, *21*, 1410–1412.
- (489) Pichon, A.; Lazuen-Garay, A.; James, S. L. Solvent-free synthesis of a microporous metal–organic framework. *CrystEngComm* **2006**, *8*, 211–214.
- (490) Stassen, I.; Campagnol, N.; Fransaer, J.; Vereecken, P.; De Vos, D.; Ameloot, R. Solvent-free synthesis of supported ZIF-8 films and patterns through transformation of deposited zinc oxide precursors. *CrystEngComm* **2013**, *15*, 9308–9311.
- (491) Mottillo, C.; Lu, Y.; Pham, M.-H.; Cliffe, M. J.; Do, T.-O.; Friščić, T. Mineral neogenesis as an inspiration for mild, solvent-free synthesis of bulk microporous metal–organic frameworks from metal (Zn, Co) oxides. *Green Chem.* **2013**, *15*, 2121–2131.
- (492) Müller-Buschbaum, K.; Schönfeld, F. The Utilisation of Solvent-Free Synthesis for the Reaction of Cobalt with Imidazole: MOF Conversion from $[Co_3(Im)_6(ImH)_2]$ via $[Co_4(Im)_8(ImH)]$ to $[Co(Im)_2]$. *Z. Anorg. Allg. Chem.* **2011**, *637*, 955–960.
- (493) Lanchas, M.; Arcediano, S.; Aguayo, A. T.; Beobide, G.; Castillo, O.; Cepeda, J.; Vallejo-Sánchez, D.; Luque, A. Two appealing alternatives for MOFs synthesis: solvent-free oven heating vs. microwave heating. *RSC Adv.* **2014**, *4*, 60409–60412.
- (494) Cliffe, M. J.; Mottillo, C.; Stein, R. S.; Bučar, D.-K.; Friščić, T. Accelerated aging: a low energy, solvent-free alternative to solvothermal and mechanochemical synthesis of metal–organic materials. *Chem. Sci.* **2012**, *3*, 2495–2500.
- (495) Chal, R.; Gérardin, C.; Bulut, M.; van Donk, S. Overview and industrial assessment of synthesis strategies towards zeolites with mesopores. *ChemCatChem* **2011**, *3*, 67–81.
- (496) Ren, L.; Zhu, L.; Yang, C.; Chen, Y.; Sun, Q.; Zhang, H.; Li, C.; Nawaz, F.; Meng, X.; Xiao, F.-S. Designed copper–amine complex as an efficient template for one-pot synthesis of Cu-SSZ-13 zeolite with excellent activity for selective catalytic reduction of NO_x by NH₃. *Chem. Commun.* **2011**, *47*, 9789–9791.
- (497) Cho, H. S.; Ryoo, R. Synthesis of ordered mesoporous MFI zeolite using CMK carbon templates. *Microporous Mesoporous Mater.* **2012**, *151*, 107–112.
- (498) Cooper, E. R.; Andrews, C. D.; Wheatley, P. S.; Webb, P. B.; Wormald, P.; Morris, R. E. Ionic liquids and eutectic mixtures as solvent and template in synthesis of zeolite analogues. *Nature* **2004**, *430*, 1012–1016.
- (499) Yang, Z.; Xia, Y.; Mokaya, R. Zeolite ZSM-5 with Unique Supermicropores Synthesized Using Mesoporous Carbon as a Template. *Adv. Mater.* **2004**, *16*, 727–732.
- (500) Cundy, C. S.; Cox, P. A. The hydrothermal synthesis of zeolites: history and development from the earliest days to the present time. *Chem. Rev.* **2003**, *103*, 663–702.
- (501) Liu, G.; Tian, P.; Zhang, Y.; Li, J.; Xu, L.; Meng, S.; Liu, Z. Synthesis of SAPO-34 templated by diethylamine: Crystallization process and Si distribution in the crystals. *Microporous Mesoporous Mater.* **2008**, *114*, 416–423.
- (502) Xu, Y.; Maddox, P. J.; Couves, J. W. The synthesis of SAPO-34 and CoSAPO-34 from a triethylamine-hydrofluoric acid-water system. *J. Chem. Soc., Faraday Trans.* **1990**, *86*, 425–429.
- (503) Prakash, A. M.; Unnikrishnan, S. Synthesis of SAPO-34: high silicon incorporation in the presence of morpholine as template. *J. Chem. Soc., Faraday Trans.* **1994**, *90*, 2291–2296.
- (504) Gougeon, R. D.; Brouwer, E. B.; Bodart, P. R.; Delmotte, L.; Marichal, C.; Chézeau, J.-M.; Harris, R. K. Solid-State NMR Studies of the As-Synthesized AlPO₄-5/TPAF Microporous Aluminophosphate. *J. Phys. Chem. B* **2001**, *105*, 12249–12256.
- (505) Jiang, F.; Tang, Z.; Zhai, J.; Ye, J.; Han, J. Synthesis of AlPO₄-5 crystals using TBAOH as template. *Microporous Mesoporous Mater.* **2006**, *92*, 129–133.
- (506) Wan, Y.; Williams, C. D.; Duke, C. V.; Cox, J. J. Systematic studies on the effect of water content on the synthesis, crystallisation, conversion and morphology of AlPO₄-5 molecular sieve. *J. Mater. Chem.* **2000**, *10*, 2857–2862.